

## INFORMATION TO USERS

This reproduction was made from a copy of a document sent to us for microfilming. While the most advanced technology has been used to photograph and reproduce this document, the quality of the reproduction is heavily dependent upon the quality of the material submitted.

The following explanation of techniques is provided to help clarify markings or notations which may appear on this reproduction.

1. The sign or "target" for pages apparently lacking from the document photographed is "Missing Page(s)". If it was possible to obtain the missing page(s) or section, they are spliced into the film along with adjacent pages. This may have necessitated cutting through an image and duplicating adjacent pages to assure complete continuity.
2. When an image on the film is obliterated with a round black mark, it is an indication of either blurred copy because of movement during exposure, duplicate copy, or copyrighted materials that should not have been filmed. For blurred pages, a good image of the page can be found in the adjacent frame. If copyrighted materials were deleted, a target note will appear listing the pages in the adjacent frame.
3. When a map, drawing or chart, etc., is part of the material being photographed, a definite method of "sectioning" the material has been followed. It is customary to begin filming at the upper left hand corner of a large sheet and to continue from left to right in equal sections with small overlaps. If necessary, sectioning is continued again—beginning below the first row and continuing on until complete.
4. For illustrations that cannot be satisfactorily reproduced by xerographic means, photographic prints can be purchased at additional cost and inserted into your xerographic copy. These prints are available upon request from the Dissertations Customer Services Department.
5. Some pages in any document may have indistinct print. In all cases the best available copy has been filmed.

**University  
Microfilms  
International**  
300 N. Zeeb Road  
Ann Arbor, MI 48106



**Glebocki, Orest Jaroslaw**

**INTERVALLEY ELECTRON-PHONON AND HOLE-PHONON  
INTERACTIONS IN SILICON, GERMANIUM AND GALLIUM PHOSPHIDE:  
EXPERIMENT AND THEORY**

*City University of New York*

PH.D. 1982

**University  
Microfilms  
International** 300 N. Zeeb Road, Ann Arbor, MI 48106

**Copyright 1982**

**by**

**Glebocki, Orest Jaroslaw**

**All Rights Reserved**



**PLEASE NOTE:**

In all cases this material has been filmed in the best possible way from the available copy. Problems encountered with this document have been identified here with a check mark ✓.

1. Glossy photographs or pages \_\_\_\_\_
2. Colored illustrations, paper or print \_\_\_\_\_
3. Photographs with dark background \_\_\_\_\_
4. Illustrations are poor copy \_\_\_\_\_
5. Pages with black marks, not original copy \_\_\_\_\_
6. Print shows through as there is text on both sides of page \_\_\_\_\_
7. Indistinct, broken or small print on several pages ✓
8. Print exceeds margin requirements \_\_\_\_\_
9. Tightly bound copy with print lost in spine \_\_\_\_\_
10. Computer printout pages with indistinct print ✓
11. Page(s) \_\_\_\_\_ lacking when material received, and not available from school or author.
12. Page(s) \_\_\_\_\_ seem to be missing in numbering only as text follows.
13. Two pages numbered \_\_\_\_\_. Text follows.
14. Curling and wrinkled pages \_\_\_\_\_
15. Other \_\_\_\_\_

**University  
Microfilms  
International**



INTERVALLEY ELECTRON-PHONON AND HOLE-PHONON INTERACTIONS  
IN SILICON, GERMANIUM AND GALLIUM PHOSPHIDE:  
EXPERIMENT AND THEORY

By

Orest J. Glembocki

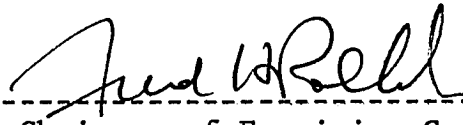
A dissertation submitted to the Graduate Faculty in  
Physics in partial fulfillment of the requirements for  
the degree of Doctor of Philosophy, The Graduate School  
of the City University of New York.

1982

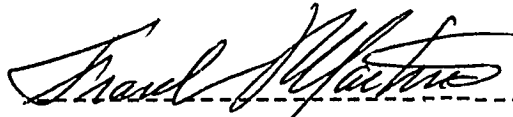
©  
Copyright by  
Orest Jaroslaw Glembocki  
1982

This manuscript has been read and accepted for the Graduate Faculty in Physics in satisfaction of the dissertation requirement for the degree of Doctor of Philosophy

7/26/82  
-----  
Date

  
-----  
Chairman of Examining Committee

7/26/82  
-----  
Date

  
-----  
Executive Officer

David E. Aspnes  
-----

Herman Cummins  
-----

Joseph B. Krieger  
-----

George Skorinko  
-----  
Supervisory Committee

The City University of New York

ABSTRACT

Intervalley Electron-Phonon and Hole-Phonon Interactions  
in Silicon, Germanium and Gallium Phosphide:  
Experiment and Theory

By

Orest J. Glembocki

Advisor: Professor Fred H. Pollak  
(Brooklyn College of C.U.N.Y.)

Intervalley electron-phonon (e-ph) and hole-phonon (h-ph) interactions play an important role in many properties of semiconductors. Understanding indirect phonon assisted transitions requires a precise knowledge of the e-ph and h-ph matrix elements. In these types of materials the fundamental absorption of light proceeds via two scattering mechanisms involving both e-ph and h-ph interactions and in such a way that they can interfere either constructively or destructively. The absorption coefficient in some indirect gap semiconductors is sensitive to the magnitudes and phases of the e-ph and h-ph matrix elements. Consequently, this area is ideal for studying the intervalley e-ph and h-ph interactions.

In this thesis, we present a study of the e-ph and

h-ph interactions in GaP, Si and Ge. A piezospectroscopic experiment is performed in GaP for the  $\Gamma$ -X phonon assisted transitions (LA,TA,LO,TO) and the ratio of the e-ph and h-ph scattering matrix elements is obtained for the LA and TA phonons. The e-ph and h-ph matrix elements are evaluated individually by comparing the above results together with experimental values for the absorption coefficient to theoretical expressions for the absorption coefficient. A similar analysis is performed for the TO phonon assisted transition in Si and its e-ph and h-ph matrix elements are also obtained.

A theoretical calculation of the  $\Gamma$ - $\Delta$  and  $\Gamma$ -L matrix elements of Si and Ge is performed. This work uses the "rigid-pseudoion" model, which represents the lattice displacements through a rigid-ion model and the potential and electronic states by local pseudopotential theory. The theoretical and experimental values of the matrix elements for the TO phonon of Si are in good agreement. Consequently, we can now account for the absolute as well as relative intensities of the indirect transitions in both Si ( $\Gamma$  -  $\Delta$ ) and Ge ( $\Gamma$  - L). The determination of the e-ph and h-ph matrix elements in GaP, Si and Ge permits us to gain insights into the mechanisms responsible for the indirect transitions in these materials.

The calculation is also performed for points midway into the Brillouin zone along  $\Delta$  for Si and Ge and along  $\Gamma$  in Ge. These results, in conjunction with the  $\Gamma$ - $\Delta$  and  $\Gamma$ -L numbers and the values in GaP allow us to probe the nature of the scattering in these materials.

To the Glembocki and Omechenko family

and to Audrey Murawski

ACKNOWLEDGEMENTS

I wish to extend to Professor Fred H. Pollak my deepest gratitude for his guidance, patience and friendship throughout the course of this work. My association with him has been not only educational and stimulating, but also very enjoyable. I thank him for all that he did for me.

To Professor M. H. Cohen, Dr. S. Pantelides and Professor P. B. Allen for useful discussions at various times and to Dr. G. Wright for his continuing encouragement I give many thanks. I am especially grateful to Dr. R. P. Silberstein for his guidance, moral support and friendship during many trying times in my graduate studies and to Professor V. Sahni for stimulating my interest in Solid State physics. I also would like to thank the members of my guidance committee for their time and efforts on my behalf.

Acknowledgement is given to S. Coltun and M. Berman of the machine shop and i. Senzon of the electronics shop for their technical support during the course of the experiments. I very grateful to Ken Davenport of the Data Acquisition Facility, who was most instru-

mental in the computer preparation of this manuscript. Without his help and friendship the final stages of this work would have been quite difficult.

This research was supported by the Office of Naval Research through Contract No. N00014-78-C0890.

TABLE OF CONTENTS

APPROVAL.....iii

ABSTRACT.....iv

DEDICATION.....vii

ACKNOWLEDGEMENTS.....viii

CHAPTER I. INTRODUCTION.....1

CHAPTER II. THEORETICAL BACKGROUND.....11

CHAPTER III. UNIAXIAL STRESS.....19

    3.1 General Theory.....20

    3.2 Stress Along [111].....22

        3.2.1 <001> Conduction Bands.....22

        3.2.2 <111> Conduction Bands.....22

        3.2.3 The Valence Band.....23

    3.3 Stress Along [001].....26

        3.3.1 <001> Conduction Bands.....26

        3.3.2 <111> Conduction Bands.....27

        3.3.3 The Valence Band.....27

    3.4 The Stress-Dependent "Oscillator Strength"...27

CHAPTER IV. THE EXPERIMENT.....30

    4.1 Experimental Details.....31

        4.1.1 The Optics and Electronics.....31

        4.1.2 The Stress Apparatus.....35

    4.2 Experimental Results.....36

        4.2.1 LA Phonon.....40

4.2.2	TA Phonon.....	43
4.2.3	TO Phonon.....	45
4.3	Evaluation of the Electron-Phonon and Hole-Phonon Scattering Matrix Elements.....	46
4.3.1	Silicon.....	46
4.3.2	Gallium Phosphide.....	51
	TA Phonon.....	52
	LA Phonon.....	54
CHAPTER V. CALCULATION OF THE ELECTRON-PHONON AND HOLE-PHONON SCATTERING MATRIX ELEMENTS.....		
5.1	The Rigid-Pseudoion Model.....	58
5.2	Application To Diamond Type Materials.....	62
5.2.1	The Fundamental Indirect Gap.....	64
	Silicon.....	64
	Germanium.....	73
5.2.2	The Secondary Indirect Gaps.....	78
	Silicon.....	69
	Germanium.....	85
5.2.3	Other Points In The Brillouin Zone.....	86
CHAPTER VI. DISCUSSION AND CONCLUSIONS.....		
6.1	The Oscillator Strength.....	88
6.2	Gallium Phosphide.....	91
6.3	Silicon.. ..	93
6.4	Germanium.....	95
6.5	Trends In Intervalley Scattering.....	97
6.6	Summary And Conclusions.....	102
6.7	Possible Future Research.....	105
APPENDIX A. OPTICAL AND PHONON SCATTERING SELECTION RULES.....		
A.1	$\Gamma$ -X( $\Delta$ ) Transitions.....	109
A.2	$\Gamma$ -L Transitions.....	114

APPENDIX B. CURVE FITTING PROGRAMS.....	115
APPENDIX C. PSEUDOPOTENTIAL CALCULATIONS.....	127
APPENDIX D. RIGID-ION LATTICE DYNAMICS.....	131
APPENDIX E. THE PROCEDURE FOR CALCULATING THE E-PH AND H-PH MATRIX ELEMENTS.....	136
REFERENCES.....	138
LIST OF TABLES.....	145
TABLES.....	150
FIGURE CAPTIONS.....	188
FIGURES.....	190
LIST OF PUBLICATIONS.....	210

## CHAPTER I. INTRODUCTION

Electron-phonon (e-ph) and hole-phonon (h-ph) interactions play an important role in many optical<sup>1-17</sup> and transport<sup>18-21</sup> properties of semiconductors. Despite nearly three decades of research into processes which involve intervalley e-ph and h-ph interactions, little is known about them either experimentally or theoretically. This deficiency in our knowledge can be traced to the difficulty in obtaining reliable experimental values for the matrix elements ( $S_{e-ph}$  and  $S_{h-ph}$ ) of these interactions. Consequently theoretical calculations had no basis for comparison and hence there could be little confidence in their results. Because of this situation, theoretical work was rarely attempted in this area.

In transport phenomena, intervalley e-ph (or h-ph) interactions provide a scattering mechanism which limits the electron (or hole) drift velocity when the crystal is placed in a high electric field.<sup>18,20</sup> A measurement of only the velocity-field curves of a semiconductor will not provide a value for the e-ph matrix element. This is a result of the fact that several valleys ( $\Gamma-X, \Gamma-L, L-X$ ) may be involved in the scattering process and one does not know the strengths of the individual contributions to drift velocity.

Furthermore, the calculations of the drift velocity are dependent on the model used to obtain the relaxation time and therefore, the e-ph matrix elements are not easily differentiated from the other unknown parameters.<sup>20</sup>

Despite these difficulties, transport calculations were still carried out. To circumvent the problem of a lack of information about the intervalley e-ph and h-ph interactions, one level scattering was assumed and the value of the e-ph matrix element was estimated.<sup>20</sup> The number for  $S_{e-ph}$  was obtained by considering the energy differences between the scattering states, band widths, sizes of energy gaps and the fact that the e-ph interaction is a perturbation to the band structure. This crude approach to obtaining a value for the e-ph (h-ph) matrix element resulted in reasonable agreement between transport measurements and theory.

Phonon-assisted absorption and luminescence in indirect gap semiconductors is an area which requires a precise knowledge of the e-ph and h-ph matrix elements. The phonon assisted transition proceeds via both e-ph and h-ph scattering mechanisms.<sup>7,8,12,15,16,22-26</sup> The "oscillator strength" of the absorption coefficient is proportional to the square of the sum of terms involving e-ph and h-ph matrix elements and thus constructive

or destructive interference can occur between the two scattering mechanisms. This is a result of the delicate balance between both the magnitudes and relative phase of the e-ph and h-ph matrix elements of a given process. In a material such as Si, where more than one indirect transition occurs, this balance is more complicated. The relative intensities of the observed processes depend upon the relationship between the pairs of matrix elements (e-ph and h-ph) of all of the allowed phonons. For example, in Si, four transitions (TO,LO,TA,LA) can occur, but only three are observed. Among the detected processes, the TO transition is much stronger than the LO and TA ones.<sup>1,5,6,13</sup> Therefore, the e-ph and h-ph matrix elements of the TO phonon are in a delicate balance with those of the LO and TA phonons.

The sensitivity of the indirect transitions to the e-ph and h-ph matrix elements makes this area ideal for the evaluation of  $S_{e-ph}$  and  $S_{h-ph}$ . However, the nature of the indirect transition, i.e., the interference phenomena does not allow us to determine the matrix elements directly by measuring only one parameter, i.e., the absorption coefficient. This difficulty was overcome by various workers, including Cardona, Pollak, Capizi, Balslev, Pikus, etc., who realized that the

application of uniaxial stress along appropriate crystallographic axes can be used to reduce the symmetry of the valence and (or) conduction bands in such a way that would produce additional transitions for each phonon-assisted process that takes place.<sup>7,8,10,22,27-29</sup> It was proposed that this extra information can be utilized in evaluating the ratio of the e-ph and h-ph scattering matrix elements.

Using this idea, Pollak, et al.<sup>7</sup> and Capizi et al.<sup>24</sup> independently performed wavelength modulated absorption (WMA) experiments on Si stressed along the [001] and [111] directions. From their results, both groups were able to determine the ratio of the contributions to the oscillator strength of the electron and hole scattering for the TO ( $\Gamma$ - $\Delta$ ) phonon-assisted transition of this material. However, a more complete analysis of the data allowed Pollak et al. to evaluate the ratio of the e-ph and h-ph scattering matrix elements. They found that  $S_{e-ph_{TO}}/S_{h-ph_{TO}} = -0.73$ .

A similar experiment was also performed for the  $\Gamma$ -L, LA phonon-assisted transition in Ge and a ratio of the e-ph and h-ph matrix elements was obtained.<sup>8</sup> However, in this material the electron scattering can proceed via two intermediate conduction band states,  $\Gamma_{2',c}$  and  $\Gamma_{15,c}$ . The  $\Gamma_{15,c}$  state lies much higher in

energy than  $\Gamma_{2,c}$  and therefore its contribution to the oscillator strength was neglected. The result of this experiment was not similar to the ratio obtained for the TO phonon of Si. In Ge, the ratio,  $S_{e-ph_{LA}}/S_{h-ph_{LA}} = -0.16$ , indicated that the conduction band coupling was much weaker than the valence band coupling, where as in Si they were comparable. This result was accepted by many, but with some reservations. It was generally felt that the e-ph and h-ph matrix elements for a given transition should be similar in magnitude and that the small  $S_{e-ph}/S_{h-ph}$  ratio for the LA phonon of Ge was a result of neglecting  $\Gamma_{15,c}$ .

This survey of the experimental progress in the study of the role of e-ph and h-ph interactions in indirect transitions brings us to the start of the present work. To this point in time, there were no known theoretical calculations of the e-ph and h-ph matrix elements of phonon-assisted absorption processes. It must be pointed out here that intervalley e-ph and h-ph matrix elements were calculated in the study of the intervalley deformation potentials in PbTe and SnTe,<sup>30</sup> the temperature dependence of the direct gaps in Ge,<sup>31</sup> PbTe and PbSe<sup>32</sup> and coupling constants in graphite.<sup>19</sup> However, in these calculations,

only the magnitudes were obtained and in the latter three cases averages were performed over various scattering mechanisms. Obviously, these calculations were not sensitive to the fine details of the e-ph and h-ph matrix elements, which become crucial in indirect transitions.

The work prior to this study left many unanswered questions, which we will address. In this thesis we will approach the problem of obtaining values for the e-ph and h-ph matrix elements from both experimental and theoretical points of view. We have performed a piezospectroscopic investigation of the WMA spectra of GaP. From an analysis similar to the ones carried out in Si and Ge, we have obtained experimental values for the  $S_{e-ph}/S_{h-ph}$  ratio for the  $\Gamma$ -X LA and TA phonon-assisted transitions in GaP. By comparing the values of  $S_{e-ph}/S_{h-ph}$  in Si (TO) and GaP (LA,TA), together with experimental numbers for the absorption coefficient to the theoretical expressions for the absorption coefficient, the e-ph and h-ph matrix elements are evaluated individually. Ge was left out of this analysis for the reasons mentioned above.

Theoretical calculations of  $S_{e-ph}$  and  $S_{h-ph}$  are carried out for the  $\Gamma$ -L and  $\Gamma$ - $\Delta$  scattering in both Ge and Si, using the "rigid-pseudion" model, which was

first proposed by M. L. Cohen twelve years ago.<sup>30</sup> In this calculation, the e-ph (h-ph) interaction is represented by a "rigid-ion" model, the scattering states by pseudopotential wave functions and local form factors ( $V_q$ ) for the potential. The previously mentioned theoretical work on intervalley scattering was performed in this fashion, but it could not test the "rigid-pseudoion" model. On the other hand, indirect transitions are sensitive to the magnitudes and relative phases of the e-ph and h-ph matrix elements. In order for the calculation to be successful, these details must be correct not only for one of the observed indirect transitions, but for all of them. Consequently, phonon-assisted transitions provide a rigorous test of the "rigid-pseudoion" model, as well as any other technique which may be used in calculating the e-ph and h-ph matrix elements.

Finally, we will calculate  $S_{e-ph}$  and  $S_{h-ph}$  for points midway into the Brillouin zone along the symmetry lines  $\Delta$  for Si and Ge and along  $\Lambda$  in Ge. From this information and the calculations for the fundamental indirect transitions, we hope to explore the  $\vec{k}$  and materials dependence of the matrix elements and find any trends which may exist.

This thesis is divided into 6 chapters and 4

appendices. In the body of the text, we try to present only the information which is needed to understand the problem and its solution. Additional details are placed in the appendices, which contain the selection rules for optical transitions and the phonon scattering processes, data fitting programs, pseudopotential band structure calculations, the rigid-ion model and their associated computer programs.

In chapter II, the results of the theory of indirect absorption are presented. Both exciton and free electron-hole pair formation are considered. The absorption coefficient is written as a product of three terms, a line shape factor, a density of states constant and an oscillator strength. The last term is considered in detail for  $\Gamma-\Delta(X)$  and  $\Gamma-L$  transitions.

Chapter III sets up the theoretical background of the experimental procedure. In this section, we consider the effects of uniaxial stress along the  $[001]$  and  $[111]$  crystallographic directions on the indirect absorption edges in diamond and zincblende (DZB) materials. Stress dependent expressions for the oscillator strength are presented.

In Chapter IV, we describe a piezospectroscopic experiment, in which we take advantage of the stress

effects described in Chapter III. From the experimental data, we determine the ratio of the e-ph and h-ph matrix elements for the LA and TA phonon assisted transitions ( $\Gamma$ -X) in GaP. These results along with those of the study of Pollak et al. in Si are then combined with the theory of Chapter II in determining  $S_{e-ph}$  and  $S_{h-ph}$  individually in Si (TO) and GaP (LA,TA).

In Chapter V, we perform a theoretical calculation of the values of the e-ph and h-ph matrix elements. This is accomplished through the use of the "rigid-pseudoion" model of Cohen.<sup>30</sup> The calculation is performed for the  $\Gamma$ - $\Delta$  and  $\Gamma$ -L scattering in both Si and Ge. We also consider the scattering to points midway along  $\Delta$  (both materials) and  $\Lambda$  (Ge).

All of the experimental and theoretical results are analyzed in Chapter VI. The mechanisms responsible for the relative as well as absolute intensities of indirect transitions in a given material are discussed in general and then applied to GaP, Si and Ge. In this section, we also make a comparison of all of the experimental and calculated matrix elements and search for any trends which may exist. Future experimental and theoretical work is discussed.

At this point, we would like to discuss the system

of units which are used in this work. We will present many of our results in atomic units in which the unit of energy is a Rydberg,  $1\text{Ry} = 13.6 \text{ eV}$ , the mass of a free electron is  $1/2$  ( $m_0=1/2$ ) and its charge,  $e$ , is  $2$ . The unit of length in this system is the Bohr radius,  $a_0$ , and  $\hbar = 1$ . In addition to this we will at times use a commonly used mixed system of units in which the unit of length is a cm and the unit of energy is an eV.

## CHAPTER II. THEORETICAL BACKGROUND

During the past twenty five years, indirect-gap semiconductors have been the subject of extensive theoretical and experimental research. It has been shown that the absorption coefficient can be expressed as the product of a density of states constant, an oscillator strength and a line shape factor. A variety of experiments such as absorption,<sup>1-5</sup> wavelength-modulated absorption,<sup>6-13</sup> electroabsorption,<sup>14</sup> luminescence,<sup>15,16</sup> resonant Raman scattering,<sup>17</sup> etc. have provided considerable information about the nature of the phonon-assisted absorption process. These studies have indentified the various phonons which participate in the absorption process. In addition, they have yielded detailed line-shape information, i.e., fine structure related to the "camel's back" effect in zincblende type materials,<sup>11</sup> etc.. However, in spite of this large body of knowledge, the underlying reasons for the observed relative intensities of the various phonon-assisted transitions have not been ellucidated. As mentioned in the first chapter, this lack in our understanding is related to the fact that phonon-assisted absorption proceeds in general via two scattering mechanisms involving both e-ph and h-ph interactions. The "oscillator strength" of these transitions contains contributions from both effects and in

such a way that they can interfere either constructively or destructively.

In this chapter, we will present the theory of the absorption coefficient. By making certain assumptions regarding the nature of the conduction and valence bands, we will be able to obtain simple expressions for the absorption coefficient. Of central interest to us is the oscillator strength, which contains the e-ph and h-ph matrix elements and hence some very important physics of indirect transitions. Expressions for this crucial quantity will be derived for both  $\Gamma$ -L and  $\Gamma$ - $\Delta$ (X) scattering of diamond and zincblende (DZB) materials.

## 2.1 The Absorption Coefficient

The absorption coefficient,  $\alpha$ , of an indirect-gap semiconductor, resulting from an electronic transition between states differing in energy by  $E_g$  and accompanied by the creation or annihilation of a phonon of the 1 th branch is given by<sup>22,24,26</sup>

$$\alpha_1 = Af_1 \{ L[\hbar\omega - E_g \mp \hbar\omega_1(\vec{Q})] / \hbar\omega \} (n_Q + 1/2 \pm 1/2) \quad (2.1)$$

where,  $\hbar\omega$  is the photon energy,  $\vec{Q}$  the wave vector of a phonon of frequency  $\omega_1(\vec{Q})$ , where the upper and lower signs of  $\mp$  and  $\pm$  refer to phonon emission and absorption respectively and  $n_Q$  is the phonon occupation

number. The frequency independent (only over small energy ranges) term,  $Af_1$ , of Eq. (2.1) is related to the "strength" of the transition.  $A$  is a density-of-states constant involving certain materials parameters such as the index of refraction, electron and hole effective masses, etc. In Equation (2.1)  $f_1$  is the "oscillator strength" of the indirect transition between the valence state  $\psi_{v,\vec{k}}$  and a conduction state  $\psi_{c,\vec{k}'}$ , and proceeding via an intermediate state  $\psi_{i,\vec{k}}$  (or  $j,\vec{k}'$ ) and is given by<sup>22</sup>

$$f_1 = \sum_{c,v} \sum_t \left| \sum_i \frac{\langle \psi_{v,\vec{k}} | \hat{e} \cdot \vec{p} | \psi_{i,\vec{k}} \rangle \langle \psi_{i,\vec{k}} | H_1^t(\vec{Q}) | \psi_{c,\vec{k}'} \rangle}{E_c(k') - E_i(k) - \hbar\omega_1(Q)} + \sum_j \frac{\langle \psi_{v,\vec{k}} | H_1^t(\vec{Q}) | \psi_{j,\vec{k}'} \rangle \langle \psi_{j,\vec{k}'} | \hat{e} \cdot \vec{p} | \psi_{c,\vec{k}'} \rangle}{E_v(k) - E_j(k') - \hbar\omega_1(Q)} \right|^2 \quad (2.2)$$

where  $H_1^t(\vec{Q})$  is the effective electronic perturbation due to the creation or annihilation of a phonon of polarization  $t$  and wave vector  $\vec{Q}$ ,  $\hat{e}$  is the unit polarization vector of the incident electric field and  $\vec{p}$  is the linear momentum of the electron.

Equation (2.2) contains the matrix elements of the e-ph and h-ph interactions. These are given by<sup>7,10</sup>

$$S_{e-ph_1} = \langle \psi_{i,\vec{k}} | H_1^t(\vec{Q}) | \psi_{c,\vec{k}'} \rangle \quad (2.3a)$$

$$S_{h-ph_1} = \langle \psi_{j,\vec{k}'} | H_1^t(\vec{Q}) | \psi_{v,\vec{k}} \rangle \quad (2.3b)$$

where for  $S_{e-ph_1}$  of DZB materials  $\gamma_{i,\vec{k}}$  is  $\Gamma_{1,c}$  ( $\Gamma_{2',c}$ ) or  $\Gamma_{15,c}$ , depending on which phonon is involved. Excluding Ge, the valence-band intermediate state  $\gamma_{j,\vec{k}}$  is  $X_{5,v}$  ( $\Delta_{5,v}$ ) for all phonon modes of these semiconductors. For Ge, the LA phonon-assisted transition proceeds via both  $\Gamma_{2',c}$  and  $\Gamma_{15,c}$ , while for the other allowed phonon (TO) scattering to  $L_1, \Gamma_{15,c}$  is the conduction band intermediate state.  $L_{3',v}$  is the valence band intermediate state for both phonons.<sup>33</sup> Figures 1-3 depict the band structures of Si, GaP and Ge and schematically represent the various scattering processes which occur in these materials. Also shown in these figures are the relevant optical transitions, which can be used to evaluate the energy denominators in Eq. (2.2). It can readily be seen that the important energy differences are given by

$$E(X_{1,c}) - E(\Gamma_{1,c}) = E_{ind} - E_0$$

$$E(X_{1,c}) - E(\Gamma_{15,c}) = E_{ind} - E'_0$$

$$E(L_{1,c}) - E(\Gamma_{2',c}) = E_{ind} - E_0$$

$$E(L_{1,c}) - E(\Gamma_{15,c}) = E_{ind} - E'_0$$

$$E(X_{5,v}) - E(\Gamma_{25',v}) = E_2 - E_{\text{ind}}$$

$$E(L_{3',v}) - E(\Gamma_{25',v}) = E_1 - E_{\text{ind}}$$

Theoretical expressions for  $f_1$  have been derived for the  $\Gamma$ -L (Ge)<sup>8,34</sup> and  $\Gamma$ -X( $\Delta$ )<sup>7,10,11,16,24</sup> phonon assisted transitions in DZB indirect-gap semiconductors. Equation (2.2) is evaluated by using the symmetry of the phonon and the various states which are involved in the process. The selection rules for the optical transitions and intervalley phonon scattering along with the details of the calculation are presented in Appendix A. In Tables I. and II. we display the equations for the  $\Gamma$ -X( $\Delta$ ) and  $\Gamma$ -L processes. Also listed in these tables are the expressions for  $f_1$  for transitions from the spin-orbit split bands. In Table II and throughout the thesis, we will take  $\bar{X}$ ,  $\bar{Y}$ , and  $\bar{Z}$  to be  $\bar{X} = (1/\sqrt{2})(X-Y)$ ,  $\bar{Y} = (1/\sqrt{6})(X+Y-2Z)$  and  $\bar{Z} = (1/\sqrt{3})(X+Y+Z)$ , where  $X=yz$ ,  $Y=xz$  and  $Z=xy$ .

The form of the line-shape factor in Eq. (2.1) depends upon whether excitons or free electron-hole pairs are formed. In the excitonic region, it is given by<sup>26,35,36</sup>

$$L_{\text{ex}}[\hbar\omega - E_g \mp \hbar\omega_1(\vec{Q})] = \left[ \hbar\omega - E_g \mp \hbar\omega_1(\vec{Q}) + \frac{R}{n^2} \right]^{1/2} \quad (2.4)$$

where  $R$  is the exciton Rydberg and  $n$  is the principal quantum number. The coefficient  $A$  is<sup>22</sup>

$$A_{\text{ex}} = \frac{2e^2 \hbar V_p}{\eta m_0^2 c} \left[ \frac{2(m_0^* + m_v^*)}{\hbar^2} \right]^{3/2} |F(0)|^2 \quad (2.5)$$

where  $c$  is the speed of light,  $e$  is the electronic charge,  $\eta$  is the index of refraction,  $m_0$  is the free electron mass,  $m_c^*$  and  $m_v^*$  are the mean conduction- and valence-band effective masses respectively and  $|F(0)|^2$  is the probability that the electron and hole occupy the same site.<sup>26</sup> In Eq. (2.5),  $V_p$  is the volume of a primitive cell, which for DZB materials is given by<sup>37</sup>

$$V_p = \frac{1}{4} a^3 \quad (2.6)$$

where  $a$  is the lattice constant.

For our work, we will assume parabolic bands and the Bohr model for the exciton. Corrections to this model (degenerate valence-bands) are made by using experimentally determined exciton rydbergs to evaluate the Bohr radius and the reduced mass of the exciton. Within the framework of this model, the exciton reduced mass is given by<sup>26</sup>

$$\frac{1}{\mu_{\text{ex}}} = \frac{1}{m_c^*} + \frac{1}{m_v^*} = \frac{e^4}{2\hbar^2 \eta^4 R} \quad (2.7)$$

and the quantity  $|F(0)|^2$  is<sup>26</sup>

$$|F(0)|^2 = \frac{1}{\pi n^3 a_{ex}^3}, \quad (2.8)$$

where  $a_{ex}$  is the Bohr radius of the exciton and is expressed as<sup>26</sup>

$$a_{ex} = \frac{e^2}{2 n^2 R}. \quad (2.9)$$

Furthermore, the anisotropic conduction band is replaced by a spherical band of mean effective mass given by

$$\frac{1}{m_c^*} = (1/3) \left[ \frac{2}{m_c^\perp} + \frac{1}{m_c^\parallel} \right], \quad (2.10)$$

where  $m_c^\perp$  and  $m_c^\parallel$  are the perpendicular and parallel conduction-band effective masses. This expression allows us to evaluate  $m_v^*$  by using Eq. (2.7)

When the photon energy is such that  $[\hbar\omega - E_g \mp \hbar\omega_1(\vec{Q})] \gg R$ , the absorption is due to the creation of free electron-hole pairs.<sup>26</sup> In this case the line shape factor is given by<sup>22,26,35</sup>

$$L[\hbar\omega - E_g \mp \hbar\omega_1(\vec{Q})] = [\hbar\omega - E_g \mp \hbar\omega_1(\vec{Q})]^2 \quad (2.11)$$

and the coefficient A becomes<sup>35,36</sup>

$$A_{e-h} = \frac{e^2 h V_p}{\pi \eta c m_0^2} \frac{[M_c^* M_v^*]^{3/2}}{\hbar^4} \quad (2.12)$$

where  $M_v^*$  is the appropriately averaged density-of-states effective mass for the valence band, while  $M_c^*$  is the conduction-band density of states effective mass and is given by<sup>26</sup>

$$M_c^* = [m_c^{\parallel} (m_c^{\perp})^2]^{1/3}, \quad (2.13)$$

where  $m_c^{\parallel}$  and  $m_c^{\perp}$  have been defined above.

This concludes the theoretical framework for indirect absorption. The relative intensities of the phonon assisted transitions in a given material are determined by the product  $f_1(n_q + 1/2 \pm 1/2)$ . The effects of the oscillator strength are clearly manifested in phonon emission processes, for which  $n_q < 1$ . For temperatures up to room temperature this condition is satisfied and  $f_1$  becomes the principal factor governing the relative strengths. For phonon absorption processes, the phonon occupation number has a large effect on the relative intensities. In this case the role of the oscillator strength is not apparent. In all of our work with relative intensities, we will include the phonon occupation number. However, only phonon creation processes will be considered when we study the role of  $f_1$  in indirect absorption.

CHAPTER III. UNIAxIAL STRESS

In the previous chapter, we presented expressions for the oscillator strengths of the various phonon-assisted indirect transitions. From these equations (see Tables I-II) it is evident that a measurement of only the absorption coefficient is inadequate for obtaining values of the e-ph and h-ph matrix elements. However, it is well known that uniaxial stress, applied along appropriate axes can be used to reduce the symmetry of the crystal and in such a way as to provide us with enough additional information so that an evaluation of the ratio  $S_{e-ph}/S_{h-ph}$  can be performed.

In this chapter, we will consider the effect of stress along (001) and (111) on the indirect absorption edge of DZB type materials. From the theory, we will be able to obtain expressions for the "oscillator strength",  $f_1$  of the strained crystal for the  $\Gamma-L$  transitions in Ge and the  $\Gamma-\Delta(X)$  processes in the other DZB indirect gap materials. For the  $\Gamma-\Delta(X)$  transitions we will also include the stress-induced coupling between the top of the valence-band and its spin-orbit split component. In Ge, the spin-orbit splitting is large (300 meV) in comparison to the stress induced splittings attainable in our work. Therefore, in Ge the stress induced effect will be neglected. The

expressions for the oscillator strength of the indirect transitions in the strained crystal will allow us to obtain the ratio of the e-ph and h-ph matrix elements from the experiment which will be described in Chapter IV.

### 3.1 General Theory

The total Hamiltonian, H for the  $|_{25}, (|_{15})$  valence band can be written as<sup>9,27,39</sup>

$$H = H_{so} + H_1 + H_2 \quad (3.1)$$

where  $H_{so}$  is the spin-orbit Hamiltonian without stress,  $H_1$  and  $H_2$  are the orbital-strain and stress-dependent spin-orbit components of the Hamiltonian respectively.

It has been shown that  $H_1$  can be written as<sup>27,39</sup>

$$H_1 = -a_1 (\epsilon_{xx} + \epsilon_{yy} + \epsilon_{zz}) - 3b_1 \left[ (L_x^2 - \frac{1}{3}L^2) \epsilon_{xx} + c\rho \right] - \sqrt{3} d_1 \left[ (L_x L_y + L_y L_x) \epsilon_{xy} + c\rho \right] \quad (3.2)$$

where,  $\epsilon_{ij}$  is the  $ij$ th component of the strain tensor,  $\vec{L}$  is the angular momentum operator,  $a_1$  is the deformation potential for the hydrostatic pressure shift, while  $b_1$  and  $d_1$  are the uniaxial stress deformation potentials. In Eq. (3.2)  $c\rho$  denotes cyclic permuta-

tions with respect to the indices x,y,z.

The stress-dependent spin-orbit Hamiltonian,  $H_2$  is given by<sup>27,39</sup>

$$\begin{aligned}
 H_2 = & - a_2 (\epsilon_{xx} + \epsilon_{yy} + \epsilon_{zz}) (\vec{L} \cdot \vec{\sigma}) \\
 & - 3 b_2 \left[ (L_x \sigma_x - \frac{1}{3} \vec{L} \cdot \vec{\sigma}) \epsilon_{xx} + c p \right] \\
 & - \sqrt{3} d_2 \left[ (L_x \sigma_y + L_y \sigma_x) \epsilon_{xy} + c p \right]
 \end{aligned} \quad (3.3)$$

where  $a_2, b_2$  and  $d_2$  are deformation potentials describing the effects of a strain on the spin-orbit interaction and  $\vec{\sigma}$  is the Pauli spin matrix.

Furthermore, uniaxial stress may also cause a shift and splitting of any equivalent conduction band minima. In the notation of Brooks, this effect can be expressed as<sup>40,41</sup>

$$\begin{aligned}
 \delta E^c = & \hat{n} \cdot \left\{ \mathcal{E}_1 (\epsilon_{xx} + \epsilon_{yy} + \epsilon_{zz}) \hat{1} \right. \\
 & \left. + \mathcal{E}_2 \left[ \vec{\epsilon} - \frac{1}{3} (\epsilon_{xx} + \epsilon_{yy} + \epsilon_{zz}) \hat{1} \right] \right\} \cdot \hat{n}
 \end{aligned} \quad (3.4)$$

where  $\hat{n}$  is a unit vector in the direction of the critical point in  $\vec{k}$  space,  $\hat{1}$  is the unit dyadic and  $\mathcal{E}_1$  and  $\mathcal{E}_2$  are the hydrostatic and shear deformation potentials.

A uniaxial stress may also result in a coupling between the conduction band minima and the next highest

(in energy) state at (or near) the zone edge, i.e.,  $\Delta_{1,c} - \Delta_{2',c}$  in Si and  $X_{1,c} - X_{3,c}$  in GaP. However, this effect is expected to be small at the stresses used in our work, about 2 meV at the higher stresses in GaP<sup>9,42</sup> and less in Si.<sup>27</sup> The magnitude of this shift is approximately equal to the energy resolution of our experiments and thus will be neglected in our analysis.

### 3.2 Stress Along [111]

#### 3.2.1 <001> Conduction Bands

For stress along (111), no intervalley splitting of the <001> conduction bands takes place. However, they experience a hydrostatic pressure shift which can be obtained from Eq. (3.4) and is given by

$$\delta E_H^c = \mathcal{E}_1 (S_{11} + 2S_{12}) X \quad (3.5)$$

where  $S_{11}$  and  $S_{12}$  are elastic compliance constants and  $X$  is the applied stress.

#### 3.2.2 <111> Conduction Bands

For the case of the <111> conduction bands, there is both a hydrostatic and shear effect. The (111) valley splits away from the  $(\bar{1}\bar{1}1)$ ,  $(1\bar{1}\bar{1})$  and  $(\bar{1}\bar{1}\bar{1})$  equivalent valleys. The energy shift of the (111)

valley is given by<sup>28</sup>

$$\delta E_{5c}^{(iii)} = \frac{1}{3} S_{44} \mathcal{E}_2 X + \delta E_H^c \quad (3.6)$$

and for the  $(\bar{1}, \bar{1}, 1)$ ,  $(1, \bar{1}, \bar{1})$ ,  $(\bar{1}, 1, \bar{1})$  valleys

$$\delta E_{2,c}^{(i\bar{i})} = -\frac{1}{9} S_{44} \mathcal{E}_2 X + \delta E_H^c \quad (3.7)$$

where,  $X$  is the applied stress,  $S_{44}$  is an elastic compliance constant and  $\mathcal{E}_2$  has been previously defined. Fig. 4 illustrates this splitting schematically.

### 3.2.3 The Valence Band

The valence band,  $\Gamma_{25',v}$  ( $\Gamma_{15,v}$ ) is p like ( $J=3/2$ ) and sixfold degenerate. The spin-orbit interaction splits the  $|1/2, 1/2\rangle_{111}$  state ( $v_3$ ) from the  $|3/2, 3/2\rangle_{111}$  and  $|3/2, 1/2\rangle_{111}$  states. A uniaxial stress along (111) removes the degeneracy of these two states and produces  $v_2$  which is purely  $|3/2, 3/2\rangle_{111}$  and  $v_1$  which is mainly  $|3/2, 1/2\rangle_{111}$ , with a stress-induced admixture of  $|1/2, 1/2\rangle_{111}$ . However, the Kramer's degeneracy still remains. Fig. 4 depicts this splitting for GaP ( $\Gamma-X$ ).

With the valence band wave functions in the  $(J, M_J)$

representation

(see Appendix A ), the Hamiltonian matrix of Eqs. (3.1)-(3.3) becomes

$$\begin{array}{ccc} |3/2, 3/2\rangle_{\alpha} & |3/2, 1/2\rangle_{\alpha} & |1/2, 1/2\rangle_{\alpha} \\ \left[ \begin{array}{ccc} -\delta E_H - \delta E_{\alpha}/2 & 0 & 0 \\ 0 & -\delta E_H - \delta E_{\alpha}/2 & \delta E'_{\alpha}/\sqrt{2} \\ 0 & \delta E'_{\alpha}/\sqrt{2} & -\Delta_0 - \delta E_H' \end{array} \right] & & (3.8) \end{array}$$

where  $\alpha=[111]$ , refers to the stress direction and

$$\delta E_H = (\alpha_1 + \alpha_2)(S_{11} + S_{12})X = \alpha(S_{11} + 2S_{12})$$

$$\delta E_H' = (\alpha_1 - 2\alpha_2)(S_{11} + 2S_{12})X = \alpha'(S_{11} + 2S_{12})$$

$$\delta E_{II} = \frac{1}{\sqrt{3}}(d_1 + 2d_2)S_{44}X = \frac{d}{\sqrt{3}}S_{44}X$$

$$\delta E_{III} = \frac{1}{\sqrt{3}}(d_1 - d_2)S_{44}X = \frac{d'}{\sqrt{3}}S_{44}X$$

where  $S_{11}, S_{12}$  and  $S_{44}$  are elastic compliance constants,  $X$  is the applied stress and  $\Delta_0$  is the spin-orbit splitting in the absence of stress. Table III lists the values of  $S_{ij}$  and  $\Delta_0$  for the various DZB materials are considered in this work.

Diagonalizing the matrix of Eq. (3.8) yields the following eigenvalues for the  $v_1$  band

$$\begin{aligned} \delta E_1 = & -\frac{1}{2} (\bar{\Delta}_0 - \frac{1}{2} \delta E_\alpha) - \delta E_H \\ & + \frac{1}{2} \left[ (\bar{\Delta}_0 + \frac{1}{2} \delta E_\alpha)^2 + 2(\delta E_\alpha')^2 \right]^{1/2} \end{aligned} \quad (3.9)$$

while, the  $v_2$  band energy eigenvalue is

$$\delta E_2 = \frac{1}{2} \delta E_\alpha - \delta E_H \quad (3.10)$$

and for the spin-orbit split band,  $v_3$  we find

$$\begin{aligned} \delta E_3 = & -\frac{1}{2} (\bar{\Delta}_0 - \frac{1}{2} \delta E_\alpha) - \delta E_H \\ & - \frac{1}{2} \left[ (\bar{\Delta}_0 + \frac{1}{2} \delta E_\alpha)^2 + 2(\delta E_\alpha')^2 \right]^{1/2} \end{aligned} \quad (3.11)$$

where,  $\bar{\Delta}_0 = \Delta_0 - \beta a_2 (S_{11} + 2S_{12})X$ .

It has previously been demonstrated that the stress dependence of  $\bar{\Delta}_0$  is very small and thus we can take  $\bar{\Delta}_0 = \Delta_0$  in our calculations.<sup>27,42</sup>

The stress dependent eigenfunctions are given by<sup>27,39,42</sup>

$$|V_\alpha\rangle_\alpha = |3/2, 3/2\rangle_\alpha \quad (3.12a)$$

$$|v_1\rangle = \left(\frac{1}{q_i}\right) \left[ (\sqrt{2} \delta E'_\alpha) |3/2, 1/2\rangle_\alpha + (n_i - m_i) |1/2, 1/2\rangle_\alpha \right] \quad (3.12b)$$

$$|v_2\rangle = \left(\frac{1}{q_i}\right) \left[ (\sqrt{2} \delta E'_\alpha) |1/2, 1/2\rangle_\alpha + (m_i - n_i) |3/2, 1/2\rangle_\alpha \right] \quad (3.12c)$$

where  $i=1$  and  $\alpha=111$  for stress along  $[111]$ . These equations have been given in general because, for stress along  $[001]$ , they will have a similar form. In Eqs (3.11)  $m_i, n_i$  and  $q_i$  are given by

$$m_i = \Delta_0 + \frac{1}{2} \delta E_\alpha \quad (3.13a)$$

$$n_i = \left[ m_i^2 + 2 (\delta E'_\alpha)^2 \right]^{1/2} \quad (3.13b)$$

$$q_i = \left[ 2n_i (n_i - m_i) \right]^{1/2} \quad (3.13c)$$

where we have used the approximation  $\bar{\Delta}_0 = \Delta_0$ .

### 3.3 Stress Along [001]

#### 3.3.1 <001> Conduction Bands

For this stress direction, the  $\langle 001 \rangle$  valleys experience a splitting, i.e., the (001) valley splits away from the (100) and (010) valleys. From Eq. (3.4), the energy shift of the singlet, (001) valley is given

by 9,12,27,40

$$\delta E_{1,c}^{(001)} = -\frac{2}{3} \epsilon_2 (S_{11} - S_{12}) X + \delta E_H^c \quad (3.14)$$

and for the (010) and (100) valleys (doublet)

$$\delta E_{2,c}^{(010)} = \frac{1}{3} \epsilon_2 (S_{11} - S_{12}) X + \delta E_H^c \quad (3.15)$$

This splitting is shown schematically in Fig. 5 .

### 3.3.2 <111> Conduction Bands

For this case, there is no splitting and only a hydrostatic pressure shift occurs. The shift is obtained from Eq. (3.4) and is the same as that given by Eq. (3.5) . Figure 4 illustrates this effect.

### 3.3.3 The Valence Band

The degeneracy of the valence band,  $\Gamma_{25'}^v$  is also lifted producing two states  $v_1$  and  $v_2$  . The Hamiltonian matrix is just Eq. (3.8) with  $\alpha = [001]$  and 9,27,39,41

$$\delta E_{001} = 2(b_1 + 2b_2)(S_{11} - S_{12})X \quad (3.16a)$$

$$\delta E'_{001} = 2(b_1 - b_2)(S_{11} - S_{12})X \quad (3.16b)$$

Equation (3.8) [ with  $\alpha=001$  ] and Eqs. (3.16) ] can be diagonalized to obtain the eigenvalues and eigenvectors of the Hamiltonian. These turn out to be just Eqs. (3.10)-(3.13) with  $\alpha=001$  and  $i=0$ .

### 3.4 The Stress-Dependent "Oscillator Strength"

In the previous section, we saw that the application of a uniaxial stress along [001] and [111] reduced the degeneracy of the valence and (or) conduction bands. Table IV summarizes the splittings which are found for both stresses.

The polarization dependent ( $\vec{E} \parallel \vec{X}$  and  $\vec{E} \perp \vec{X}$ ) relative as well as absolute intensities of the above transitions have been calculated by using Eq. (1.2) for the oscillator strength, Eqs. (3.12) for the stress dependent valence band wave functions and the optical and phonon scattering selection rules from Appendix A. The results of this calculation are presented in Tables V-VII. The terms  $\eta_1^j$  and  $\gamma$  represent the contribution of the stress-induced mixing of the  $|3/2, 1/2\rangle_c$  and  $|1/2, 1/2\rangle_c$  states.<sup>42</sup> If this effect is neglected,  $\eta_1^j=1$  and  $\gamma=0$ , our results are identical to those of Ref. 11 for GaP and Refs. 15 and 25 for Si. The fact

that the ratios  $W_1/V_1$  and  $U_1/V_1$  are real allows us to write these expressions in the simplified form presented in Tables V-VII.

In Table VII are displayed the polarization dependent oscillator strengths for the LA phonon assisted  $\Gamma$ -L transitions. In these expressions, the stress-induced coupling of the top of the valence band and its split off component have been neglected. The reason for this is the fact that Ge is the only DZB indirect gap material in which the fundamental absorption proceeds via  $\Gamma$ -L transitions and in this material, the spin-orbit splitting is large enough so that in our experiment  $\Delta_0 \gg \delta E_\alpha$ . Therefore, the stress-induced mixing of the  $|3/2, 1/2\rangle_\alpha$  and  $|1/2, 1/2\rangle_\alpha$  states can be neglected (see Eqs. 3.12 and 3.13). This concludes the discussion of the effects of uniaxial stress on the indirect absorption edge of DZB type materials.

#### CHAPTER IV. THE EXPERIMENT

Having established the theoretical framework of the effects of uniaxial stress on the indirect transitions in DZB materials, we can now apply these results to the experimental evaluation of the e-ph and h-ph matrix elements. The experiment was performed in GaP using a technique which had previously been utilized for this purpose in Si<sup>7</sup> and to study the effects of stress on the indirect gap of Ge.<sup>8</sup> From this work we obtained the ratio  $K = S_{e-ph}/S_{h-ph}$  for the LA and TA phonons of GaP.

The experimental procedure involves measuring the wavelength modulated absorption (WMA) spectrum of the strained crystal for stresses along [001] and [111] with the electric field vector of the incident light polarized parallel and perpendicular to the stress axis. For a given phonon, ratios of the relative intensities of the extra transitions resulting from the stress will be compared to the corresponding theoretical expressions derived in the previous Chapter. By performing this analysis for both stress directions and light polarizations, we can obtain the ratio  $K = S_{e-ph}/S_{h-ph}$  for the phonon assisted transition under consideration.

By comparing the ratios found in Si by Pollak et. al and our results in GaP, along with experimental values of the absorption coefficient to the theoretical expressions for  $f_1$  from Chapter II., we can evaluate individually the e-ph and h-ph matrix elements in these materials. Ge will be left out of this analysis because the LA transition proceeds via two intermediate conduction band states and therefore, the ratio,  $K_{LA}$  cannot be determined uniquely. In this Chapter, we present the details of the experiment, its results and the evaluation of the e-ph and h-ph matrix elements.

#### 4.1 Experimental Details

##### 4.1.1 The Optics and Electronics

The transmission measurements were made using a Jarrel-Ash 1/4 meter Ebert design grating monochromator, with a 5000Å blaze grating. The wavelength modulation was produced by vibrating the 45° mirror (located behind the entrance slit) about its axis at 450 Hz by means of a General Scanning AX200 oscillator. The slit width resolution was approximately 5Å.

The modulation was measured by attaching a small mirror ( 1 cm<sup>2</sup> in area ) to the rotating shaft of the monochromator mirror. A laser beam was then reflected

from the mirror onto a distant wall approximately 20 feet away. The rotation of the shaft produced a rectangular image, whose length was measured. The vibration was then turned off and the monochromator mirror was rotated in such a way that the image of the laser spot was displaced by one half of the length of the rectangle. This resulted in a shift of the zero of the grating equal to the modulation amplitude and thus a comparison of the "zero-grating" spectrum prior to and after the shift provided this value.

The light source used in the experiment was a quartz halogen lamp. The transmitted light was detected with a Hamamatsu R375, S-20 photomultiplier. The a.c. signal was extracted by an Ithaco Dynatrac 391A lockin amplifier. The d.c. level was held constant by a servomechanism applied to the photomultiplier power supply, similar to that which has extensively been used for electroreflectance measurements.<sup>41,42</sup> This procedure, i.e., normalized WMA gives a line shape which is proportional to the derivative of the absorption coefficient.

In the region of the indirect exciton, the transmitted intensity,  $I_T$  can be written as<sup>7,42</sup>

$$I_T = I_0(1 - R)^2 e^{-\alpha t} \quad (4.1)$$

where  $I_0$  is the incident intensity,  $R$ , is the reflection coefficient,  $\alpha$ , is the absorption coefficient and  $t$  is the thickness of the sample. The effects of multiple reflection can be shown to be negligible. The wavelength derivative of  $I_0$  is given by

$$\frac{dI_T}{d\lambda} = I_0(1 - R)^2 e^{-\alpha t} (-t) \frac{d\alpha}{d\lambda} \quad (4.2)$$

where we have neglected the wavelength dependence of  $R$ . The spectrum of the grating was taken in the region of the exciton and it exhibited no structure from  $I_0$ . Thus the wavelength dependence of  $I_0$  can be neglected.

A normalized WMA spectrum is one in which  $dI_T/d\lambda$  is divided by  $I_T$  resulting in

$$(dI_T/d\lambda) / I_T = -t \frac{d\alpha}{d\lambda} \quad (4.3)$$

Therefore, from a knowledge of the sample thickness,  $t$ , and the amplitude of the modulation,  $d\lambda$ , one can obtain  $d\alpha/dE$  where  $E$  is the photon energy.

The samples used in the experiment were obtained from Metal Specialties and were silicon doped to a

carrier concentration of  $n = 3 \times 10^{17} \text{ cm}^{-3}$ . The bulk pieces were x-ray oriented to  $\pm 1^\circ$  and cut along the stress direction ( $[111]$  or  $[001]$ ) into parallelepipeds of dimensions  $1.3 \times 1.3 \times 13 \text{ mm}^3$ . Two opposite faces of the long edge were mechanically polished with various abrasives down to  $0.05 \mu\text{m}$  alumina powder and then etched in a 1:10 solution of bromine and methanol for about one minute. This procedure allowed us to obtain spectra with a large signal to noise ratio.

The measurements were performed at 77 K using a glass dewar, capable of holding approximately one liter of liquid nitrogen. The dewar was shaped to have a 4" diameter cylindrical bulb, connected to a 1" diameter long neck. The dewar was covered with tape, except for approximately 2" near the bottom of the neck, which served as an optical window.

The temperature was kept constant by a temperature controller, which utilized a Si diode as a temperature sensor. A nicrome wire through which a current was passed served as a heating element. The sample temperature was kept several degrees above 77 K so that a small current was constantly being passed through the wire. In this fashion, minor changes in temperature could be compensated for by appropriately adjusting the current through the nicrome wire.

Figure 6 shows a schematic diagram of the optics used in the experiment. Figure 7 shows the stress apparatus and the location of the heating element.

#### 4.1.2 The Stress Apparatus

The stress rig used was of the type extensively described in the literature and shown in Fig. 7 (Refs. 39,42). The sample was mounted by epoxying approximately 1/4 of its length (at the ends) into tightly fitting flat-bottom holes in brass plugs, which were inserted into copper pistons. Before the epoxy set, the pistons were rotated to insure that the sample was vertical. If this procedure was not carried out, the sample would readily crack at low stresses.

The force on the sample was applied in the following manner. By turning the knob ( see Fig. 7 ), the spring which is connected to a lever arm of ratio 10:1, was elongated. This caused the pull rod to move the pull frame upward. A pin connected to the pull frame forced the pistons and the sample up against the stress frame, thereby producing a compressive stress.

The extension of the spring was measured by a linear differential transducer (LVDT) mounted inside the spring.<sup>44</sup> The change in inductance of the transformer caused by the moveable core attached to the

spring was balanced by another matched LVDT, whose core was mounted in a micrometer. These LVDT's formed two arms of an a.c. bridge and were accurately balanced with a voltmeter. Thus the extension of the spring was measured by the micrometer and the stress could be computed to  $\pm 1\%$ .

#### 4.2 Experimental Results

Shown in Fig. 8 is the normalized WMA spectrum  $d\alpha/dE$  at  $X = 0$  which displays three well resolved phonon-assisted transitions, involving the emission of LA, TA and TO phonons. This spectrum is quite similar to the zero stress results of Mathieu et al..<sup>9</sup> In the remaining portion of the figure, we show spectra for  $\vec{E} \parallel \vec{X}$  and  $\vec{E} \perp \vec{X}$  at  $X = 2.63 \times 10^9 \text{ dyn-cm}^{-2}$  and  $X = 7.35 \times 10^9 \text{ dyn-cm}^{-2}$  applied along [111]. For this stress direction, the  $\Gamma_{8,v}$  valence band is split, but the  $X_{1,c}$  conduction band minima remain equivalent and hence two transitions ( $A_1$  and  $A_2$ ) are observed for each phonon mode. We have labelled the various observed structures  $A_1^{\parallel}(\text{LA})$ ,  $A_1^{\perp}(\text{LA})$ , etc., where the superscript refers to the polarization direction and the quantity in parenthesis is the phonon mode.

The complexity of the stressed spectra (two lines per phonon mode for  $\vec{X} \parallel [111]$ ) did not allow us to

observe well resolved lines for both the LA and TA phonons at a given stress. An examination of the spectrum for  $X = 2.63 \times 10^9 \text{ dyn-cm}^{-2}$  (see Fig. 8) reveals that the  $A_1^\perp(\text{LA})$  line shows up as a low energy shoulder of the more intense  $A_2^\perp(\text{LA})$  peak and therefore cannot be separated from it. However, at this stress both TA phonon lines  $A_1(\text{TA})$  and  $A_2(\text{TA})$  are well resolved for both polarizations. On the other hand, at  $X = 7.35 \times 10^9 \text{ dyn-cm}^{-2}$  the LA peaks are separated, while the weaker TA lines are seen only in the perpendicular polarization mode. For stresses between  $3 \times 10^9 \text{ dyn-cm}^{-2}$  and  $7 \times 10^9 \text{ dyn-cm}^{-2}$  we observed interference between the  $A_2(\text{TA})$  and  $A_1(\text{LA})$  lines for both polarizations. For all of the stresses used in this experiment, the  $A_2^{\parallel}(\text{TA})$  structure was too weak to be seen (i.e., see Fig. 8). In order to obtain complete sets of data for  $\vec{X} \parallel [111]$ , it was necessary to use  $X = 7.35 \times 10^9 \text{ dyn-cm}^{-2}$  for the LA peaks and  $X = 2.63 \times 10^9 \text{ dyn-cm}^{-2}$  for the TA phonon lines.

In GaP, the WMA spectrum of the indirect transition is more complex in relation to Si and Ge. The lack of inversion symmetry opens up a gap in the lowest conduction band at the X point, i.e.,  $X_{1,c}$  and  $X_{3,c}$  are no longer degenerate. The  $\vec{k} \cdot \vec{p}$  interaction between the two bands introduces a "camel's back" in the dispersion

relations for  $X_{1,c}$  in the vicinity of the X point, i.e., an  $M_0$  minimum occurs at  $\vec{k} = (0.015)(2\pi/a)$  away from the zone edge and an  $M_1$  saddle point is found at the X point.<sup>11,45,46,47</sup> Consequently, the dispersion relations are no longer parabolic. The WMA line shape exhibits fine structure and cannot be represented by the function  $F(W')$  which was successfully used in Si<sup>7,43,48-49</sup> and Ge<sup>8,43,49</sup>. The function  $F(W')$  is given by

$$F(W') = \frac{[(W'^2 + 1)^{1/2} + W']^{1/2}}{(W'^2 + 1)^{1/2}} \quad (4.4)$$

where  $W' = [(E - E_{ex})/\Gamma']$  and  $\Gamma'$  is the broadening parameter and ex denotes exciton.

A linear combination of  $F(W'_1)$  and  $F(-W'_2)$  (where the subscripts 1,2 refer to the two minima) can be tried as an approximation to the actual line shape. The high resolution work of Humphreys et al.<sup>11</sup> which was performed at 4.2 K resolved the fine structure and showed that the spectra indeed resemble  $F(W'_1)$  at the minimum and  $F(-W'_2)$  at the saddle point, commonly referred to as the hump of the "camel's back". When these lines broaden, due to an increase of temperature or an application of stress, the doublet becomes a sin-

gle structure which can be fit by a Gaussian. This effect is illustrated in Ref. 11 where stress-induced broadening is considered.

In our experiment, which was performed at 77 K, temperature broadening of the lines and lack of high resolution did not allow us to resolve the fine structure. We were not successful in fitting the spectra to  $F(W')$ , linear combinations of  $F(W'_1)$  and  $F(-W'_2)$  or a Lorentzian line shape. However, we did find that the best fit to the data was accomplished through the use of a Gaussian given by

$$D(W) = D_0 e^{-W^2} \quad (4.5)$$

where  $D_0$  is the height of the line and  $W = (E - E_{ex})/\sqrt{2}\Gamma$  and  $\Gamma$  is the Gaussian broadening parameter. In addition, the background was not logarithmic as in Si and Ge. However, we successfully fit it to a quadratic equation given by

$$G(E) = A \epsilon^2 + B \epsilon + C \quad (4.6)$$

where  $A, B$  and  $C$  were adjustable parameters and  $\epsilon = E - E_{ex}$ .

The fit was performed on a Tektronix 4051 graphics computer. The fitting program which is listed in Appendix B allowed for both automatic and visual adjustments of the parameters. At the beginning of the procedure, an approximate background was subtracted from the experimental data. The new points were then used to compute  $D_0$ ,  $E_{ex}$  and  $\Gamma$  and the resulting  $D(W)$ , along with the adjusted data were displayed. The iteration process which followed consisted of subtracting the experimental points from  $D(W)$  and using the difference in a least squares adjustment of the parameters  $A, B$  and  $C$ . The new background would then be subtracted from the original experimental points and  $D_0$ ,  $E_{ex}$  and  $\Gamma$  would be recomputed. This procedure along with visual adjustment of all of the parameters was repeated until the differences in  $D_0$ ,  $E_{ex}$  and  $\Gamma$  between successive iterations were less than 1%.

#### 4.2.1 LA Phonon

In Fig. 9 we have plotted the experimental values (solid line) of  $d\alpha/dE$  for the  $A_2(LA)$  peak of Fig. 8 for  $X=7.53 \times 10^9 \text{ dyn-cm}^{-2}$  after an appropriate subtraction of the background given by Eq. (4.6). Also shown in Fig. 9 is the theoretical fit (dashed line) from Eq. (4.5). The agreement between the line shapes is very good. Similar results have been obtained for the other

LA peaks for both [111] and [001] uniaxial stress. The fit for the  $A_1''(\text{LA})$  peak is shown in Fig. 10. In order to obtain a measure of the integrated intensity  $dd$ , we have multiplied the value  $dd/dE$  by the broadening parameter  $\Gamma$ .

Listed in Table IX are the experimentally determined relative and actual (in parenthesis) values of  $[dd/dE \times \Gamma]$  for the various A and B peaks of the LA-phonon assisted transitions at the indicated stresses for  $\vec{E} \parallel \vec{X}$  and  $\vec{E} \perp \vec{X}$ . Although  $A_2''(\text{LA})$  is allowed (see Table V) we find experimentally that it is so weak that its intensity is taken to be zero in Table IX. Similar results have been obtained at several other applied stresses for both stress directions for the various LA-phonon assisted peaks.

Comparison of the theoretical expressions of Table V and the experimental results listed in Table IX enable the ratio  $K_{\text{LA}} = W_{\text{LA}}/V_{\text{LA}}$  to be determined. Values of  $\eta_j^i$  and  $\gamma$  were calculated from the equations in Table V and the known spin-orbit splitting (0.090 eV), the deformation potentials and elastic constants of GaP listed in Table III. We find that the best overall agreement with the experimental numbers in Table IX is achieved for a value of  $K_{\text{LA}} = -4.5$ . Using this number for the ratio we have calculated the

relative theoretical values listed in Table IX. There is good agreement between experiment and theory.

From the ratio  $K_{LA} = -4.5$  we can obtain a value for  $S_{e-ph_{LA}}/S_{h-ph_{LA}}$ . This quantity can be evaluated from a knowledge of the ratio of the matrix elements of  $\vec{p}$  and the appropriate phonon energy  $\hbar\omega_{LA}$ . The energy differences in the denominators of  $W_{LA}$  and  $V_{LA}$  can be obtained from various experimentally determined quantities. From Fig. 2 it can be seen that these energy denominators are related to known optical transitions in the following manner

$$E(X_{1,c}) - E(\Gamma_{1,c}) = E_{ind} - E_0 \quad (4.7a)$$

$$E(\Gamma_{8,v}) - E(X_{5,v}) = E_2 - E_{ind} \quad (4.7b)$$

The various values of the optical transitions used in Eqs. (4.7) are listed in Table X. The  $E_0$  and  $E_{ind}$  numbers are 77 K values, while  $E_2$  is obtained from 2 K reflectivity measurements. Since  $E_2$  is large in comparison to any difference which may arise between the 77 K and 2 K values, we have taken it to be the same at both temperatures. From the values of the phonon energy listed in Table XI and the above considerations

we find that

$$E(X_{1,c}) - E(\Gamma_{1,c}) - (\hbar\omega)_{LA} = -0.58 \quad (4.8a)$$

$$E(\Gamma_{8,v}) - E(X_{5,v}) + (\hbar\omega)_{LA} = +2.92 \quad (4.8b)$$

The ratio of the optical matrix elements cannot be obtained from experiment, but can be deduced from a  $\vec{k} \cdot \vec{p}$  band structure calculation.<sup>45</sup> The values of these matrix elements are listed in Table XII. From the above considerations and the number for  $K_{LA} = -4.5$  we obtain

$$S_{e-ph_{LA}} / S_{h-ph_{LA}} = 0.6$$

#### 4.2.2 TA Phonon

The situation for the TA phonon is somewhat more difficult in relation to the LA phonon case. The former transitions are weaker than the latter, as shown in Fig. 8 for  $X = 0$ . Therefore, for  $\vec{X} || [001]$  not all of the four TA-phonon lines can be resolved because of the destructive interference between some of the weak TA-phonon lines and the stronger LA ones. Similar problems were encountered in Ref. 9.

We have, however, been able to clearly observe the  $B_1''(\text{TA})$  and  $B_4''(\text{TA})$  peaks for  $\vec{X} \parallel [001]$  at several stresses. For  $\vec{X} \parallel [111]$  all of the lines  $A_1(\text{TA})$ ,  $A_2''(\text{TA})$ ,  $A_1^\perp(\text{TA})$  and  $A_2^\perp(\text{TA})$  are clearly seen for  $X = 2.63 \times 10^9 \text{ dyn-cm}^{-2}$  ( see Fig. 8). Displayed in Figs. 11 and 12 are the fits to the  $A_1''(\text{TA})$  and  $A_2^\perp(\text{TA})$  peaks. The agreement between experiment and theory is quite good. The experimental value of  $B_4''/B_1'' = 0.6$  and the theoretical expressions of Table VI yield that  $K_{\text{TA}} (= U_{\text{TA}}/V_{\text{TA}})$  can be either -1.6 or -0.7. This ambiguity is resolved by an examination of the results for  $\vec{X} \parallel [111]$ , where agreement between experiment and theory is good only for  $K_{\text{TA}} = -1.6$ . Using this result for the ratio we have calculated the relative theoretical values listed in Table XIII.

As in the case of the LA phonon a value for the ratio,  $S_{\text{e-ph}_{\text{TA}}}/S_{\text{h-ph}_{\text{TA}}}$  can be found. Figure 2 shows that

$$E(X_{1,c}) - E(\Gamma_{15,c}) - (\hbar\omega)_{\text{TA}} = E_{\text{ind}} - E_0' - (\hbar\omega)_{\text{TA}}$$

and

$$E(\Gamma_{8,v}) - E(X_{5,v}) + (\hbar\omega)_{TA} = E_2 - E_{ind} + (\hbar\omega)_{TA}$$

number for  $K_{TA}$  we find that

$$S_{e-ph_{TA}}/S_{h-ph_{TA}} = 1.1$$

#### 4.2.3 TO Phonon

The TO phonon transition is approximately equal in magnitude to the TA peak. However, its stress induced components are very weak and can not be readily extracted from the background. The recent study of Mathieu et al.<sup>9</sup>, which was carried out at 4 K has shown that for  $\vec{X} \parallel [111]$ ,  $A_1(TO)$  and  $A_2(TO)$  are observed simultaneously only for stresses above  $12 \times 10^9 \text{ dyn-cm}^{-2}$  [for  $X < 12 \times 10^9 \text{ dyn-cm}^{-2}$  they observed only  $A_2(TO)$ ]. For  $\vec{X} \parallel [001]$ , their study yielded only  $B_4(TO)$ .

From our work which was carried out at 77 K, we obtained similar results. For  $\vec{X} \parallel [111]$  we clearly observed  $A_2(TO)$  for stresses below  $X = 5 \times 10^9 \text{ dyn-cm}^{-2}$ . At higher stresses this line became broadened and obscured by the background. For  $\vec{X} \parallel \vec{E}$  and low stress ( $X < 5 \times 10^9 \text{ dyn-cm}^{-2}$ ), we found two unresolved peaks, which are labelled with some uncertainty as  $A_1(TO)$  and  $A_2(TO)$ . At higher stresses, these two lines rapidly broadened and became indistinguishable from the

background. The  $X = 2.63 \times 10^9 \text{ dyn-cm}^{-2}$  spectrum of Fig. 8 illustrates these results. For  $X \parallel [001]$  we observed only  $B_4(TO)$ . Since we could see just  $A_2(TO)$  and  $B_4(TO)$  clearly, it was not possible to determine the ratio of the e-ph and h-ph matrix elements for the TO phonon.

### 4.3 Evaluation of the Electron-Phonon and Hole-Phonon Scattering Matrix Elements

Having obtained values for the ratio of the e-ph and h-ph scattering matrix elements for the LA and TA phonons of GaP and having this ratio for the TO phonon of Si, we now turn our attention to evaluating the matrix elements individually. This can be accomplished by comparing the ratio  $K_1$  along with experimental values of the absorption coefficient to the theoretical expressions for the absorption coefficient.

#### 4.3.1 Silicon

The case of Si will be considered first. The piezospectroscopic investigation of Pollak et al.,<sup>7</sup> found that for  $\langle 001 \rangle$  scattering,  $K_{TO} = U_{TO}/V_{TO} = 1.0$ , where

$$u_{T0} = \frac{\langle \Gamma_{2s',\nu}^z | p_x | \Gamma_{1s,c}^y \rangle \langle \Gamma_{1s,c}^y | \mathcal{R}_{T0}^x | \Delta_{1,c} \rangle}{E(\Delta_{1,c}) - E(\Gamma_{1s,c}) - (\hbar\omega)_{T0}} \quad (4.9a)$$

and

$$v_{T0} = \frac{\langle \Gamma_{2s',\nu}^z | H_{T0}^x | \Delta_{5,\nu}^x \rangle \langle \Delta_{5,\nu}^x | p_x | \Delta_{1,c} \rangle}{E(\Gamma_{2s',\nu}) - E(\Delta_{5,\nu}) + (\hbar\omega)_{T0}} \quad (4.9b)$$

The study of Macfarlane, McLean, Quarrington and Roberts (MMQR) provides us with absorption data in both the excitonic and free-pair energy regions.<sup>2</sup> MMQR were able to decompose the absorption coefficient into a sum of components, each having the same line shape and corresponding to the creation or annihilation of TA and T0 phonons. In Fig. 13, where  $(\alpha \hbar\omega)^{1/2}$  (this function is convenient for the analysis of the Si data) is plotted against  $\hbar\omega$ , we exhibit the decomposition which MMQR obtained for the absorption coefficient at 4.2 K. Since at this temperature  $n_Q \approx 0$ , we do not observe the phonon annihilation processes and thus the data of Fig. 13 correspond to transitions accompanied by phonon creation. The low energy component is a result of the emission of TA phonons, while the higher energy one is a consequence of T0 phonon creation. A further examination of the figure reveals that each component begins with a well defined knee and ultimately rises linearly with energy. In the "knee" region excitons are

created, while in the linear regime free electron-hole pairs are formed.

More accurate studies of the indirect absorption in Si have revealed LO-phonon assisted transitions.<sup>3,13,48</sup> This process is found just below the TO line and is approximately a factor of 7 weaker than the TO absorption. Since MMQR did not resolve this transition, we can assume that it is part of their TO phonon data. The error introduced by not accounting for this is on the order of 15%, which is approximately equal to the accuracy of the experimental values of the  $K_1$  ratio. Because the more accurate data is available only at 1.6 K, while the study of MMQR produced numbers at various temperatures for both phonon emission and absorption, we will use MMQR's results. From this, we should be able to establish the consistency of our procedure enroute to obtaining the e-ph and h-ph matrix elements. The results of the evaluation using the more accurate numbers will also be given.<sup>3,48</sup>

In the knee (or excitonic ) region of Fig. 13, MMQR were able to obtain empirical expressions for the components of the absorption coefficient. For the TO phonon, they found the following relationship

$$\alpha_{T_0} = \frac{B_{T_0}}{\hbar\omega} \left[ \hbar\omega - E_g - (\hbar\omega)_{T_0} + R \right]^{1/2} \quad (4.10)$$

where  $B_{T_0} = 26.9 \times 10^{-9} \text{ Ry}^{1/2}/a_0$  and  $a_0$  is the Bohr radius ( $=5.29 \times 10^{-9} \text{ cm}$ ).

The value of  $B_{T_0}$  enables us to evaluate  $S_{e-ph_{T_0}}$  and  $S_{h-ph_{T_0}}$ . The theoretical expression for the absorption coefficient in this energy region is given by Eqs. (2.1), (2.2), (2.4), (2.5) and hence  $B_{T_0} = A_{ex} f_{T_0}$ . The constant  $A_{ex}$  can be evaluated by using the expressions for  $V_p$ ,  $m_c^*$ ,  $m_v^*$  and  $|F(0)|^2$  from Eqs. (2.6)-(2.10) and the values for  $a$ ,  $m_c''$ ,  $m_c^\perp$ ,  $R$  and  $\mathcal{N}$  from Table XII. Thus we can obtain a value for  $f_{T_0} (=B_{T_0}/A_{ex})$ . Using this value, the expression for the oscillator strength listed in Table I and the experimentally determined ratio  $K_{T_0} = 1.0$  we compute  $U_{T_0}$  and  $V_{T_0}$  individually. From these values, the expressions for  $U_{T_0}$  and  $V_{T_0}$  from Eqs. (4.9), the optical matrix elements (obtained from  $\vec{k}p$  calculations) listed in Table XII and the energy denominators obtained from the optical transitions and phonon frequencies listed in Tables X-XI, we find

$$S_{e-ph_{T_0}} = 17.4 \pm 2.6 \times 10^{-3} \text{ Ry}$$

$$S_{h-ph_{T_0}} = -22.9 \pm 3.4 \times 10^{-3} \text{ Ry}$$

Since the quantity  $Af_1$  is an absolute magnitude of the sum electron and hole scattering terms, it is sensitive only to the phase of the ratio  $S_{e-ph}/S_{h-ph}$ . Therefore, the phases of the individual matrix elements are arbitrary to within a common factor. We have chosen this phase factor such that  $S_{e-ph_{T0}}$  is real and positive, making  $S_{h-ph_{T0}}$  real and negative. This sign convention will be followed throughout the thesis.

In the linear region of Fig. 13 the theoretical expression for the absorption coefficient is given by Eqs. (2.1), (2.2), (2.11) and (2.12). Multiplying this equation for  $\alpha_{T0}$  by  $\hbar\omega$  and taking the square root produces a function linear in energy. Equating the slope of this function with the experimentally determined slope of  $(\alpha_{T0}\hbar\omega)^{1/2}$  ( in the linear region of Fig. 13 ) allows us to obtain a value for  $f_{T0}$ . The constant  $A_{e-h}$  (Eq. 2.12) is computed by using  $M_v^*$  from Table XII and Eq. (2.13) for  $M_c^*$ . From here, proceeding as we did in the excitonic case we find

$$S_{e-ph_{T0}} = 17.9 \pm 2.7 \times 10^{-3} \text{ Ry}$$

$$S_{h-ph_{T0}} = -23.6 \pm 3.5 \times 10^{-3} \text{ Ry}$$

We have also performed this evaluation in the linear region for the phonon creation and annihilation at 170 K and phonon absorption at 363 K. Table XIV lists the values of the slopes used in this work. In addition to this, we have used more accurate data for the quantity  $B_{T0}$ . The absorption study of Dean et al. found this number to be  $B_{T0} = 21.0 \times 10^{-9} \text{ Ry}^{1/2}/a_0$ , while the WMA work of Nishino et al. found that  $B_{T0} = 30.0 \times 10^{-9} \text{ Ry}^{1/2}/a_0$ . We have evaluated the e-ph and h-ph matrix elements using these values. Our results from all of the computations are listed in Table XV. Averaging over all of these numbers and estimating the error at 15% we obtain

$$S_{e-ph_{T0}} = 17.3 \pm 2.6 \times 10^{-3} \text{ Ry}$$

$$S_{h-ph_{T0}} = -22.9 \pm 3.4 \times 10^{-3} \text{ Ry}$$

#### 4.3.2 Gallium Phosphide

Now we turn our attention to GaP. As previously stated, the "camel's back" effect plays a significant role in the WMA spectrum of this material. The dispersion relations for the conduction band are no longer

parabolic and the analysis of the previous section is not exact in this case. However, the study of Dean et al. showed that the excitonic absorption coefficient can be fitted to an equation which is proportional to the square root of the energy and thus has the form of Eq.(2.1) with a line shape factor given by Eq. (2.4).<sup>5</sup> This indicates that as a first order approximation, we can neglect the "camel' back" effect and treat GaP as we did Si. We will use this approximation in our analysis.

From transmission studies, Dean et al.<sup>5</sup>, were able to perform a decomposition of the absorption coefficient into components resulting from the creation and annihilation of LA, TA and TO phonons. Their analysis was performed only in the excitonic region. Consequently, we will restrict our evaluation to this energy regime.

#### TA Phonon

First we consider the TA phonon, whose symmetry and intermediate states are similar to those of the TO phonon of Si. Consequently, the expression for the "oscillator strength" of the TA phonon is identical in form to  $f_{TO}$  (see Table I). Dean et al. found that at 1.6 K the TA component of the absorption coefficient

can be written as<sup>5</sup>

$$\alpha_{TA} = D_{TA} \left[ \hbar\omega - E_g - (\hbar\omega)_{TA} + R \right] \quad (4.11)$$

where  $D_{TA} = 3.32 \times 10^{-7} a_0^{-1} (\text{Ry})^{-1/2}$ .

This expression differs in form from Eq. (4.10) for the TO phonon. In Eq. (4.11),  $\hbar\omega$  is included in  $D_{TA}$  while in Eq. (4.10) it was not contained in  $B_{TO}$ . This approximation can be used, since the energy range of the exciton is much smaller than the photon energy and thus  $h$  does not change very much in this energy regime. For our evaluations we will let  $\hbar\omega = E_g - \hbar\omega_{TA} = 172. \times 10^{-3} \text{ Ry}$ . Once again, the absorption coefficient is given by Eqs. (2.1), (2.2), (2.4) and (2.5). The quantity  $A_{ex}$  can be computed from the values of the parameters comprising it listed in Table XII. Thus from Eq. (4.12) we obtain the oscillator strength  $f_{TA} (= \hbar\omega D_{TA} / A_{ex})$ . Utilizing  $K_{TA} = -1.6$  and the procedure used for Si, we find

$$S_{e-ph_{TA}} = 19.8 \pm 2.9 \times 10^{-3} \text{ Ry}$$

$$S_{h-ph_{TA}} = 17.7 \pm 2.6 \times 10^{-3} \text{ Ry}$$

We have performed this evaluation for the data of Dean et al. for both absorption and phonon emission processes at 77 K, 120 K and 218 K. Table XVI lists the values of  $D_{TA}$  which were used in our computation. In all of this work, the phonon occupation number was included. The results of these evaluations are presented in Table XVII. By averaging these values and estimating the error at 15% we obtain

$$S_{e-ph_{TA}} = 19.2 \pm 2.8 \times 10^{-3} \text{ Ry}$$

$$S_{h-ph_{TA}} = 17.4 \pm 2.5 \times 10^{-3} \text{ Ry}$$

#### LA Phonon

For the LA phonon, the conduction band intermediate state is different from that of the TA phonon i.e.,  $\Gamma_{1,c}$  instead of  $\Gamma_{15,c}$ . As a consequence of this and the different phonon symmetry involved, the expression for the oscillator strength is not the same as that of the transverse phonons (see Table I).

For the LA phonon at 1.6 K, Dean lists the absorption coefficient as

$$d_{LA} = D_{LA} [\hbar\omega - E_g - (\hbar\omega)_{LA} + R]^{1/2}$$

where  $D_{LA} = 1.25 \times 10^{-6} a_0^{-1} (\text{Ry})^{-1/2}$ . Using  $\hbar\omega = 173. \times 10^{-3} \text{ Ry}$ ,  $K_{LA} = -4.5$  and the procedure employed for the TA phonon, we find

$$S_{e-ph_{LA}} = -8.3 \pm 1.2 \times 10^{-3} \text{ Ry}$$

$$S_{h-ph_{LA}} = -13.6 \pm 2.1 \times 10^{-3} \text{ Ry}$$

where the phase factor was chosen to facilitate comparison to the theoretical values of Si and Ge, which will be calculated in the next chapter.

Table XVII contains the results of our evaluations for the various values of  $D_{LA}$  listed in Table XVI. From these numbers we obtain the following averages

$$S_{e-ph_{LA}} = -7.6 \pm 1.1 \times 10^{-3} \text{ Ry}$$

$$S_{h-ph_{LA}} = -13.0 \pm 2.0 \times 10^{-3} \text{ Ry}$$

An examination of Table XV reveals that the

results for Si from the excitonic region are very close to those of the free-pair range. This indicates that the simplifying assumptions made in performing the evaluations in the excitonic regime are valid. The validity of the assumptions is important in the case of GaP, for which we have no data from the free-pair region. Furthermore, we notice from Tables XV and XVII that for both Si and GaP the values of the matrix elements are consistent over all of the temperatures considered and are independent of the phonon process (absorption or emission) involved. The 218 K values fall somewhat out of the range of the others because Dean et al. experienced some experimental difficulties at this temperature. A detailed analysis of our results will be presented in Chapter VI.

CHAPTER V. CALCULATION OF THE ELECTRON-PHONON AND HOLE-PHONON SCATTERING MATRIX ELEMENTS

The calculation of the e-ph and h-ph scattering matrix elements is a difficult problem. Its complexities are summarized by Ziman and Sham in an excellent review article in "Solid State Physics" (vol. 15, 1963).<sup>61</sup> They point out the fact that many degrees of freedom are involved, i.e., a quasi-infinite lattice of ions is imbedded in a sea of electrons. The ions and electrons interact with each other through Coulomb forces. This is a many body problem, in which the actions of a given electron or ion will effect the whole ensemble, thereby introducing a complicated screening of the bare particle potential. For example, the displacement of an ion in such a system is expected to cause not only a shift of the core potential, but also a redistribution of the outer-electrons which are not tightly bound to the ion.<sup>31,61,62</sup> Thus, the calculation of the e-ph and h-ph matrix elements should be done self consistently.

Ziman's book, "Electrons and Phonons" and the review article of Ziman and Sham consider this problem in detail.<sup>62</sup> Various approximations, such as the "rigid-ion" and "deformable-ion" models and long wavelength approaches are developed. Of particular

interest to us is an application of the "rigid-ion" model, the "rigid-pseudoion" model first proposed by M.L. Cohen in 1970 (Ref. 50). This approach combines the rigid-ion description of the lattice displacements and local pseudopotential theory to provide the first step in calculating e-ph and h-ph interactions. In short, it neglects such effects as charge redistribution and the nonlocal nature of the pseudopotential. These effects should ultimately be included, however, their neglect seems to provide a reasonable starting point for calculating e-ph and h-ph interactions.

### 5.1 The Rigid-Pseudoion Model

The foundation of the "rigid-pseudoion" model is the "rigid-ion" description of the lattice dynamics, which was introduced by Nordheim in 1931 (Ref. 63). In this approximation, the ion-core potential of an atom moves rigidly with it, when the atom is displaced from equilibrium. Thus, the potential seen by an electron due to a lattice of such atoms is just<sup>61,64</sup>

$$V(\vec{r}) = \sum_{j,\beta} V_{j,\beta}(\vec{r} - \vec{R}_{j,\beta}^0) \quad (5.1)$$

where  $V_{j,\beta}(\vec{r} - \vec{R}_{j,\beta}^0)$  is the atomic potential of an atom in its equilibrium position,  $\vec{R}_{j,\beta}^0$ , having a lat-

tice index,  $j$ , and basis index  $\beta$ . Within this approximation, the e-ph (h-ph) interaction Hamiltonian due to small displacements from equilibrium resulting from a phonon of mode  $l$  and polarization,  $t$ , is given by<sup>30,32,35</sup>

$$H_l^t = \sum_{j,\beta} \delta \vec{R}_{j,\beta}^{l,t} \cdot \vec{\nabla} V_{j,\beta}(\vec{r} - \vec{R}_{j,\beta}) \quad (5.2)$$

where  $\delta \vec{R}_{j,\beta}^{l,t}$  is the displacement of the atom from equilibrium and can be written in terms of phonon coordinates as<sup>31,30,35</sup>

$$\delta \vec{R}_{j,\beta}^{l,t} = \left[ \frac{\hbar}{2M_\beta \omega_l(\vec{Q})} \right]^{1/2} \hat{e}_{l,\beta}^t e^{i\vec{Q} \cdot \vec{R}_{j,\beta}^0} \quad (5.3)$$

where the phonon creation and annihilation operators are implied. In Eq (5.3),  $\vec{Q}$  is the phonon wave vector,  $\hat{e}_{l,\beta}^t$  is the polarization vector of the  $\beta$  th atom of mass  $M_\beta$  and  $\omega_l(\vec{Q})$  is the phonon frequency. The index  $t$  is used to distinguish between any degenerate phonons of a given mode,  $l$ . In the above equation,  $N$  is the number of primitive cells in the crystal. Since  $N$  is ultimately cancelled out in calculating measureable quantities such as absorption coefficients, it will be left out of the square root in any subsequent discussions. We can Fourier analyze the potential to obtain

$$V_{j,\beta}(\vec{r}-\vec{R}_{j,\beta}^0) = \frac{\Omega}{(2\pi)^3} \int d\vec{q} V_{\vec{q},\beta} e^{i\vec{q}\cdot(\vec{r}-\vec{R}_{j,\beta}^0)} \quad (5.4)$$

where  $\Omega$  is the volume of a primitive cell. Writing  $\vec{R}_{j,\beta}^0 = \vec{R}_j^0 + \vec{r}_\beta$  where  $\vec{R}_j^0$  is a lattice vector and  $\vec{r}_\beta$  is a basis vector of the  $\beta$ th atom. By putting Eqs. (5.3) and (5.4) into (5.2) we obtain for the e-ph(h-ph) interaction

$$H_{el}^t = \sum_{\beta \vec{G}} i \left( \frac{\hbar}{2M_\beta \omega_{\vec{q}}(\vec{Q})} \right)^{1/2} \hat{e}_{\vec{q},\beta}^t \cdot (\vec{Q}-\vec{G}) \times \\ V_{\vec{Q}-\vec{G},\beta} e^{i\vec{G}\cdot\vec{r}_\beta} e^{i(\vec{Q}-\vec{G})\cdot\vec{r}} \quad (5.5)$$

where  $\vec{G}$  is a reciprocal lattice vector and where we used Bloch's theorem in the form

$$\sum_j e^{i\vec{R}_j^0 \cdot (\vec{Q}-\vec{G})} = N \delta_{\vec{G}, \vec{Q}-\vec{G}}$$

and changed the integral over  $q$  into a sum by the following relationship

$$\frac{\Omega N}{(2\pi)^3} \int d\vec{q} \rightarrow \sum_{\vec{q}}$$

In order to calculate the matrix elements of Eq.(5.5), which is a general result within the context of the "rigid-ion" model, the atomic potential and

electronic states must be known. In principle, this can become a very difficult program. However, pseudopotential theory provides an elegant method of obtaining the electronic band structure of a solid.<sup>64-69</sup> It takes advantage of the fact that between lattice sites, the potential is weak and thus the electron can be considered as being nearly-free. Under these conditions, the electronic wave functions can be chosen to be plane waves, whose overlap with the core states is removed through the use of an effective potential, the pseudopotential. If we assume that the pseudopotential is just a function of  $|\vec{r} - \vec{R}_j^0|$  then we are within the regime of local pseudopotential theory<sup>64-69</sup> In our work, we will use this approximation. Sham has demonstrated that if the scattering is on the Fermi sphere (i.e., the phonon energy can be neglected), then using pseudopotential wave functions and potential is equivalent to the use of the real wave function and actual potential.<sup>70</sup> With this choice, the wave functions are pseudo-plane-waves (ppw's) and can be written as<sup>30,64-69</sup>

$$\psi_{\vec{k},s}(\vec{r}) = \sum_{\vec{G}} C_{\vec{G}}^{\vec{k},s} e^{i(\vec{k} + \vec{G}) \cdot \vec{r}} \quad (5.7)$$

By using Eq. (5.7) in Eq. (5.6) we find the matrix

element of the electron (hole) - phonon Hamiltonian to be

$$\begin{aligned}
 S_{e-ph} &= \langle \psi_{\vec{k}',s'} | H_{ph}^{\dagger} | \psi_{\vec{k},s} \rangle \\
 &= i \sum_{\beta, \vec{G}} \left( \frac{\hbar}{2M_{\beta} \omega_{\beta}(\vec{Q})} \right)^{1/2} V_{\vec{Q}-\vec{G},\beta} e^{i \vec{G} \cdot \vec{\tau}_{\beta}} \\
 &\quad \hat{e}_{1,\beta}^{\dagger} \cdot (\vec{Q}-\vec{G}) \sum_{\vec{G}'} \left( C_{\vec{G}'+\vec{G}}^{\vec{k}',s'} \right)^* \left( C_{\vec{G}}^{\vec{k},s} \right)
 \end{aligned} \tag{5.8}$$

where  $\vec{k}$  and  $\vec{k}'$  are related through  $\vec{Q} = \vec{k}' - \vec{k}$ . For hole scattering, the subscript h-ph replaces e-ph. Equation (5.8) is the general form of the e-ph (h-ph) matrix elements within the "rigid-pseudoion" model. We will now apply it to the calculation of the e-ph and h-ph matrix elements in Si and Ge, which are diamond type materials.

### 5.2 Application To Diamond Type Materials

In Eq. (5.8), the phonon polarization vectors, are complex numbers. However, in diamond type materials, such as Si and Ge, with two similar atoms within the basis ( $\beta=1,2$ ) a simplification can be made. If we choose the origin for  $\vec{\tau}_{\beta}$  to lie midway between the two atoms, we find that  $\vec{\tau}_2 = -\vec{\tau}_1 = \tau = (a/8)(111)$ . By employing time reversal invariance and inversion symmetry, we find that the polarization vectors  $\hat{e}_{1,1}^{\dagger}$  and

$\hat{e}_{1,1}^t$  are related in the following manner<sup>71</sup>

$$\hat{e}_{l,1}^t = (\hat{e}_{l,2}^t)^* \quad (5.9)$$

This relationship between the polarization vectors allows us to make a transformation to a real set of vectors,  $\hat{e}_{+,1}^t$  and  $\hat{e}_{-,1}^t$ , which are given by<sup>31,71</sup>

$$\hat{e}_{l,-}^t = \frac{1}{\sqrt{2}} (\hat{e}_{l,1}^t + \hat{e}_{l,2}^t) \quad (5.10a)$$

$$\hat{e}_{l,+}^t = \frac{1}{i\sqrt{2}} (\hat{e}_{l,1}^t - \hat{e}_{l,2}^t) \quad (5.10b)$$

where  $(\hat{e}_{+,1}^t)^2$  and  $(\hat{e}_{-,1}^t)^2$  correspond to the fraction of the mode which is "acoustic" and "optic", respectively. Using Eqs. (5.10) in Eq. (5.8) and expanding  $e^{i\vec{G}\cdot\vec{r}_1}$  and  $e^{i\vec{G}\cdot\vec{r}_2}$  we obtain

$$\begin{aligned} S_{e-ph_l} = & i \left( \frac{\hbar}{2m\omega_l(\vec{Q})} \right)^{1/2} \sum_{\vec{G}} V_{\vec{Q}-\vec{G}} (\vec{Q}-\vec{G}) \cdot \\ & (\hat{e}_{l,+}^t \cos \vec{G}\cdot\vec{r} + \hat{e}_{l,-}^t \sin \vec{G}\cdot\vec{r}) \times \\ & \times \sum_{\vec{G}'} \left( C_{\vec{G}'+\vec{G}}^{\vec{k},s'} \right)^* \left( C_{\vec{G}'}^{\vec{k},s} \right) \end{aligned} \quad (5.11)$$

where we used the fact that for a diamond type material  $m_1 = m_2 = m$  and  $V_{\vec{Q}-\vec{G},1} = V_{\vec{Q}-\vec{G},2} = V_{\vec{Q}-\vec{G}}$ . The computa-

tion is further simplified because the plane wave expansion coefficients can be chosen to be real numbers for these types of semiconductors, i.e., the Hamiltonian matrix is real. Thus, Eq. (5.11) is just two sums of real numbers.

In the following section, we will apply Eq. (5.11) to Si and Ge. For both materials, we will consider the fundamental indirect gap, referred to as the "primary" indirect gap and the next highest phonon-assisted transition, which is called the "secondary" indirect gap. In the interest of comparing Si and Ge, and in order to obtain some idea of the  $\vec{k}$  dependence of the matrix elements, we have also evaluated Eq. (5.11) for points midway into the Brillouin zone along  $\Delta$  and  $\Gamma$ .

### 5.2.1 The Fundamental Indirect Gaps

#### Silicon

In Si, the conduction band minimum is at  $\Delta$  ( $\vec{k}=(2\pi/a)(0,0,0.85)$ ) and ( $\Gamma$ - $\Delta$ ) indirect transitions, assisted by TO, LO, TA and LA phonons are allowed. A subsidiary conduction band minimum is found at L and thus at a photon energy of 1.65 eV at 1.6 K, indirect processes ( $\Gamma$ -L) can occur with the aid of LA and TO phonons. In this section, we will concentrate on the e-ph and h-ph interactions for the  $\Gamma$ - $\Delta$  scattering,

which are associated with the primary gap. The secondary gap will be considered in section 5.2.2.

The evaluation of Eq. (5.11) was performed by using a 67 plane wave expansion for the wave functions and a local pseudopotential form factor  $V_q$ , in the range  $V_{0.85} < V_q < V_{\infty}$  (Ref. 72).  $V_q$  was interpolated through the values of Pantelides, which were used to calculate the band structure. The form of Pantelides reproduces the Cohen-Bergstresser form factors  $V_3$ ,  $V_8$  and  $V_{11}$  (Ref. 74). Convergence was checked by comparing the wave functions from 59 and 74 plane wave expansions and by examining the value of a given matrix element as the calculation was performed, i.e., the program would print out the value of the matrix element for each plane wave component which was used. Computational difficulties with the subroutine, which diagonalized the band structure Hamiltonian limited the number of plane waves to 89. The pseudopotential calculation is discussed in Appendix C, where we also describe the computer program used to generate the band structure.

In evaluating Eq. (5.11). we used experimental values of the phonon frequencies, listed in Table XI. The phonon polarization vectors were obtained from a second nearest neighbor "rigid-ion" model calculation,

which utilized experimentally determined phonon frequencies at  $\vec{k}=0$  and at the Brillouin zone edges at X and L.<sup>71</sup> Such an approach to the lattice dynamics is inadequate for calculating dispersion curves and elastic constant  $s$ .<sup>75,76</sup> However, it was found to yield phonon polarization vectors which were within 2% of those derived from the more exact Weber "bond-charge" model.<sup>77</sup> This surprising result was obtained for both Si and Ge and seems to indicate that for diamond type materials, the phonon polarization vectors may be model independent and not a major source of error in our calculation. Thus within the context of the model, the most uncertain quantities are the interpolation of the form factor and the pseudowave-functions. The lattice dynamics of the "rigid-ion" model and the program which was used to diagonalize the dynamical matrix are described in Appendix D.

Now, we will consider the the wave function and form factors. These two parameters are intimately related, since the form factor is the potential in the Fourier transformed Schroedinger equation, whose solution ultimately determines the wave function (see Appendix C). However, because of the structure factor, only a few select values of  $V_q$  are needed to determine the band structure.<sup>68</sup> The values of  $q^2$  which are

important for diamond type materials are 3, 8, and 11 [in units of  $(2\pi/a)^2$ ].<sup>65,68</sup> Larger values of  $q^2$  do not enter, because the form factor approaches zero at large values of the wave vector. It is not uncommon to take  $V_q = 0$  beyond  $q=4$  (Ref. 68). On the other hand as  $q \rightarrow 0$ , the form factor should approach a value of  $(-2/3)E_f$ , where  $E_f$  is the Fermi energy.<sup>66-69</sup> In the calculation of the e-ph and h-ph matrix elements, the relevant values of  $q$  are reciprocal lattice vectors shifted by the wave vector of the phonon. In addition to this, the structure factor is different (see Eq. 5.11). Consequently, the form factors which we use are not those of the band structure work. In particular, the values of  $q^2 < 3$  and  $q^2 > 11$  are important.<sup>77</sup> Since the form factor is not known in these regions, we have a substantial amount of freedom in interpolating  $V_q$ . This  $q=0$  limit is exact in the case of metals, but can be relaxed for semiconductors to some number near  $(-2/3)E_f$  (Refs. 31,57).

From the above discussion, we see that there are many form factors which can be used and that we have no way of telling which one is right for our purposes. However, as stated in Chapter I., the resulting  $S_{e-ph}$  and  $S_{h-ph}$  must be in a delicate balance in order to account for the relative as well as absolute intensi-

ties of the indirect transitions in Si. In addition, the values of the matrix elements for the T0 phonon should be in accord with the experimental ones presented in the previous chapter. The large and small  $q$  limits and the above requirements were used as guidelines in choosing the interpolation of the form factor. In this thesis, we will only present the form factors which gave the best results.

Our first calculations utilized a histogram interpolation of  $V_q$  (Ref. 72). The relevant values of  $q^2$  were chosen to be integers between 1 and 25 [ units of  $(2\pi/a)^2$  ] and for each of these, a value of  $V_q$  was assigned from curve (a) of Fig. 14. Thus each point in this set was used to approximate two neighboring points which entered the calculation, i.e., the point at  $q=1$  represented points at  $q=0.85$  and  $q=1.15$ . The results of this calculation for all four phonons, along with the experimental values for the T0 phonon are listed in Table XVIII. The agreement between theory and experiment is excellent for the T0 phonon. At this point, it must be noted that the phase of the ratio  $S_{e-ph_1}/S_{h-ph_1}$  is fixed. However, the phases of the individual matrix elements are arbitrary to within a common factor. This factor has been chosen so that the  $S_{e-ph_{T0}}$  is real and positive, thereby making  $S_{h-ph_{T0}}$  real and negative.

A further test of the calculation comes from the quantity  $Af_1$ , which apart from the line shape factor, describes the relative as well as absolute intensities of the indirect transition. We have evaluated  $Af_1$  in the excitonic region for each of the  $\Gamma-\Delta$  phonons of Si. For this computation, we used Eqs. (2.5)-(2.10) for  $A_{ex}$ , equations for  $f_1$  from Table I, values of the energy denominators obtained from the numbers in Tables X and XI and the relationships presented in Chapter II, the optical matrix elements and various materials parameters listed in Table XII. The results of these calculations along with experimental values from several sources are listed in Table XIX (Ref. 78). Excellent agreement is found between experiment and theory for the values of the relative as well as absolute intensities of the  $\Gamma-\Delta$  transitions and thus a correct description of the strengths of these processes is obtained.

However, a histogram interpolation of  $V_q$  may not be an accurate representation of the potential. In a more detailed calculation, we fit the form factor of Fig. 14 to a cubic equation of the form

$$V_q = aq^3 + bq^2 + cq + d \quad (5.12)$$

where  $a$ ,  $b$ ,  $c$  and  $d$  were adjustable parameters. The actual form factor was a piecewise smooth curve constructed from Eq. (5.12) in three regions,  $q^2 < 3$ ,  $3 \leq q^2 \leq 11$  and  $q^2 > 11$ . The values of the fitting parameters in the three regimes are given in Table XX. The results of this calculation are presented in Tables XVIII and XIX, just below those of the "histogram" potential. A comparison of the two sets of numbers reveals the sensitivity of the calculation to the form factor. The values of  $S_{e-ph}$  and  $S_{h-ph}$  have changed somewhat, with those of the TA phonon showing the largest variation. The quantity  $Af_1$  is also effected. Once again the the most sensitive phonon is the TA phonon, whose "intensity" has decreased by more than a factor of two. Even though the ordering of the relative intensities is still correct, the quantity  $Af_{TA}$  is in poor agreement with experiment.

Various interpolations of the form factor were tried and similar effects were observed. In particular, the ordering of the relative intensities of the TA and LA phonons was found to be very sensitive to  $V_q$  for all values of  $q$ . For many form factors, the LA transition was stronger than the TA one.

The sensitivity of the relative intensities of the LA and TA phonons can be traced to the destructive

interference between the e-ph and h-ph scattering, which the LA phonon experiences and the small magnitudes of the matrix elements of the TA phonon. Consequently, there exists a very delicate balance between these two phonons, which serves to eliminate many of the possible interpolations of the form factor which may otherwise work well for the less sensitive TO and LO phonons.

The best overall fit to  $Af_1$  was obtained through the use of the above form factor, but having an oscillating tail, which decays to zero for large  $q$ . Curve (b) of Fig. 14 shows this interpolation. For  $q^2 < 11$ ,  $V_q$  coincides with curve (a), while for  $q^2$  it is given by

$$V_q = \frac{V_0}{q^2} \cos(R_c q + \theta) \quad (5.13)$$

where  $V_0 = 0.88$ ,  $R_c = 1.57$  and  $\theta = -5.2$ .

The results using this form factor are presented in Tables XVIII and XIX along with those of the other two interpolations. In this case, the agreement between theory and experiment is much better than for the previous two potentials.

The reason why a form factor with an oscillating tail works better than the usual one, which is cut off

near  $q=4$ , is not known. This may be an indication that nonlocality is important in Si, i.e., the core potential is not properly cancelled out.<sup>66-69</sup> It may also simulate effects due to charge redistribution.<sup>61</sup>

In a similar calculation, Bednarek and Rossler also had to use an unusual potential in order to get good agreement between experiment and theory for the LA and TA phonon assisted absorption.<sup>79</sup> In their case, the form factor was cut off at  $q=4$  and approached zero for small values of  $q$ . They felt that their potential simulated nonlocal and charge redistribution effects.<sup>61</sup>

A more detailed analysis is required to pin point the source of the difficulty in obtaining good agreement between theory and experiment for the LA and TA phonons. In particular, a nonlocal calculation would be a good starting point for such an analysis.

However, the agreement which we have obtained through our potential is good and can be taken as a demonstration of the validity of the "rigid-pseudoion" model for calculating e-ph and h-ph matrix elements. An examination of Table XIX reveals that only small changes in the e-ph and h-ph matrix elements of the LA and TA phonons would be required to produce very good accord between experiment and theory. For example, a

5% change in the ratio  $S_{e-ph}/S_{h-ph}$  for both phonons would be adequate. Thus our calculation provides a reasonable description of the e-ph and h-p interactions in Si.

### Germanium

Ge, just like Si is a diamond type material and thus Eq. (5.11) can be used to calculate its e-ph and h-ph matrix elements. However, in Ge, the fundamental absorption results from  $\Gamma$ -L indirect processes assisted by LA and TO phonons. The LA transition has two intermediate conduction band states,  $\Gamma_2',c$  and  $\Gamma_{15},c$ , while the TO phonon proceeds via  $\Gamma_{15},c$ . Both phonons have  $L_{3',v}$  as their valence band intermediate state.

Experimental data exists only for  $Af_{LA}$  and the polarization dependent relative intensities of the LA phonon in the strained crystal. For the TO phonon transition, which is approximately one tenth as strong as the LA process, there is no accurate experimental data. The 1/10th estimate comes from the WMA work of Pollak et al.. In Fig. 15 we display their zero stress data. A careful examination of the figure reveals that there is a weak structure approximately 9 meV beyond the stronger LA peak. This is exactly the amount by which the LA and TO phonon energies differ at the L

point. Consequently, the weak feature can be attributed to TO phonon assisted transitions. Since, in Ge there are only two phonon-assisted absorption processes, the test of the "rigid-pseudoion" model is not as rigorous as it was in Si.

We have evaluated Eq (5.11) by using a 70 plane wave expansion for the wave function and a form factor given by

$$V_q = \frac{u_0 \cos(r_1 q)}{q^2 + k_0^2} \exp \left[ k_1^2 (3 - q^2) + k_2^2 (q - 3.4)^2 \right] \quad (5.14)$$

where the parameters  $u_0$ ,  $r_1$  and  $k_0^2$  are determined by the known form factors  $V_3$ ,  $V_8$  and  $V_{11}$ . The other quantities are used to control the form factor in the regions  $q^2 > 11.2$  and  $q^2 < 3$ . The values of the potential parameters are listed in Table XXI and the form factor is displayed in Fig. 16. The phonon polarization vectors for Ge were obtained in the same manner as they were for Si.

In Table XXII, we list the calculated values of  $S_{e-ph}$  and  $S_{h-ph}$  for the LA and TO phonons ( $\Gamma-L$ ). For the LA phonon, e-ph matrix elements are presented for the two allowed conduction band intermediate states,  $\Gamma_{15,c}$  and  $\Gamma_{2',c}$ .

The TO phonon hole scattering requires two matrix elements. This is a consequence of the fact that  $\Gamma_{25',v}$  is compatible with  $\Lambda_{3,v} + \Lambda_{1,v}$  and each component couples to  $L_{3,v}$  through the TO phonon.<sup>15</sup>  $\Lambda_1$  transforms as  $\bar{Z} = \frac{1}{\sqrt{3}}(X + Y + Z)$  while  $\Lambda_3$  transforms as  $\bar{X} = \frac{1}{\sqrt{2}}(X - Y)$  and  $\bar{Y} = \frac{1}{\sqrt{6}}(X + Y - 2Z)$ , where  $X = yz$ , etc. Table XXII displays both of the matrix elements for hole scattering. Our results for the two components are consistent with the luminescence study of Smith and McGill who found that  $\left| \frac{S_{\bar{Z}}}{S_{\bar{X}}} \right|_{h-ph_{TO}} < 1.0$  in order to explain their experimental data.<sup>15</sup> From Table XXII we see that this ratio is 1/2.6.

In Ge there are no experimental values for the e-ph and h-ph matrix elements and therefore, the quantity  $Af_1$  becomes crucial in testing the calculation. MMQR provide a value for  $Af_1$  for the LA phonon, but they could not resolve the TO transition and thus there is no known value (to us) for the quantity  $Af_{TO}$ .

The lack of data for the TO phonon can be remedied by making use of the WMA spectra of Pollak et al.,<sup>8</sup> which was used in their piezospectroscopic study of the LA transition. Figure 15 shows their results at 77 K and zero stress. As previously stated, a line is found approximately 9 meV higher in energy than the strong LA

peak and is a result of TO phonon assisted indirect transitions. This conclusion is based on the fact that, at L the LA and TO phonons differ in energy by 9 meV, a result which was obtained from the study of Brockhous and Iyengar.

By using the procedures described in Chapter IV., we were able to fit this peak to the function  $F(W')$ .<sup>4b</sup> The fit is shown in Fig. 17. From this data and Eqs. (2.1) and (2.4) and by accounting for broadening, we obtained a value for the quantity  $Af_{TO}$ . As a check of the procedure, we also evaluated  $Af_{LA}$  (see Fig. 18) and found it to be in good agreement with the value of MMQR.<sup>1</sup> This result gave us confidence in this method, which had previously been successful in Si at 1.6 K (Ref. 48). Consequently, we now have a value of  $Af_{TO}$  with which we can compare the theoretical number. The results of this analysis are presented, along with those of MMQR and the theory in Table XXIII.

We have made a theoretical evaluation of the quantity  $Af_1$  for the LA and TO phonon assisted transitions of Ge. In the case of the LA phonon, the conduction band energy difference,  $E(\Gamma_{2',c}) - E(L_{1,c}) - \hbar\omega_{LA}$ , is on the order of magnitude of  $S_{e-ph_{LA}}$  for the  $\Gamma_{2',c} \rightarrow L_{1,c}$  scattering and thus the usual first-order perturbation term of Eq. (2.2) ( $S_{e-ph}$  divided by an

energy denominator) is not adequate in calculating  $Af_{LA}$ . In our work, we used an exact expression for the  $\Gamma_{2',c} \rightarrow L_{1,c}$  coupling coefficient, which is based on a two band model and is given by<sup>10</sup>

$$d(y_l) = \frac{[1 - (1 + 4y_l^2)^{1/2}]}{\{4y_l^2 + [1 - (1 + 4y_l^2)^{1/2}]^2\}^{1/2}} \quad (5.15)$$

where

$$\begin{aligned} y_l &= \frac{S_{e-ph_l}}{E(L_{1,c}) - E(\Gamma_{2',c}) - \hbar\omega_l} \\ &= S_{e-ph_l} / \Delta E_c \end{aligned} \quad (5.16)$$

with this expression,  $W_1$  is replaced by

$$W_l = d(y_l) \langle \Gamma_{25',\bar{v}} | P_{\bar{z}} | \Gamma_{2',c} \rangle \quad (5.17)$$

It is easy to see that as  $\Delta E_c \rightarrow 0$ ,  $d(\infty) \rightarrow -1/\sqrt{2}$  and that as  $\Delta E_c$  becomes much larger (in magnitude) than  $S_{e-ph_1}$ ,  $d(y_1) \approx y_1$  and the result of Eq. (2.2) is recovered. Thus, the transition intensity increases asymptotically as  $\Delta E_c \rightarrow 0$ , instead of becoming infinitely large. This phenomena is also important in other

materials such as ternary compounds, whose fundamental gap can be changed from direct to indirect by alloying.<sup>81-83</sup>

Listed in Table XXIII are the experimental and theoretical values of  $Af_1$  for the LA and TO phonons of Ge. Included in this Table are the results obtained from our analysis of the piezospectroscopic data of Pollak et al.. The agreement between experiment and theory is good even though the theory overestimates  $Af_{TO}$ .

As a further test of the calculation, we have evaluated the polarization dependent intensities of the LA phonon assisted transitions in the strained crystal for stresses along [001] and [111].<sup>8</sup> This was accomplished through the use of the equations listed in Table VIII along with Eqs. (5.16)-(5.18). The results of this calculation along with the experimental values of Ref. 8 are presented in Table XXIV. The agreement between experiment and theory is quite good for both of the stresses, for the electric field vector, E polarized parallel and perpendicular to the stress axis.

### 5.2.2 The Secondary Indirect Gap

Having established the validity of the model for calculating the e-ph and h-ph matrix elements of the

primary indirect transitions in Si and Ge, we now will turn our attention to the secondary indirect gaps of these materials. The calculation will follow the procedure, which was used in the last section. The zone center wave functions and the form factors are the same as in the previous work. The wave functions at the other points ( $L$  for Si and  $\Delta$  for Ge) are computed from the program described in Appendix C and new phonon eigenvectors are obtained from the calculation of Appendix D.

### Silicon

The secondary indirect gap of Si results from  $\Gamma$ - $L$  transitions, which have been observed to begin at 1.65 eV in the experiments of Forman<sup>54</sup>. Transmission studies show a break in absorption data in this energy range<sup>84</sup> and  $\sqrt{d\hbar\omega}$  which is postulated to be a straight line extrapolates to 1.65 eV. Consequently, a theoretical calculation of the  $\Gamma$ - $L$  e-ph and h-ph matrix elements may have a basis for comparison.

Since we are dealing with  $\Gamma$ - $L$  transitions, the results of this calculation should be similar to those in Ge. We expect the electron scattering by LA phonons to proceed via  $\Gamma_{2,c}$  and  $\Gamma_{15,c}$ , while for the TO phonon hole scattering, two matrix elements will be required.

We have evaluated Eq. (5.11) for the  $\Gamma$ -L scattering of Si. The phonon frequencies were experimental values of Brockhouse et al. and the phonon eigenvectors were obtained using the procedure of Appendix D. In this case, we used only curves (a) and (b) for our extrapolation of the pseudopotential form factor. The "histogram" potential was not used, because the  $\Gamma$ - $\Delta$  work showed that this was not an accurate representation of the form factor. The results of our evaluation of Eq. (5.11) for  $\Gamma$ -L scattering are presented in Table XXV.

We can test our calculation by accounting for the absorption in the vicinity of the secondary indirect gap. Displayed in Fig. 19 are the experimental values for  $\chi$  for photon energies between 1.4 eV and 3.0 eV. The low energy portion (below 1.65 eV) results from  $\Gamma$ - $\Delta$  transitions, while the higher energy portion is a consequence of  $\Gamma$ -L processes.<sup>84</sup> The LA and TO phonon components have not been resolved. However, we can presumably extract from the absorption curve the total  $\Gamma$ -L contribution. This would be accomplished by subtracting from the slope of  $\sqrt{\alpha\hbar\omega}$  beyond 1.65 eV, the slope of the portion of the curve which corresponds to the  $\Gamma$ - $\Delta$  transitions. In this manner, we obtained an experimental value for the quantity  $A_{e-h}(f_{TO}+f_{LA})$ . In

Table XVII we list both  $\Gamma$ -L and  $\Gamma$ - $\Delta$  contributions to the absorption coefficient.

Using the theoretical values from Tables XVIII and XXV [only those of curve (a)], along with the equations for  $f_1$  listed in Tables I and II and Eq. (2.12) for  $A_{e-h}$ , we calculated the theoretical slopes for the  $\Gamma$ -L and the  $\Gamma$ - $\Delta$  contributions to the absorption near 1.65 eV. Figure 20 shows the phonon dispersion curves for Si, which we used in our work.<sup>57</sup> In this evaluation, the spin-orbit split band was included. The results of this computation are also presented in Table XXVI.

The disagreement between experiment and theory is substantial. In addition, the experimental value for the  $\Gamma$ - $\Delta$  transition is about 20% larger than the theoretical one. This is not consistent with the results of the previous section, in which the theory overestimated the "strength" of the absorption. From Table XXVI we see that the experimental value of  $S_{e-ph_{T0}}$  is smaller than the theoretical one and that the h-ph matrix elements agree. This suggests that in the region of the  $\Gamma$ -L transitions the theoretical  $\Gamma$ - $\Delta$  contribution to the absorption coefficient would be larger than the experimental one. Consequently, we conclude that something is wrong.

The fact that there is poor agreement between experiment and theory for the  $\Gamma$ - $\Delta$  transitions gives us a clue to the source of the trouble. A careful examination of Fig. (19) reveals that the experimental points actually lie between 1.5 eV and 3.0 eV. This energy range is quite large and begins approximately 0.3 eV higher than the fundamental gap. The linear extrapolation in the free electron-hole region is based on the assumption that  $A_{e-h}^{f_1}$  is energy independent. However, this assumption is valid only for photon energies near the primary indirect gap. As the photon energy increases, the energy of the final state begins to approach that of the intermediate scattering state. From Eq. (2.2), we see that this will result in an enhancement of the oscillator strength.

Two other effects must be taken into account. First, the density of states constant  $A_{e-h}$  may change when the final state is not near the conduction band minimum. Secondly, the e-ph and h-ph matrix elements can also change with the scattering states.

Based on the above considerations, we conclude that a linear extrapolation of  $\sqrt{\alpha \hbar \omega}$  will not be representative of the actual absorption coefficient for energies which are much larger than that of the fundamental gap. In particular, if we neglect any changes

in the density of states and the e-ph and h-ph matrix elements, we expect the slope of  $\sqrt{\alpha\hbar\omega}$  to increase with energy.

An extensive study of the absorption coefficient in Si near 1.65 eV is beyond the scope of this thesis. However, in order to gain some insight into the  $|\vec{k}|$  dependence of the e-ph and h-ph matrix elements, we evaluated Eq. (5.11) at  $\vec{k}=\frac{2\pi}{a}(0,0,0.5)$ . Indirect transitions to this state will occur at a photon energy of approximately 1.65 eV to 1.8 eV. In the absence of experimental data, this value for the photon energy was obtained by assuming that the actual energy difference in  $\Delta_{1,c}$  between  $\vec{k}=\frac{2\pi}{a}(0,0,0.5)$  and the band minimum could be obtained from a band structure calculation.

The results of our calculation for scattering midway into the zone are listed in Table XXVII. Below the values of the matrix elements, we display  $A_{e-h}f_1$ . In computing this quantity, we assumed that  $A_{e-h}$  was a constant. From Tables XVIII and XXVII, we see that all of the matrix elements increase in magnitude. In particular, the absolute value of  $S_{e-ph_{TA}}$  is substantially larger than it was at the  $\vec{k}=\frac{2\pi}{a}(0,0,0.85)$ . Therefore,  $f_1$  is enhanced by the changes in both the matrix elements and the energy denominators (which have the greatest effect). The slope of  $\alpha\hbar\omega$  also increases

from

$76.0 \text{ (eV-cm)}^{-1/2}$  which is extrapolated from the fundamental gap to  $102.0 \text{ (eV-cm)}^{-1/2}$ . This is consistent with our contention that the slope is energy dependent.

We can take this analysis one step further and calculate a theoretical value for  $\sqrt{\alpha \hbar \omega}$  for energies beyond 1.65 eV. If we do this, we find that theory yields  $A_{e-h} f_{\text{total}} = 150.0 \text{ (eV-cm)}^{-1/2}$ , whereas from experiment we obtain  $A_{e-h} f_{\text{total}} = 214.0 \text{ (eV-cm)}^{-1/2}$ . Here,  $f_{\text{total}}$  is the total oscillator strength due to both  $\Gamma-L$  and  $\Gamma-\Delta$  transitions. In this case, the agreement between experiment and theory is much better than if we just linearly extrapolated from the fundamental gap. A more detailed analysis would require that a calculation be made at each photon energy of both  $f_1$  and  $A_{e-h}$ .

From the above results, we see that a simple linear extrapolation of  $\sqrt{\alpha \hbar \omega}$  could easily lead to a miscalculation of the contributions to the absorption coefficient of various scattering processes, such as  $\Gamma-L$  and  $\Gamma-\Delta$ . A linear extrapolation can be used only over small energy regions. However, when large energy regimes are considered, such as the one in Fig. 19, a

more detailed analysis must be made to account for changes in the density of states, the e-ph and h-ph matrix elements, the optical matrix elements and the energy denominators of the oscillator strength.

### Germanium

In Ge, the secondary indirect gap results from  $\Gamma$ - $\Delta$  "transitions" and occurs at a photon energy of approximately 1 eV, which is higher than that of the direct transitions from  $\Gamma_{25',v}$  to  $\Gamma_{2',c}$ . Thermoabsorption measurements provides some evidence of these processes.<sup>85</sup> The study found a weak structure near 1 eV, but it was never analyzed in detail. Consequently, there is no experimental value for the strength of this absorption.

We have calculated the e-ph and h-ph matrix elements for each of the allowed (TO,LO,TA,LA)  $\Gamma$ - $\Delta$  transitions in Ge [  $\Gamma$  to  $\vec{k} = \frac{2\pi}{a}(0,0,0.85)$  ]. The form factors used in this evaluation were the same as in the  $\Gamma$ -L work.<sup>86</sup> The phonon frequencies were the experimental values of Brockhouse and Iyengar and the eigenvectors were obtained from the procedure of Appendix D. The quantity  $Af_1$  was not evaluated because there is no basis for comparison. The results of our calculation of the matrix elements are listed in Table XXVIII.

### 5.2.3 Other Points In The Brillouin Zone

Once the e-ph and h-ph matrix elements of the fundamental and secondary indirect transitions are known, one would like to know how  $S_{e-ph}$  and  $S_{h-ph}$  vary as a function of  $|\vec{k}|$  along symmetry lines such as  $\Delta$  and  $\Lambda$ . In order to obtain this information, one should calculate the matrix elements at several points along various symmetry lines. Such a study is beyond the scope of this thesis and will not be considered here.

However, in order to gain some insights into the dependence of the matrix elements on  $\vec{k}$  and materials properties, we have calculated them for scattering midway into the zone along  $\Delta$  for both Si and Ge and along  $\Lambda$  for Ge. The results of these calculations are displayed in Tables XXVII-XXIX. This work should allow us to explore the nature of the e-ph and h-ph scattering. A detailed discussion will be presented in the next chapter.

## CHAPTER VI. DISCUSSION AND CONCLUSIONS

In the preceding chapters, we presented the results of a piezospectroscopic experiment in GaP, evaluations of e-ph and h-ph matrix elements in Si and GaP and various calculated values of the matrix elements and strengths of absorption coefficients in Si and Ge. We found good agreement in Si and Ge between various experiments and the theoretical work, thereby establishing the validity of the "rigid-pseudion" model for calculating e-ph and h-ph matrix elements in these materials.

In this chapter, we will take a closer look at the results of the previous sections and try to gain an understanding of the mechanisms which are responsible for the relative as well as absolute intensities of phonon-assisted transitions in indirect-gap materials. First, we will present a general discussion of the quantity  $Af_1$ , which ultimately determines the relative strength of a given indirect transition. After this we will present a specific discussion of phonon-assisted absorption (luminescence) in GaP, Si and Ge. Finally, an examination of all of the e-ph and h-ph matrix elements (experimental and theoretical) will allow us to examine trends which may occur. In the conclusion to the thesis, we will present some possible directions

for future research in this area.

### 6.1 The Oscillator Strength

An important consequence of our results lies in understanding the mechanisms responsible for the relative as well as absolute intensities of indirect transitions. The following discussion applies to phonon emission processes. For the case of phonon absorption, the occupation number must be included. In a given indirect gap material, apart from the line shape factor, the quantity  $Af_1$  determines the strength of a particular phonon assisted transition. The oscillator strength depends on the square of the sum of electron ( $U_1$  or  $W_1$ ) and hole ( $V_1$  or  $X_1$ ) scattering terms. By considering the various parameters comprising these terms, we will be able to show that the energy denominators of  $U_1$ ,  $W_1$ , etc. and the magnitudes and phases of the e-ph and h-ph matrix elements are responsible for the strength of  $f_1$ . Both the electron and hole scattering contributions have the same form: the product of an optical matrix element and  $S_{e-ph}$  ( $S_{h-ph}$  divided by an energy difference (e.g. see Table I). For the case of Ge, we must use the exact expression from Chapter V, which is given by Eq. (5.15).

We will first consider the optical matrix ele-

ments. For a given phonon-assisted transition the optical matrix elements associated with the electron and hole scattering contributions are not too different in magnitude, e.g. in GaP the ratio of the optical matrix element at  $\Gamma$  to the one at X is 1.2 for the TA phonon process and 1.4 for the LA mode. Furthermore, the optical matrix elements for different intermediate states at  $\Gamma$  ( $\Gamma_{1,c}$ ,  $\Gamma_{15,c}$  in GaP) are also not too different. Table X illustrates this for all of the materials which we are studying. Consequently, the optical matrix elements can in general be ruled out as the source of large variations in the oscillator strength. However, it must be noted that they are important in the case when there is a large degree of cancellation between the electron and hole scattering processes.

We now focus on the e-ph and h-ph matrix elements. From our experimental and theoretical results, we see that the magnitudes of  $S_{e-ph}$  and  $S_{h-ph}$  can vary substantially. In addition, the relative signs of the e-ph and h-ph matrix elements are vital because they determine whether the scattering processes interfere constructively or destructively. If the signs of  $S_{e-ph_1}$  and  $S_{h-ph_1}$  are the same, the electron and hole scattering interfere destructively (the valence band energy difference is opposite in sign to that of the

conduction band) and vice versa. The effect of this phenomena can be pronounced and is best illustrated by the expression for  $f_{LO}$  of GaP. For this case, if  $U_{LO} = -V_{LO}$ , the oscillator strength vanishes.

The remaining parameter to be considered is the energy denominator in the scattering terms  $U_1$ ,  $W_1$ ,  $X_1$  and  $V_1$ . The values of this parameter can show considerable differences not only for a particular phonon process (for  $U_1$  and  $V_1$  of  $f_1$ ), but also among the various allowed transitions of a given material (e.g. LA and TA of GaP). In materials such as Ge and GaP, the energy difference for scattering proceeding via  $\Gamma_{2',c}$  ( $\Gamma_{1,c}$ ) is much smaller than any of the other relevant energy denominators. A resonance can occur in the electron scattering term if  $S_{e-ph} / \Delta E_c \approx 1.0$ . This effect will be discussed further when we deal with Ge and GaP.

The preceding arguments enabled us to understand which parameters are responsible for large variations in the relative intensities of indirect transitions. We established that both the magnitudes and phases of the e-ph and h-ph matrix elements and their corresponding energy denominators are the causes of substantial variations in the "oscillator strengths" of the indirect transitions in a particular semiconductor. In

J

the following sections, we will apply these arguments to the indirect transitions of GaP, Si and Ge.

## 6.2 Gallium Phosphide

In GaP the fundamental absorption results from LA, TA, TO and LO phonon assisted  $\Gamma$ -X transitions. The most intense process is the LA phonon one, while the TA and TO transitions are approximately a factor of three weaker. The LO phonon transition is not observed. Based on the experimental results and the considerations of the last section, we can understand the mechanisms which are responsible for the relative intensities in this material.

The LA transition, which is the strongest of the ones observed, is the only process which has  $\Gamma_{1,c}$  as a conduction band intermediate state. The energy difference for this state,  $E(X_{1,c}) - E(\Gamma_{1,c}) - \hbar\omega_{LA}$  is much smaller than any of the other relevant energy separations, including the one for valence band scattering. The ratio  $W_{LA}/V_{LA} = -4.5$  indicates that the e-ph scattering dominates over the h-ph process and that destructive interference occurs between them. Since  $S_{e-ph_{LA}}$  and  $S_{h-ph_{LA}}$  are comparable in magnitude and have the same phase, i.e.,  $S_{e-ph_{LA}}/S_{h-ph_{LA}} = 0.6$ , the strength of

the electron scattering can be attributed to the small energy denominator in  $W_{LA}$ .

On the other hand, the TA transition, which also experiences destructive interference and has comparable e-ph and h-ph matrix elements ( $S_{e-ph_{TA}}/S_{h-ph_{TA}}=1.1$ ) is weak. The conduction band intermediate state of this process is  $\Gamma_{15,c}$  which is much higher in energy than  $\Gamma_{1,c}$ . In this case, no "resonance" occurs in the electron scattering and the ratio  $U_{TA}/V_{TA}=-1.6$  confirms this. Consequently, destructive interference makes this transition weak.

The TO phonon assisted transition is somewhat stronger than the TA one, but also much weaker than the LA process. In the absence of values for the e-ph and h-ph matrix elements, we do not know which mechanism is responsible for its relative intensity. The only thing that we can say with certainty, is that a resonance does not occur for this phonon assisted process, i.e., it has the same intermediate states as the TA mode.

The LO phonon assisted transition is so weak that it is not observed experimentally. As stated in the previous section, the expression for  $f_{LO}$  shows that total destructive interference can occur between the electron and hole scattering processes. This

phenomenon is probably responsible for the fact that the LO transition is too weak to detect.

### 6.3 Silicon

For Si, we have both experimental (TO) and theoretical (all phonons) values for the  $\Gamma$ - $\Delta$  matrix elements. In this material, the energies of  $\Gamma_{15,c}$  and  $\Gamma_{2',c}$  intermediate states are similar and well separated from that of the conduction band minimum at  $\Delta$ . The valence band energy separation is not too different from those of the conduction band. Thus, a resonance in the oscillator strength can be ruled out as a mechanism responsible for the dominance of the intensity of any indirect transition in this material.

In the following discussion, we will show that a delicate balance between the magnitudes and phases of the e-ph and h-ph matrix elements is responsible for the observed relative strengths of these transitions. From Table XVIII we see that constructive interference is responsible for the dominance of the TO phonon. Although the TA phonon also exhibits constructive interference, it is weak because  $S_{e-ph_{TA}}$  and  $S_{h-ph_{TA}}$  are substantially smaller in magnitude than the e-ph and h-ph matrix elements of the other phonons. For both the LO and LA modes, the electron and hole

scattering interfere destructively. In the case of the LA phonon, the transition is very weak despite the fact that its matrix elements are large in magnitude. The ratio  $S_{e-ph_{LA}}/S_{h-ph_{LA}}$  is such that almost complete destructive interference occurs. On the other hand, for the LO phonon,  $S_{e-ph_{LO}}/S_{h-ph_{LO}}=0.36$ , indicating that the effect of destructive interference is reduced. Furthermore, we see from Table I that the hole scattering term can never totally cancel the term for the electron scattering, i.e., even if  $V_{LO}=-U_{LO}$ , the e-ph process will still contribute to the oscillator strength.

The above discussion allows us to understand the sensitivity of the relative intensities of the LA and TA phonons. In the case of the LA phonon, if the balance between  $S_{e-ph_{LA}}$  and  $S_{h-ph_{LA}}$  is not just right, its intensity could become stronger than that of the TA phonon. In the case of the TA phonon, the matrix elements are small, indicating that a large amount of cancellation occurs in the sums of Eq. (5.11). If some of the terms do not add properly, the matrix elements could easily change phase and thereby result in poor agreement with experiment. These effects were illustrated in the last chapter, in which we saw that two form factors which differed only at large values of  $q$

produced significant differences in the relative intensities of these two phonons.

From these considerations, we see that accounting for the relative, as well as the absolute intensities provides a rigorous test of the "rigid-pseudoion" model. The calculation must yield the correct magnitudes and phases of the e-ph and h-ph matrix elements for each of the  $\Gamma$ - $\Delta$  transitions in Si.

#### 6.4 Germanium

In the case of Ge, the fundamental absorption comes from  $\Gamma$ -L transitions, in which only LA and TO phonons participate. The LA phonon process has both  $\Gamma_{2',c}$  and  $\Gamma_{15,c}$  as its conduction band intermediate states, while the TO phonon transition proceeds via only  $\Gamma_{15,c}$ .  $L_{3',v}$  is the valence band intermediate state for phonons. The LA transition is at least a factor of 10 stronger than the TO one.

In Ge, the energy separation,  $E(L_{1,c}) - E(\Gamma_{2',c})$  is substantially smaller than the valence band or  $L_{1,c} - \Gamma_{15,c}$  energy differences. Therefore, the electron scattering via  $\Gamma_{2',c}$  dominates the oscillator strength for the LA phonon. However, the other scattering mechanisms contribute to polarization dependent relative intensities in the strained crystal.

Without these processes, we would have  $A_3^{\parallel}/A_1^{\parallel}=A_4^{\perp}/A_2^{\perp}=A_3^{\perp}/A_1^{\perp}=3$  and  $A_2^{\perp}/A_3^{\perp}=1$  ( see Table VIII). From Table XXIV, we see that this is clearly not the case, indicating that the  $\Gamma_{15,c} \rightarrow L_{1,c}$  electron scattering and the hole process are important in understanding the indirect absorption in Ge.

The role of the  $\Gamma_{15,c}$  scattering in the oscillator strength can be understood by considering the magnitudes and phases of the matrix elements of this phonon.  $S_{e-ph}$  for the  $\Gamma_{15,c}$  process is greater in magnitude by a factor of 2.3 than  $S_{e-ph}$  for  $\Gamma_{2',c}$  and opposite in sign. Since the hole and  $\Gamma_{2',c}$  electron scattering interfere constructively, the transition proceeding via  $\Gamma_{15,c}$  reduces the effective "electron scattering" or enhances the effective "hole scattering". This phenomenon manifests itself when we use the experimental data of Table XXIV to obtain a value for the ratio of  $S_{e-ph_{LA}}$  for  $\Gamma_{2',c}$  scattering and  $S_{h-ph_{LA}}$ . By neglecting  $\Gamma_{15,c}$  in the analysis we find that  $S_{e-ph_{LA}}/S_{h-ph_{LA}} = -0.16$  (Ref. 8), whereas from Table XXII we see that this ratio is actually  $-0.43$ . Thus the hole scattering is "artificially" enhanced, in accord with the picture presented above for the role of the  $\Gamma_{15,c}$  scattering.

The fact that the TO phonon transition is much weaker than the LA one can easily be understood in terms of the fact that  $S_{e-ph_{TO}}$  is much smaller in magnitude than the e-ph matrix elements of the LA phonon. The h-ph matrix elements of both phonons are comparable in magnitude. Therefore, the combined effect of a small e-ph and h-ph matrix element and the lack of a resonance in its energy denominator, make the TO phonon transition much weaker than the LA one.

#### 6.5 Trends in Intervalley Scattering

In addition to understanding the indirect transitions in GaP, Si and Ge, we can use the results which we obtained to explore the nature of the intervalley scattering in DZB semiconductors. In order to do this more effectively, we have summarized the  $\Gamma-\Delta(X)$  (also midway into the zone) and the  $\Gamma-L$  numbers into two tables, one for each scattering direction. All of the materials which we studied are represented here. For Si and Ge we listed the theoretical values and for GaP, the experimental numbers are presented. Tables XXX and XXXI contain this information. In this discussion, we will first compare the matrix elements of different materials along a given direction and then we will study the  $\vec{k}$  dependence of the scattering in a particular semiconductor.

An examination of Table XXX allows us to explore the differences between the  $\Gamma-\Delta$  matrix elements of Si and Ge. Excluding the TA phonon, the magnitude and phase of the ratio  $S_{e-ph}/S_{h-ph}$  for a given phonon is similar in both materials. However, the individual matrix elements of Si are consistently larger in magnitude than the corresponding Ge numbers. This analysis also applies to the  $\Gamma-L$  matrix elements.

The TA phonon  $\Gamma-\Delta$  scattering exhibits the greatest difference between the two materials. For example the phases and the magnitudes of the ratio  $S_{e-ph}/S_{h-ph}$  are not the same in Si and Ge, e.g., the absolute values of  $S_{e-ph}/S_{h-ph}$  differ by at least a factor of two. We should note that in both cases the matrix elements are substantially smaller in magnitude than those of the other phonons. In addition, the GaP values for this phonon are substantially different from the Si and Ge numbers<sup>4</sup>. This indicates that the TA phonon e-ph and h-ph matrix elements are the most sensitive to materials properties.

A comparison of the  $\Gamma-\Delta$  and  $\Gamma-L$  numbers for Ge listed in Tables XXX and XXXI reveals that the longitudinal phonon matrix elements for the two scattering processes are similar, while those of the transverse phonons are not. We notice that the longitudinal

phonons which have  $\Gamma_{2',c}$  as an intermediate state (LA for  $\Gamma-L$  and LO for  $\Gamma-\Delta$ ) have similar matrix elements for both scattering directions. This also holds true for the longitudinal phonon processes proceeding via  $\Gamma_{15,c}$ . For the valence band, the analysis is not straight forward, since for  $\Gamma-\Delta$  both LA and LO phonons have  $\Delta_{5',v}$  as an intermediate state. In this case, we notice a similarity between  $S_{e-ph}$  of the LA phonon for both scattering directions. This analysis seems to indicate that the longitudinal phonon matrix elements are  $\vec{k}$  independent, provided that the initial and final states are at points of special symmetry. However, the matrix elements of Ge midway into the zone along support this idea only for the  $\Gamma_{2',c}$  and the valence band scattering.

We will now compare the  $\Gamma-\Delta$  longitudinal phonon scattering in Ge to similar processes in Si and GaP. In GaP, the LA phonon ( $\Gamma-X$ ) has  $\Gamma_{1,c}$  as its conduction band intermediate state. The e-ph matrix element for this phonon,  $S_{e-ph_{LA}} = -7.6 \pm 1.1 \times 10^{-3} \text{Ry}$  is very similar to those of Ge for the  $\Gamma-\Delta$  (LO) scattering. However, the h-ph matrix element of the LA phonon in GaP is somewhat smaller in magnitude than the corresponding one in Ge, indicating that the hole scattering is materials dependent.

In the case of Si, our previous discussion showed that all of its  $\Gamma$ - $\Delta$  matrix elements differed from those of Ge. Furthermore, an examination of the results for the scattering from  $\Gamma$  to L and from  $\Gamma$  midway into the zone along  $\Delta$  reveals a  $\vec{k}$  dependence of the matrix elements.

In order to gain further insights into our results, we will examine the nature of the lowest conduction bands at  $\Gamma$  of these three materials. From Figs. 2 and 3 we see that Ge and GaP are similar in that the  $\Gamma_{2',c}(\Gamma_{1,c})$  state is the lowest conduction band at  $\vec{k}=0$  and is well separated from the next highest conduction band,  $\Gamma_{15,c}$ . The energy of  $\Gamma_{2',c}$  lies just above that of the conduction band minimum (X in GaP and L in Ge). In GaP this separation is approximately 0.5 eV and in Ge it is 0.1 eV. In Si (see Fig. 1), on the other hand, the ordering of  $\Gamma_{2',c}$  and  $\Gamma_{15,c}$  is reversed and both bands are much higher in energy than the conduction band minimum at  $\Delta$ . Our results suggest that the location of  $\Gamma_{2',c}(\Gamma_{1,c})$  has a bearing on the  $\vec{k}$  dependence of the scattering by longitudinal phonons from this state.

We will finally examine the scattering from  $\Gamma$  to a point midway into the zone along  $\Delta$ . This calculation

was performed only in Ge and is included because of its interesting results. For this scattering, the LA and LO phonons have the same symmetry. This is also true for the transverse phonons. From Table XIX, we see that the matrix elements of the LA and LO modes are very similar and that their sum is approximately equal to  $S_{e-ph_{LA}}$  at L. The transverse phonons also exhibit this feature. The  $\vec{k}$  independence which was discussed previously, applies in this case if we consider both LA and LO phonons as a single mode with an "effective" matrix element given by

$$S_{e-ph}^{eff} = \left[ S_{e-ph_{LA}}^2 + S_{e-ph_{LO}}^2 \right]^{1/2}$$

This value is somewhat smaller than the matrix element for  $\Gamma$ -L scattering, but it is close enough to the other so that the scattering seems to be "isotropic".

We conclude this discussion by summarizing our results. We find that:

- (a) The scattering along both  $\Delta$  and  $\Lambda$  in Si and Ge is somewhat different, with most of the matrix elements of Si being larger in magnitude than the corresponding ones of Ge.

- (b) The TA phonon matrix elements are the most sensitive to materials properties.
- (c) The location of  $\Gamma_{2',c}(\Gamma_{1,c})$  has a bearing on the  $\vec{k}$  independence of the "s-like" scattering which proceeds via this state.
- (d) The  $\Gamma-\Delta$  scattering, midway into the zone also exhibits the  $k$  independence, if both the LA and LO phonons are considered in the event.

Thus, we found some trends in the intervalley scattering in Si, Ge and GaP. The underlying reasons for these trends are presently not understood and can only be elucidated through a more detailed study of the scattering mechanism.

#### 6.6 Summary And Conclusions

In summary, we have performed an experimental study in GaP of the intervalley e-ph and h-ph matrix elements for  $\Gamma-X$  scattering by LA and TA phonons. Using these results and similar experimental numbers for the  $\Gamma-\Delta$  TO phonon transition in Si, experimental values and theoretical expressions for the absorption coefficient, we were able to evaluate certain e-ph and h-ph matrix elements in Si (TO) and GaP (LA,TA).

We then performed theoretical calculations of the

e-ph and h-ph matrix elements in Si and Ge, using the "rigid-pseudoion" model.  $\Gamma$ - $\Delta$  and  $\Gamma$ -L processes were considered in both materials, as well as scattering midway into the zone along  $\Delta$  (Si, Ge) and  $\Lambda$  (Ge). From the results of this work, we were able to account for the relative as well as absolute intensities of the indirect transitions occurring at the fundamental gaps of both Si and Ge. In Ge, we were also able to calculate the correct polarization dependent relative intensities of the LA transition in the strained crystal. Based on the success of the calculations, we concluded that the "rigid-pseudoion" model provides a good description of the e-ph (h-ph) interaction in Si and Ge.

The results of both the theoretical and experimental work allowed us to understand which mechanisms governed the intensities of indirect transitions. We found that both the magnitudes and phases of the scattering matrix elements were important as well as the energy separation of the final and intermediate states. The phases of the matrix elements determined whether the electron and hole scattering processes interfered constructively or destructively. The effect of the interference was found to be crucial in Si, while in Ge, the energy denominator was most important.

In GaP, both effects were utilized in explaining the intensities of the indirect transitions.

In studying the secondary indirect gap of Si, we found that a simple linear extrapolation of  $\sqrt{\hbar\omega}$  in the free electron-hole pair energy region was not appropriate for analyzing the absorption process. This was a result of the fact that both  $A_{e-h}$  and the oscillator strength were energy dependent over large range of photon energies. This effect was demonstrated for the quantity  $f_1$ .

The study of the dependence of the matrix elements on material and scattering direction revealed some interesting trends. We found that the matrix elements for a given direction were somewhat different in Si and Ge. The TA phonon values were found to vary substantially within Si, Ge and GaP. In examining the  $\vec{k}$  dependence of the scattering, we found that in the "s-like" electron scattering by longitudinal phonons, the location of the  $\Gamma_{2',c}(\Gamma_{1,c})$  state was important. In Si this type of scattering was anisotropic and  $|\vec{k}|$  dependent, while in Ge and GaP it was not.

In conclusion, this thesis has provided considerable information about the nature of indirect transitions and their associated intervalley e-ph and h-ph

scattering elements in GaP, Si and Ge. We also gained some insights into other scattering along other high symmetry directions. From a theoretical point of view we showed that the "rigid-pseudoion" model is a good description of the e-ph and h-ph interaction in Si and Ge. In the next section, we will briefly consider some possible future directions for research in this area.

### 6.7 Possible Future Research

In this thesis, we established the utility of indirect transitions in studying intervalley e-ph and h-ph scattering and demonstrated experimental and theoretical techniques for obtaining e-ph and h-p matrix elements. It is now possible to perform a systematic study of these interactions in various semiconductors. The experiment, described here can be used in other indirect gap materials such as AlAs and AlSb. This would provide experimental values of the matrix elements, which can be used as a basis for comparison with a theoretical calculation.

From a theoretical point of view, the "rigid-pseudoion" model can be extended to the III-V materials. In this application many new aspects of the calculation will be encountered. One of these lies in calculating the phonon eigenvectors. In a recent arti-

cle, Martin showed that the eigenvectors of the transverse zone edge phonons in GaAs are model dependent.<sup>87</sup> Therefore, an accurate calculation of the lattice dynamics will be required. At this point, it is not certain which model should be used. Another problem which arises in these types of materials is the fact that the electron distribution is not the same around the two atoms of the basis. This may have an effect on the form of the e-ph (h-ph) interactions. In addition to this, the lack of inversion symmetry complicates the evaluation of Eq.(5.8), which must be used instead of Eq.(5.11).

From the point of view of basic solid state physics, the assumptions of the "rigid-pseudoion" model should be examined. This can be accomplished by first performing the calculation nonlocally and then changing the form of the screening. In our calculation, we displaced a screened potential, whereas in a more accurate approach the bare ion e-ph interaction is first calculated and then it is screened nonlocally. Ziman and Sham discuss this in more detail.<sup>61</sup> A study such as this should permit us to understand the reason why the usual local form factor (as in Ge) does not work well for the LA and TA phonons of Si.

Other theoretical applications can come from a

study of phonon scattering in ternary compounds whose gap can be adjusted from direct to indirect by alloying. In these materials, we can study the effect of alloying on the e-ph interaction. We can also consider nonuniform alloying of ternary compounds.

APPENDIX A : OPTICAL AND PHONON SCATTERING SELECTION RULES

The various expressions for the oscillator strength,  $f_1$ , which were derived in the text, used the selection rules presented in this appendix. The  $|J, M_J\rangle$  wave functions are given by the equations which are listed below. Along the [001] direction, we have

$$|3/2, 3/2\rangle_{001} = (1/\sqrt{2})|(X + iY)\uparrow\rangle \quad (\text{A.1a})$$

$$|3/2, 1/2\rangle_{001} = (1/\sqrt{6})|2Z\uparrow - (X + iY)\downarrow\rangle \quad (\text{A.1b})$$

$$|1/2, 1/2\rangle_{001} = (1/\sqrt{3})|Z\downarrow + (X + iY)\uparrow\rangle \quad (\text{A.1c})$$

while along [111] we have

$$|3/2, 3/2\rangle_{111} = (1/\sqrt{2})|(\bar{X} + i\bar{Y})\uparrow\rangle \quad (\text{A.2a})$$

$$|3/2, 1/2\rangle_{111} = (1/\sqrt{6})|2\bar{Z}\uparrow + (\bar{X} + i\bar{Y})\downarrow\rangle \quad (\text{A.2b})$$

$$|1/2, 1/2\rangle_{111} = (1/\sqrt{3})|\bar{Z}\uparrow - (\bar{X} - i\bar{Y})\downarrow\rangle \quad (\text{A.2c})$$

where  $\bar{X}$ ,  $\bar{Y}$ , and  $\bar{Z}$  have been defined in the text.

In the following section, we will present the selection rules for  $\Gamma - X(\Delta)$  and  $\Gamma - L$  processes. The latter processes will not be treated in detail because they can be derived from the  $\Gamma - X(\Delta)$  selection rules.

A.1  $\Gamma - X(\Delta)$  Transitions

Optical Selection Rules

The matrix elements of  $\hat{e} \cdot \vec{p}$  between  $\Gamma_{8,v}$  (or  $\Gamma_{7,v}$ ) and  $\Gamma_{1,c}$  are given by

$$\begin{aligned} \langle \Gamma_{8,v}^x | p_x | \Gamma_{1,c} \rangle &= \langle \Gamma_{8,v}^y | p_y | \Gamma_{1,c} \rangle = \\ \langle \Gamma_{8,v}^z | p_z | \Gamma_{1,c} \rangle &\neq 0 \end{aligned} \quad (\text{A.3})$$

For the case of  $\Gamma_{8,v}$  (or  $\Gamma_{7,v}$ ) and  $\Gamma_{15,c}$ , the only non-zero matrix elements of  $\hat{e} \cdot \vec{p}$  are

$$\begin{aligned} \langle \Gamma_{8,v}^y | p_x | \Gamma_{15,c}^z \rangle &= \langle \Gamma_{8,v}^z | p_x | \Gamma_{15,c}^y \rangle = \\ \langle \Gamma_{8,v}^x | p_y | \Gamma_{15,c}^z \rangle &= \langle \Gamma_{8,v}^z | p_y | \Gamma_{15,c}^x \rangle = \\ \langle \Gamma_{8,v}^x | p_z | \Gamma_{15,c}^y \rangle &= \langle \Gamma_{8,v}^y | p_z | \Gamma_{15,c}^x \rangle \neq 0 \end{aligned} \quad (\text{A.4})$$

At the zone edge, the only non-vanishing matrix elements of  $\hat{e} \cdot \vec{p}$  between  $X_{5,v}$  and  $X_{1,c}$  are:

$$\langle X_{1,c} | p_y | X_{5,v}^y \rangle = \langle X_{1,c} | p_z | X_{5,v}^z \rangle \neq 0 \quad (\text{A.5})$$

along (100) and

$$\langle X_{bc} | P_x | X_{5,\nu}^x \rangle = \langle X_{bc} | P_z | X_{5,\nu}^z \rangle \neq 0 \quad (\text{A.6})$$

along (010) and

$$\langle X_{bc} | P_x | X_{5,\nu}^x \rangle = \langle X_{bc} | P_y | X_{5,\nu}^y \rangle \neq 0 \quad (\text{A.7})$$

along (001).

Selection Rules for LA Phonon Scattering

The only non-zero matrix elements of  $H_{LA}$  for  $\Gamma_{1,c} \rightarrow X_{1,c}$  scattering are:

$$\langle \Gamma_{bc} | H_{LA} | X_{1,c} \rangle \neq 0 \quad (\text{A.8})$$

for all of the valleys.

The only non-zero matrix elements of  $H_{LA}$  for  $X_{5,\nu} \rightarrow \Gamma_{8,\nu}$  scattering along the (100) valley are:

$$\langle \Gamma_{8,\nu}^y | H_{LA} | X_{5,\nu}^y \rangle = \langle \Gamma_{8,\nu}^z | H_{LA} | X_{5,\nu}^z \rangle \neq 0 \quad (\text{A.9})$$

while along (010) the only non-vanishing matrix elements of  $H_{LA}$  are:

$$\langle \Gamma_{8,\nu}^x | H_{LA} | X_{5,\nu}^x \rangle = \langle \Gamma_{8,\nu}^z | H_{LA} | X_{5,\nu}^z \rangle \neq 0 \quad (\text{A.10})$$

and along (001) the only non-vanishing matrix elements

of  $H_{LA}$  are:

$$\langle \Gamma_{2,\nu}^x | H_{LA} | X_{5,\nu}^x \rangle = \langle \Gamma_{2,\nu}^y | H_{LA} | X_{5,\nu}^y \rangle \neq 0 \quad (\text{A.11})$$

Selection Rules for Transverse Phonon Scattering

Since both the TA and TO phonons have the same symmetry (in this case), we will use the subscript T to represent TA and TO scattering. For  $\Gamma_{15,c} \rightarrow X_{1,c}$  scattering along the (100) valley, the only non-zero matrix elements of  $H_T$  are:

$$\langle \Gamma_{15,c}^y | H_T^y | X_{1,c} \rangle = \langle \Gamma_{15,c}^z | H_T^z | X_{1,c} \rangle \neq 0 \quad (\text{A.12})$$

while along (010), the only non-vanishing matrix elements of  $H_T$  are:

$$\langle \Gamma_{15,c}^x | H_T^x | X_{1,c} \rangle = \langle \Gamma_{15,c}^z | H_T^z | X_{1,c} \rangle \neq 0 \quad (\text{A.13})$$

and along (001), the only non-zero matrix elements of  $H_T$  are:

$$\langle \Gamma_{15,c}^x | H_T^x | X_{1,c} \rangle = \langle \Gamma_{15,c}^y | H_T^y | X_{1,c} \rangle \neq 0 \quad (\text{A.14})$$

For  $X_{5,v} \rightarrow \Gamma_{8,v}$  scattering along the (100) valley, the only non-zero matrix elements of  $H_T$  are:

$$\langle \Gamma_{8,v}^x | H_T^y | X_{5,v}^z \rangle = \langle \Gamma_{8,v}^x | H_T^z | X_{5,v}^y \rangle \neq 0 \quad (\text{A.15})$$

while along (010), the only non-vanishing matrix elements of  $H_T$  are:

$$\langle \Gamma_{8,v}^y | H_T^x | X_{5,v}^z \rangle = \langle \Gamma_{8,v}^y | H_T^z | X_{5,v}^x \rangle \neq 0 \quad (\text{A.16})$$

and along (001), the only non-zero matrix elements of  $H_T$  are:

$$\langle \Gamma_{8,v}^z | H_T^x | X_{5,v}^y \rangle = \langle \Gamma_{8,v}^z | H_T^y | X_{5,v}^x \rangle \neq 0 \quad (\text{A.17})$$

#### Selection Rules for L0 Phonon Scattering

For  $\Gamma_{15,c} \rightarrow X_{1,c}$  scattering along the (100) valley, the only non-zero matrix elements of  $H_{L0}$  are:

$$\langle \Gamma_{15,c}^x | H_{L0}^x | X_{1,c} \rangle \neq 0 \quad (\text{A.18})$$

while along (010) the only non-vanishing matrix elements of  $H_{L0}$  are:

$$\langle \Gamma_{15c}^y | H_{L0}^y | X_{1,c} \rangle \neq 0 \quad (\text{A.19})$$

and along (001) the only non-zero matrix elements of  $H_{L0}$  are:

$$\langle \Gamma_{15c}^z | H_{L0}^z | X_{1,c} \rangle \neq 0 \quad (\text{A.20})$$

For  $X_{5,v} \rightarrow \Gamma_{8,v}$  scattering along the (100) valley, the only non-zero matrix elements of  $H_{L0}$  are:

$$\langle \Gamma_{8,v}^y | H_{L0}^x | X_{5,v}^z \rangle = \langle \Gamma_{8,v}^z | H_{L0}^x | X_{5,v}^y \rangle \neq 0 \quad (\text{A.21})$$

while along (010), the only non-vanishing matrix elements of  $H_{L0}$  are:

$$\langle \Gamma_{8,v}^z | H_{L0}^y | X_{5,v}^x \rangle = \langle \Gamma_{8,v}^x | H_{L0}^y | X_{5,v}^z \rangle \neq 0 \quad (\text{A.22})$$

and along (001), the only non-zero matrix elements of  $H_{L0}$  are:

$$\langle \Gamma_{8,v}^x | H_{L0}^z | X_{5,v}^y \rangle = \langle \Gamma_{8,v}^y | H_{L0}^z | X_{5,v}^x \rangle \neq 0 \quad (\text{A.23})$$

## A.2 $\Gamma$ - L Transitions

The selection rules for  $\Gamma$  - L processes can be derived in terms of the above selection rules and the fact that  $H_{LA}$  transforms as  $L_{2,1} = (1/\sqrt{3})(x+y+z)$  [along (111)] and that  $H_{T0}$  transforms as  $L_{3,1}$ , which can be either  $L_{3,1}^{\bar{x}} = (1/\sqrt{2})(x-y)$  or  $L_{3,1}^{\bar{y}} = (1/\sqrt{6})(x+y-2z)$ .

For example, we will consider the optical matrix element for the transition from  $\Gamma_{25',v}(\Gamma_{8,v})$  to  $\Gamma_{2',c}(\Gamma_{1,c})$ , with the wave functions oriented along the (111) axis. We write the optical matrix element along (111) as:

$$\begin{aligned} \langle \bar{z} | P_{\bar{z}} | \Gamma_{2',c} \rangle &= \frac{1}{3} \langle X+Y+Z | P_x+P_y+P_z | \Gamma_{2',c} \rangle \\ &= \langle X | P_x | \Gamma_{2',c} \rangle \\ &= \langle Y | P_y | \Gamma_{2',c} \rangle \\ &= \langle Z | P_z | \Gamma_{2',c} \rangle \end{aligned} \tag{A.24}$$

where we used  $P_{\bar{z}} = (1/\sqrt{3})(P_x+P_y+P_z)$  and  $|\bar{z}\rangle = (1/\sqrt{3})|X+Y+Z\rangle$ .

The electron and hole scattering can be treated in a similar manner by expressing the states and  $H_1$  in terms of their components along the x, y, and z axes [the (001) system] and proceeding as we did above.

## APPENDIX B. CURVE FITTING PROGRAMS

In this appendix, we will discuss the procedure used to fit the experimental WMA spectra to theoretical curves. The two programs which are presented here were specifically written to run on a Tektronix 4051 computer and extensively utilize its graphics capabilities.

The first program serves as a filter for the second, which performs the actual fit. Raw data, obtained from a chart or automatically taken from the experiment is inputted into a file in a specific format. The first program then displays the complete spectrum and allows the user to choose which portion of the data is to be fitted. The resulting set of points is then placed into a temporary file on tape.

The second program reads the temporary data file and plots its contents. The user then chooses an approximate background, which is subtracted from the data. A Gaussian (Eq. 4.5) is then fit to the new experimental points. The amplitude of the Gaussian is chosen to correspond to the largest experimental value of  $dd/dE$ . The broadening parameter is obtained from the condition  $\epsilon^2/(2\Gamma^2) = 1$ .

The iteration process is carried out in the same

fashion as described in Chapter IV. The advantages of this technique lie in the fact that visual adjustments of the fit provide an accurate aid to a very simple procedure and allow one the option of terminating the program when the best fit is attained. For the case of Si and Ge, the function  $F(W')$  (Eq. 4.4) replaces the Gaussian and a logarithmic background is used instead of a parabola. The program listing begins on the next page.

1 REM: SI PLOT NORMALIZING VER I(USED FOR ALSB)

2 REM file #7

3 END

4 GO TO 110

5 GO TO 280

6 PAGE

7 GO TO 320

8 GO TO 380

9 GO TO 430

10 PRINT "M4=";

11 INPUT M4

12 GO TO 450

13 WINDOW 0,1,0,M4

14 END

15 FIND 46

16 OLD

17 FIND 66

18 OLD

19 PAGE

20 GO TO 470

21 GO TO 560

22 GO TO 700

23 GO TO 760

24 PAGE

25 LIST

26 END

27 GO TO 5000

28 EHD

29 IHIT

30 A=0

31 B=0

32 J9=0

33 K#="I"

34 PAGE

35 PAGE

36 PAGE

37 PAGE

38 PAGE

39 PAGE

40 PAGE

41 PAGE

42 PAGE

43 PAGE

44 PAGE

45 PAGE

46 PAGE

47 PAGE

48 PAGE

49 PAGE

50 PAGE

51 PAGE

52 PAGE

53 PAGE

54 PAGE

55 PAGE

56 PAGE

57 PAGE

58 PAGE

59 PAGE

60 PAGE

61 PAGE

62 PAGE

63 PAGE

64 PAGE

65 PAGE

66 PAGE

67 PAGE

68 PAGE

69 PAGE

70 PAGE

71 PAGE

72 PAGE

73 PAGE

74 PAGE

75 PAGE

76 PAGE

77 PAGE

78 PAGE

79 PAGE

80 PAGE

81 PAGE

82 PAGE

83 PAGE

84 PAGE

85 PAGE

86 PAGE

87 PAGE

88 PAGE

89 PAGE

90 PAGE

91 PAGE

92 PAGE

93 PAGE

94 PAGE

95 PAGE

96 PAGE

97 PAGE

98 PAGE

99 PAGE

100 PAGE

101 PAGE

102 PAGE

103 PAGE

104 PAGE

105 PAGE

106 PAGE

107 PAGE

108 PAGE

109 PAGE

110 PAGE

111 PAGE

112 PAGE

113 PAGE

114 PAGE

115 PAGE

116 PAGE

117 PAGE

118 PAGE

119 PAGE

120 PAGE

121 PAGE

122 PAGE

123 PAGE

124 PAGE

125 PAGE

126 PAGE

127 PAGE

128 PAGE

129 PAGE

130 PAGE

131 PAGE

132 PAGE

133 PAGE

134 PAGE

135 PAGE

136 PAGE

137 PAGE

138 PAGE

139 PAGE

140 PAGE

141 PAGE

142 PAGE

143 PAGE

144 PAGE

145 PAGE

146 PAGE

147 PAGE

148 PAGE

149 PAGE

150 PAGE

151 PAGE

152 PAGE

153 PAGE

154 PAGE

155 PAGE

156 PAGE

157 PAGE

158 PAGE

159 PAGE

160 PAGE

161 PAGE

162 PAGE

163 PAGE

164 PAGE

165 PAGE

166 PAGE

167 PAGE

168 PAGE

169 PAGE

170 PAGE

171 PAGE

172 PAGE

173 PAGE

174 PAGE

175 PAGE

176 PAGE

177 PAGE

178 PAGE

179 PAGE

180 PAGE

181 PAGE

182 PAGE

183 PAGE

184 PAGE

185 PAGE

186 PAGE

187 PAGE

188 PAGE

189 PAGE

190 PAGE

191 PAGE

192 PAGE

193 PAGE

194 PAGE

195 PAGE

196 PAGE

197 PAGE

198 PAGE

199 PAGE

200 PAGE

201 PAGE

202 PAGE

203 PAGE

204 PAGE

205 PAGE

206 PAGE

207 PAGE

208 PAGE

209 PAGE

210 PAGE

211 PAGE

212 PAGE

213 PAGE

214 PAGE

215 PAGE

216 PAGE

217 PAGE

218 PAGE

219 PAGE

220 PAGE

221 PAGE

222 PAGE

223 PAGE

224 PAGE

225 PAGE

226 PAGE

227 PAGE

228 PAGE

229 PAGE

230 PAGE

231 PAGE

232 PAGE

233 PAGE

234 PAGE

235 PAGE

236 PAGE

237 PAGE

238 PAGE

239 PAGE

240 PAGE

241 PAGE

242 PAGE

243 PAGE

244 PAGE

245 PAGE

246 PAGE

247 PAGE

248 PAGE

249 PAGE

250 PAGE

251 PAGE

252 PAGE

253 PAGE

254 PAGE

255 PAGE

256 PAGE

257 PAGE

258 PAGE

259 PAGE

260 PAGE

261 PAGE

262 PAGE

263 PAGE

264 PAGE

265 PAGE

266 PAGE

267 PAGE

268 PAGE

269 PAGE

270 PAGE

271 PAGE

272 PAGE

273 PAGE

274 PAGE

275 PAGE

276 PAGE

277 PAGE

278 PAGE

279 PAGE

280 PAGE

281 PAGE

282 PAGE

283 PAGE

284 PAGE

285 PAGE

286 PAGE

287 PAGE

288 PAGE

289 PAGE

290 PAGE

291 PAGE

292 PAGE

293 PAGE

294 PAGE

295 PAGE

296 PAGE

297 PAGE

298 PAGE

299 PAGE

300 PAGE

301 PAGE

302 PAGE

303 PAGE

304 PAGE

305 PAGE

306 PAGE

307 PAGE

308 PAGE

309 PAGE

310 PAGE

311 PAGE

312 PAGE

313 PAGE

314 PAGE

315 PAGE

316 PAGE

317 PAGE

318 PAGE

319 PAGE

```
150 PRINT " ENTER DATA FILE NUMBER"  
160 INPUT F  
165 FIND F  
169 READ @33:L$,M$,N$,X$,Z$,  
170 I=0  
175 ON EOF @> THEN 200  
180 READ @33:H  
185 I=I+1  
190 GO TO 175  
200 X=1  
202 X1=I  
205 DELETE 560,660  
206 DELETE 5000,6000  
207 DELETE H  
208 DIM D(I)  
210 FIND F  
220 READ @33:L$,M$,N$,X$,Z$,D  
221 D$=" "  
230 H4=4096  
240 WINDOW 0,I,0,H4  
250 VIEWPORT 10,130,10,90  
260 GO TO 310  
270 END  
280 PRINT "ENTER A,B"  
290 INPUT A,B  
300 END  
310 PAGE  
320 AXIS 10,1000  
330 MOVE 1,D(I)+B  
340 FOR J=1 TO I  
350 MOVE J,D(J)+A*J+B  
351 DRAW J,D(J)+A*J+B  
360 NEXT J  
370 END  
380 HOME
```

```
390 PRINT L$,M$
400 PRINT N$;" " ;0$
410 PRINT "A=" ;A;"IB=" ;B
420 END
430 PRINT "ENTER CUTOFF X VALUES"
440 INPUT X,X1
450 WINDOW X,X1,0,W4
460 GO TO 310
470 PRINT "ENTER FREQUENCY OF POINTS TO BE SENT"
480 INPUT F0
490 FIND 4
500 FOR J=X1 TO X STEP -F0
510 D9=D(J)+A*J+B
520 PRINT @33:D9
530 NEXT J
540 FIND 4
550 END
560 A$=CHR(13)
570 CALL "TCRLF",3,2,0
580 CALL "TSTRIN",",",",", "000000", " *"
590 CALL "RSTRIN",",",",", " "
600 CALL "EOLCHR",13,A$,0
610 CALL "PROMPT",0,200,"?"
620 CALL "MARGIN",1,0,0
630 CALL "BREAK",7,"@","@"
640 PRINT "GG ERNIE HERE GG";MEMORY
650 CALL "TERMIN"
660 END
700 J9=J9+2
710 MOVE J9,D(J9)+A*J9+B
711 PRINT @32,18:5
720 PRINT @32,24:K$
730 J9=J9*(J9<X1)+X*(J9=>X1)
740 END
760 PRINT K$;" ";J9;" ";D(J9);"G";
```

```
781 PRINT @32,18:0
782 MOVE J9,D<J9>
790 END
5000 PRINT "NUMBER OF POINTS TO BE DELETED"
5010 INPUT D9
5011 IF D9=0 THEN 5050
5020 FOR J=1 TO I-D9
5030 D<J>=D<J+D9>
5040 NEXT J
5050 PRINT "SCALING FACTOR"
5060 INPUT S
5070 D=D*S
5080 FIND F
5100 WRITE @33:I-D9,L$,M$,N$,O$,D
5110 GO TO 170
```

```
1 REM: CURVE FITTING FOR NONLINEAR BACKGROUND<+E>
2 REM: FILE #10
3 END
4 GO TO 100
8 GO TO 1310
12 GOSUB 1370
15 GOSUB 1070
17 END
20 GOSUB 1140
21 END
24 GOSUB 480
25 GO TO 440
28 GO TO 340
29 END
32 GOSUB 1370
33 GO TO 1310
40 FIND ?
41 OLD
100 PAGE
110 DEF FNA(J)=12398/(R+(M-J))*1.11*G
120 DEF FNB(J)=(FNA(J)-X0)/X3
130 DEF FNC(W)=Y0*EXP(-0.5*(W-0.5)^2)
131 DEF FNZ(J)=12398/FNA(J)^2
140 DIM A(4),C(3)
150 DEF FND(J)=A(3)*J^2+A(2)*J+A(1)
160 FIND 4
170 DELETE Y
180 J=0
190 ON EOF (0) THEN 230
200 INPUT @33:H
210 J=J+1
220 GO TO 190
230 M=J
240 DIM Y(M)
```

```
241 PRINT "STEP SIZE=";
242 INPUT G
250 PRINT "PAR=";
260 INPUT P
270 PRINT "KTLY=";
280 INPUT K
290 PRINT "SERVO=";
300 INPUT S
301 PRINT "SAMPLE THICKNESS<IN CM>=";
302 INPUT T
303 PRINT "DISPERSION<IN ANGSTROM>=";
304 INPUT U
305 U=P/(K*S*T*U*10)
320 PRINT "REF WAVELEH=";
330 INPUT R
340 FIND 4
350 FOR J=1 TO M
360 INPUT @33:Y(J)
361 Y(J)=FNZ(J)*Y(J)
370 NEXT J
380 GOSUB 480
391 GOSUB 560
390 GOSUB 680
400 GOSUB 1240
410 END
420 GOSUB 480
430 GOSUB 560
440 GOSUB 680
450 GOSUB 760
460 GOSUB 850
470 END
480 Y1=0
490 FOR J=1 TO M
500 IF Y1>Y(J) THEN 530
510 Y1=Y(J)
```

```
J1=J
520 NEXT J
530 PAGE
540 RETURN
550 Y0=Y1/2.71828
560 FOR L=1 TO 1
570 FOR J=J1 TO 1 STEP -1
580 IF Y(J)<Y0 THEN 610
590 NEXT J
600 J0=J
610 NEXT L
620 X0=FNA(J0)
640 X1=FNA(J1)
650 X3=X1-X0
660 RETURN
670 VIEWPORT 0,130,0,100
680 WINDOW 0,M,-Y1/10,Y1
691 S9=(M-1)/((FNA(M)-FNA(1))*1000)
700 AXIS S9,5.0E+7,J0,0
710 MOVE 0,Y(1)
720 FOR J=1 TO M
730 DRAW J,Y(J)
740 NEXT J
750 RETURN
760 FOR J=2 TO M STEP 2
770 W2=FNB(J-1)
780 W3=FNB(J)
790 MOVE J-1,FNC(W2)
800 DRAW J,FNC(W3)
810 NEXT J
811 MOVE J0,Y1
812 PRINT "JHhhdhHh__JHhde"
820 MOVE J0,0
830 PRINT USING 831:"JJ ";FNA(J0);" eV"
831 IMAGE 3A,1D.4D,3A
```

```
932 MOVE J0,0
933 PRINT @32,18:5
934 PRINT "K{1 meV"
935 MOVE J0+S9,0
936 PRINT "KH:"
937 PRINT @32,18:0
940 RETURN "↑"
950 PRINT " " PEAK HT=";Y1*U
960 PRINT " " PEAK PT=";X1;"eV"
970 PRINT " " DIM FACTOR U=";U
980 PRINT " " WAVELEN AT PEAK=";12398/X1;"A"
990 PRINT " " INDEX AT PEAK=";J1
998 PRINT " " C(1)=";Y0*U
999 PRINT " " C(2)=";X3
999 PRINT " " C(3)=";X0
940 C(1)=Y0*U
950 C(2)=X3
960 C(3)=X0
990 PRINT USING 991: " A=";A
991 IMAGE8A,/,4D.4D,/,4D.4D,/,4D.4D,/,4E
1010 RETURN
1020 FIND 4
1030 FOR J=1 TO M
1040 PRINT @33:INT(Y(J))
1041 Y(J)=FNZ(J)*Y(J)
1050 NEXT J
1060 END
1070 PRINT "WHICH A-VALUE? ";
1080 INPUT F
1090 IF F<1 OR F>4 THEN 1260
1100 PRINT "ENTER NEW A(";F;"): ";
1110 INPUT A(F)
1120 GO TO 1070
1140 PRINT "CHANGE WHICH C-VALUE ";
```

```
1150 INPUT L
1160 IF L<1 OR L>3 THEN 1200
1170 PRINT "ENTER NEW C(1);L(1)";
1180 INPUT C(L)
1190 GO TO 1140
1200 Y0=C(1)/U
1210 X0=C(3)
1220 X3=C(2)
1230 GO TO 760
1240 PRINT " ENTER A VALUES"
1250 INPUT A
1260 MOVE 1,FND(1)
1270 FOR J=1 TO M STEP 2
1280 DRAW J,FND(J)
1290 NEXT J
1300 RETURN
1310 FIND 4
1320 FOR J=1 TO M
1321 INPUT @33:Y(J)
1322 Y(J)=FHZ(J)*Y(J)
1330 Y(J)=Y(J)-FND(J)
1340 NEXT J
1350 GO TO 420
1370 FIND 4
1380 FOR J=1 TO M
1390 INPUT @33:Y(J)
1391 Y(J)=FHZ(J)*Y(J)
1400 Y(J)=Y(J)-FNC(FNB(J))
1410 NEXT J
1420 PAGE
1430 GOSUB 680
1440 HOME
1450 PRINT USING 1460:"OLD A'S=";A
1460 IMAGE 8A,4D,4D,4D,4D,4E
1461 A(4)=Y1/8
```

```
1470 A(1)=EXP(Y(1)/A(4))
1480 J8=M
1490 J9=M-10
1500 Y7=Y(1)+FND(1)
1510 Y8=Y(J8)+FND(J8)
1520 Y9=Y(J9)+FND(J9)
1530 A(1)=Y1/8
1540 Z1=1+J9+J8
1550 Z2=1+J9↑2+J8↑2
1560 Z3=1+J9↑3+J8↑3
1570 Z4=1+J8↑4+J9↑4
1580 K1=A(1)*Z1-(Y(1)+Y(J8)*J8+Y(J9)*J9)
1590 K2=A(1)*Z2-(Y(1)+Y(J8)*J8↑2+Y(J9)*J9↑2)
1600 A(2)=(-K2*Z3+K1*Z4)/(Z3↑2-Z2*Z4)
1610 A(3)=(-K2-A(2)*Z3)/Z4
1620 PRINT USING 1460:"NEW A'S=";A
1630 GO TO 1260
```

### APPENDIX C. PSEUDOPOTENTIAL CALCULATIONS

In this appendix, we describe the local pseudopotential technique and present a computer program, written in Fortran IV, which calculates the energy levels and wave functions of Si and Ge.

Within pseudopotential theory, the Hamiltonian for an electron in the crystal can be written as

$$H = \frac{\vec{p}^2}{2m_0} + V_{ps} \quad (C.1)$$

where  $m_0$  is the electron mass,  $\vec{p}$  is its momentum and  $V_{ps}$  is the appropriately screened pseudopotential. When the full theory is employed,  $V_{ps}$  is an operator. A simplification which is often made is the assumption that the pseudopotential is a weak function of position, i.e.,  $V_{ps} = V_{ps}(r)$ . This approximation leads to the "local pseudopotential" technique. The wave functions are plane waves and are given by Eq. (5.7) of Chapter V. By Fourier analyzing  $V_{ps}$  and using Eq. (5.7) for the wave functions, we obtain the following matrix Schrödinger equation

$$\det \left| \left[ \frac{\hbar^2}{2m_0} (\vec{k} - \vec{G})^2 - E \right] \delta_{\vec{G}, \vec{G}'} + \mathcal{U}_{\vec{G} - \vec{G}'} \right| = 0 \quad (C.2)$$

where E is the energy, k is the wave vector in the Brillouin zone and  $\mathcal{U}_{\vec{G} - \vec{G}'}$  is the Fourier transform of the local pseudopotential.  $\mathcal{U}_{\vec{G} - \vec{G}'}$  is called the form factor.

The form factor of Eq. (C.2) is appropriately screened. and includes the structure factor which contains information about the geometry of the crystal. The form factor can be written as

$$\mathcal{U}_{\vec{q}} = S(\vec{q}) V_{\vec{q}} \quad (C.3)$$

where  $V_{\vec{q}}$  is the atomic form factor and  $S(\vec{q})$  is the structure factor and is given by

$$S(\vec{q}) = \frac{1}{N_t} \sum_j e^{i\vec{q} \cdot \vec{R}_j^0} \quad (C.4)$$

where  $N_t$  is the total number of atoms and  $\vec{R}_j^0$  is the atomic position. For diamond type materials,  $S(\vec{q})$  becomes

$$S(\vec{q}) = \cos(\vec{q} \cdot \vec{\tau}) \quad (\text{C.5})$$

where  $\vec{\tau}$  is a basis vector and has been defined previously in Chapter V.

In Eq. (C.4),  $V_{\vec{q}}$  is the screened atomic form factor and is given by

$$V_{\vec{q}} = V_{\vec{q}}^b / \epsilon(\vec{q}) \quad (\text{C.6})$$

where  $V_{\vec{q}}^b$  is the Fourier transform of the local bare-ion pseudopotential and  $\epsilon(\vec{q})$  is the dielectric function. The approach, which we are using for our work does not consider the division of Eq. (C.6) explicitly, i.e., the values of  $V_{\vec{q}}$  are empirical and not a result of a model potential and dielectric function. In our calculation we have used the analytic form of  $V_{\vec{q}}$  from Pantelides, which is given by:<sup>73</sup>

$$V_{\vec{q}} = \frac{2}{\Omega} \left[ b_1 \left( \frac{\pi}{a_1} \right)^{3/2} e^{-\frac{q^2}{4a_1}} + b_2 \left( \frac{\pi}{a_2} \right)^{3/2} e^{-\frac{q^2}{4a_2}} \right] \quad (\text{C.7})$$

where  $\Omega$  is the volume of a primitive cell,  $b_1=20$ ,

$b_2 = -17.7$ ,  $a_1 = 0.633$  and  $a_2 = 0.459$ . This form factor reproduces the empirical values of Cohen and Bergstresser (C-B).<sup>74</sup> For Ge, we used the C-B values.

The computer program, which we used is an adaptation of one written by S. Pantelides. It is written in Fortran IV and is designed to run on an IBM computer, which contains an International Mathematical and Statistical Library (IMSL). The subroutine, which performs the diagonalization of Eq. (C.2) is called DIAGRS and can easily handle matrices up to dimensions of  $100 \times 100$ . The subroutine allows one to output the eigenvectors and (or) eigenvalues, thus facilitating calculations of the band structures of Si and Ge. Since the program is fairly straightforward, we will not present it here. However, it is available from the author upon request.

An adaptation to zincblende materials can readily be made by modifying Eqs. (C.3) and (C.5). In this case two form factors, symmetric and antisymmetric must be used.

APPENDIX D. RIGID-ION LATTICE DYNAMICS

In this appendix, we will outline the lattice dynamics which were used to calculate the phonon eigenvectors. The treatment presented here closely follows that of Lax.<sup>71</sup>

In the rigid-ion approximation, the dynamical equation is given by

$$\sum_{\beta} \overleftrightarrow{R}_i^{\alpha\beta} \cdot \hat{e}_{\beta} = M_{\alpha} \omega^2 \hat{e}_{\alpha} \quad (D.1)$$

where  $\hat{e}_{\beta}$  is a polarization vector with a basis index  $\alpha$ .  $\overleftrightarrow{R}^{\alpha\beta}$  is the dynamical matrix, which is related to the forces between the atoms of the crystal through

$$\overleftrightarrow{R}_i^{\alpha\beta} = \sum_j \overleftrightarrow{K}_i^{\alpha\beta} (\vec{R}_{j,\beta}^0 - \vec{R}_{i,\alpha}^0) e^{i\vec{q} \cdot (\vec{R}_{j,\beta}^0 - \vec{R}_{i,\alpha}^0)} \quad (D.2)$$

where  $\overleftrightarrow{K}_i^{\alpha\beta}$  is the force matrix between the particles located at  $\vec{R}_{j,\beta}^0$  and  $\vec{R}_{i,\alpha}^0$ .

In our calculations, we will consider only the second nearest neighbors in diamond type materials. For these semiconductors, there are four nearest

neighbors. By considering the symmetry operations which leave the forces between the atoms located at  $\vec{r}_1 = (a/4)(000)$  and  $\vec{r}_2 = (a/4)(111)$  invariant, we can show that the force matrix between these two particles is given by

$$K_1^{1,2} = \begin{bmatrix} \alpha & \beta & \beta \\ \beta & \alpha & \beta \\ \beta & \beta & \alpha \end{bmatrix} \quad (\text{D.3})$$

And in a similar manner, for the second nearest neighbor, which are located at  $(a/2)(1,1,0)$  we find

$$K_2^{1,2} = \begin{bmatrix} \mu & \nu & \delta \\ \nu & \mu & \delta \\ \delta & \delta & \lambda \end{bmatrix} \quad (\text{D.4})$$

where the subscript in Eqs. (D.3) and (D.4) refers to the neighbor type, i.e., first or second nearest. The force constants for the remaining three first nearest and seven second nearest neighbors are obtained by

appropriate rotations of Eqs. (D.3) and (D.4). With this, we find the elements of the dynamical matrix to be.

$$\begin{aligned}
 R''_{xx} &= 4d + 4\mu \left\{ 2 - \cos(\pi p_x) [\cos(\pi p_y) + \cos(\pi p_z)] \right. \\
 &\quad \left. + 4\lambda [1 - \cos(\pi p_y) \cos(\pi p_z)] \right. \\
 R''_{xy} &= 4\nu \sin(\pi p_x) \sin(\pi p_y) \\
 R''_{xz} &= -4d \left[ \cos\left(\frac{\pi}{2} p_x\right) \cos\left(\frac{\pi}{2} p_y\right) \cos\left(\frac{\pi}{2} p_z\right) - \right. \\
 &\quad \left. i \sin\left(\frac{\pi}{2} p_x\right) \sin\left(\frac{\pi}{2} p_y\right) \sin\left(\frac{\pi}{2} p_z\right) \right] \quad (D.5) \\
 R''_{yz} &= 4\beta \left[ \cos\left(\frac{\pi}{2} p_z\right) \cos\left(\frac{\pi}{2} p_x\right) \sin\left(\frac{\pi}{2} p_y\right) - \right. \\
 &\quad \left. i \sin\left(\frac{\pi}{2} p_z\right) \cos\left(\frac{\pi}{2} p_x\right) \cos\left(\frac{\pi}{2} p_y\right) \right]
 \end{aligned}$$

where  $\vec{p}$  is in units of  $2\pi/a$ . The remaining components of the matrix can be obtained by using its symmetry properties. List all of the relationships between the various elements of  $R^{\alpha\beta}$ . Here, we will only present those which are derived by interchanging the indices. These are given by

$$\begin{aligned}
 R^{\alpha\beta}_{yy}(p_x, p_y, p_z) &= R^{\alpha\beta}_{xx}(p_y, p_x, p_z) \\
 R^{\alpha\beta}_{zz}(p_x, p_y, p_z) &= R^{\alpha\beta}_{xx}(p_z, p_y, p_x) \quad (D.6)
 \end{aligned}$$

In our work , we made the dynamical matrix equation real by using the transformations of Eqs. (5.10). The force constants were obtained by solving the following equations at the X point:

$$\begin{aligned} M \omega_{LA}^2(001) &= 4\alpha + 16\mu \\ M \omega_{TA}^2(001) &= 4\alpha + 8(\mu + \lambda) - 4\beta \\ M \omega_{TO}^2(001) &= 4\alpha + 8(\mu + \lambda) + 4\beta \end{aligned} \tag{D.7}$$

and at the L point we used

$$M \omega_{TA}^2(1,1,1) = 2\alpha - 2\beta + 8\mu + 4\lambda - 4\nu \tag{D.8}$$

and at the zone center

$$M \omega_{Lo}^2(0,0,0) = 4\alpha \tag{D.9}$$

These relationships were obtained by diagonalizing the dynamical matrix at the particular symmetry point. Our program sets up and diagonalizes the dynamical equation along  $\Delta$  and  $\Lambda$  and provides the eigenvectors. It also yields the eigenvalues, which as stated in the

text are not very accurate.

APPENDIX E. THE PROCEDURE FOR CALCULATING THE E-PH AND H-PH MATRIX ELEMENTS

The evaluation of Eq. (5.11) is straightforward. The form factors are obtained from the interpolations given in Chapter V and the plane wave expansion coefficients come from the procedure of Appendix C. The phonon polarization vectors are obtained from the program described in the previous appendix.

The only difficulty occurs in determining the orientation of the wave functions which are obtained from the pseudopotential program. The diagonalization program does not distinguish between equivalent orthogonal axes. For example, the  $\Gamma_{15,c}$  and  $\Gamma_{25',v}$  states were oriented along (111), (101) and (121), while the  $A_{5,v}$  states along the (001) valley were oriented along (110) and (110).

This problem necessitated an analysis of the output of the pseudopotential program. The orientation was determined by performing successive interchanges of the components of the  $\vec{G}$  vectors. Once the orientation was determined, the coefficients were entered into the program. This resulted in the use of separate programs for the e-ph and h-ph calculations.

The program to calculate the e-ph matrix elements

in Si was written in Fortran IV. It is designed in such a way that several form factors may be used. In an actual run one changes the potential simply by exchanging the comment ( the c at the beginning of a given statement)indicator. Furthermore, this version can output the result of each step of the computation. This is accomplished by removing the c's at the start of each write statement. If this is not done, only the final values of the matrix elements will be printed. A listing of this program is available from the author upon request.

REFERENCES

1. G. G. MacFarlane, T. P. McLean, J. E. Quarrington and V. Roberts, Phys. Rev. 111, 1245 (1958).
2. *ibid.*, Phys. Rev. 108, 1377 (1957).
3. P. J. Dean, Y. Yafet and J. R. Haynes, Phys. Rev. 184, 837 (1969).
4. M. R. Lorenz, R. Chicotka and G. D. Pettit, Solid State Comm. 8, 693 (1970).
5. P. J. Dean and D. G. Thomas, Phys. Rev. 150, 690 (1966).
6. T. Nishino, M. Takeda and Y. Hamakawa, Solid State Comm. 14, 627 (1974).
7. F. H. Pollak, A. Feldblum, H. D. Park and P. E. Vanier, Solid State Comm. 28, 161 (1978). This paper contains two errors; one in the expression for  $U_{T0}$  and the other in the ratio of the energy denominators. The denominator of  $U_{T0}$  should be  $E(\Delta_{1,c}) - E(\Gamma_{15,c})$  and the ratio should be  $[E(\Gamma_{15,c}) - E(\Delta_{1,c})] / [E(\Gamma_{25',v}) - E(\Delta_{5,v})] = 0.77$ . Thus the ratio  $S_{e-ph}/S_{h-ph}$  for the T0 phonon, becomes -0.73 instead of +1.4.
8. *ibid.*, Proc. 14th int. Conf. on the Physics of Semiconductors, Edinburgh, 1978, ed. by B. L. H. Wilson (Institute of Physics, Bristol and London, 1979), p. 867. This paper contains an error in the expression for  $U_{LA}$ . The denominator should be  $E(L_{1,c}) - E(\Gamma_{2',c})$ . With this, the ratio  $S_{e-ph}/S_{h-ph}$  for the LA phonon becomes -0.16 instead of +0.16.
9. H. Mathieu, P. Merle, E. L. Ameziane, B. Archilla and J. Camassel, Phys. Rev. B 19, 2209 (1979).

10. O. J. Glebocki and F. H. Pollak, Phys. Rev. B 25, 1179 (1982); ibid. Phys. Rev. B 25, 1193 (1982).
11. R. G. Humphreys, U. Rossler and M. Cardona, Phys. Rev. B 18, 5590 (1978).
12. L. D. Laude, M. Cardona and F. H. Pollak, Phys. Rev. B 1, 1436 (1970) and references therein.
13. K. L. Shaklee and R. E. Nahory, Phys. Rev. Lett. 24, 942 (1970).
14. D. F. Blossey and P. Handler, Semiconductors and Semimetals, ed. by R. K. Willardson and A. C. Beer, Vol. 9 (Academic Press, New York, 1972), p. 305.
15. See for example, D. L. Smith and T. C. McGill, Phys. Rev. B 14, 2448 (1976).
16. See for example, N. V. Alkeev, A. S. Kaminski and Ya. E. Pokrovskii, Sov. Solid State 18, 410 (1970) and references therein.
17. M. Udagawa, S. Ushioda, P. E. Forsyth and J. B. Valdez, Proc. 15th int. Conf. Physics of Semiconductors, Kyoto, 1980, J. Phys. Soc. Japan, 49 (1980) Suppl. A. p. 555 ; W. Von der Osten and J. Weber, Solid State Comm. 15, 1561 (1974) and P. B. Klein, H. J. Masui, J. Song and R. K. Chang, Solid State Comm. 14, 1163 (1974).
18. See for example, B. R. Nag, Electron Transport in Compound Semiconductors, (Springer Verlag, New York, 1980).
19. T. Inoshita and H. Kamimura, Synthetic Metals, 3, 225 (1981). 14, 2448 (1976) and references therein.
20. P. N. Butcher and W. Fawcett, Proc. Phys. Soc., ed. C. Hilsum, Vol. 86, p. 1205 (1965).
21. See for example, J. D. Wiley in Semiconductors and Semimetals, ed. by R. K. Willardson and A. C. Beer (Academic Press, New York) Vol. 10, p.91.
22. J. O. Dimmock, Semiconductors and Semimetals, ed. by R. K. Willardson and A. C. Beer (Academic Press, New York), Vol. 3, pgs. 295-297.

23. E. Erlbach, Phys. Rev. 150, 676 (1969).
24. M. Capizzi, J. C. Merle, P. Fiorini and A. Frova, Phys. Rev. B 17, 4821 (1978).
25. G. E. Pikus, Sov. Phys. Solid State, 18, 965, (1977).
26. R. J. Elliott, Phys. Rev. 108, 1384 (1957).
27. L. D. Laude, F. H. Pollak and M. Cardona, Phys. Rev B 3, 2623 (1971).
28. I. Balslev, Phys. Rev. 143, 636 (1966).
29. ibid., Phys. Soc. Jpn. Suppl. 21, 101 (1966)
30. M. L. Cohen and Y. W. Tsang, Proc. of Conf. on the Physics of Semimetals and Narrow-Gap Semiconductors, ed. by D. L. Carter and R. T. Bates (Pergamon, New York, 1971), p. 303.
31. P. B. Allen and M. Cardona, Phys. Rev. B 23, 1495 (1981).
32. M. Schluter, G. Martinez and M. L. Cohen, Phys. Rev. B 12, 650 (1975).
33. M. Lax and J. J. Hopfield, Phys. Rev. 124, 115 (1961).
34. In Ref. 8, the scattering via  $\Gamma_{15,c}$  was left out of the expression for the oscillator strength of the LA phonon.
35. F. Bassani and G. P. Parravicini, Electronic States and Optical Transitions in Solids, (Pergamon, New York, 1975).
36. E. J. Johnson, in Semiconductors and Semimetals, ed. by R. K. Willardson and A. C. Beer (Academic Press, New York, 1967), vol. 3, p. 190.
37. See for example, C. Kittel, Introduction to Solid State Physics, (Wiley, New York, 1976).
38. N. O. Lipari and A. Baldereschi, Phys. Rev. B 8, 2497 (1971).

39. F. H. Pollak and M. Cardona, Phys. Rev. 172, 816 (1968) and references therein.
40. H. Brooks, in Advances in Electronics and Electron Physics, ed. L. Marton (Academic Press, New York, 1955).
41. F. H. Pollak, Surf. Sci. 37, 863 (1973).
42. M. Cardona, Modulation Spectroscopy, (Academic Press, New York, 1969).
43. M. Chandresekhar, Ph.D. Thesis, Brown University, 1977, unpublished.
44. F. H. Pollak, Phys. Rev. 138, A618 (1965); A Feldman, Phys. Rev. 150, 748 (1966).
45. M. Cardona and F. H. Pollak, Phys. Rev. 142, 530 (1966); F. H. Pollak, C. W. Higginbottom and M. Cardona, Proc. Int. Conf. on Physics of Semicond., Kyoto, 1966 [J Phys. Soc. Jpn. Suppl. 21, 20 (1966)]; C. W. Higginbottom, F. H. Pollak and M. Cardona, Proc. Int. Conf. Physics of Semicond., Moscow, 1968 (Nauka, Leningrad, 1968), p. 57.
46. P. Lawaetz, Solid State Comm. 16, 65 (1975).
47. M. Altarelli and R. A. Sabatini, Solid State Comm. 16, 1101 (1978).
48. T. Nishino, M. Takeda, and Y. Hamakawa, Solid State Comm. 12, 1137 (1973).
49. B. Batz, in Semiconductors and Semimetals, ed. by R. K. Willardson and A. C. Beer, (Academic Press, New York, 1967), vol. 3, p. 296.
50. J. S. Kline, F. H. Pollak and M. Cardona, Helvetica Physica Acta, 41, 968 (1968).
51. M. Chandresekhar and F. H. Pollak, Phys. Rev. B 15, 2127 (1977).
52. P. J. Dean, G. Kaminsky and R. B. Zetterstrom, J. Appl. Phys. 38, 3351 (1957).
53. S. E. Stokowski and D. D. Sell, Phys. Rev. B 5, 1636 (1972).

54. R. A. Forman, W. R. Thurber and D. E. Aspnes, Solid State Comm. 14, 1007 (1974).
55. B. N. Brockhouse, Phys. Rev. Lett. 2, 256 (1959).
56. B. N. Brockhouse and P. K. Iyengar, Phys. Rev. 111, 747 (1958).
57. R. M. Martin, Phys. Rev. Lett. 21, 536 (1968).
58. J. I. Pankove, Optical Processes in Semiconductors, (Dover, New York, 1971).
59. J. M. Woodall, Science 208, 908 (1980).
60. The 218 K values are not included in the the averages because of the difficulty encountered in Ref. 5, in their analysis of the data at this temperature.
61. L. J. Sham and J. M. Ziman, in Solid State Physics, ed. by F. Seitz and D. Turnbull (Academic Press, New York, 1963).
62. J. M. Ziman, Electrons and Phonons, (Oxford Univ. Press, London and New York, 1960).
63. L. Nordheim, Ann. Physik, 9, 607 (1931).
64. J. C. Phillips and L. Kleinman, Phys. Rev. 116, 287 (1959).
65. M. H. Cohen and V. Heine, Phys. Rev. 122, 1821 (1961).
66. W. A. Harrison, Pseudopotentials in the Theory of Metals, (Benjamin, New York, 1966).
67. V. Heine, Solid State Physics, ed. by H. Ehrenreich, F. Seitz and D. Turnbull, (Academic Press, New York, 1970).
68. M. L. Cohen and V. Heine, Solid State Physics, ed. by H. Ehrenreich, F. Seitz and D. Turnbull, (Academic Press, New York, 1970). This article and the one of the previous reference present excellent reviews of pseudopotential theory.
69. J. M. Ziman, Theory of Solids, (Cambridge Univ. Press, London and New York, 1972), 2nd ed.. This book has a very good description of the

pseudopotential technique, in particular; the non-local nature of the pseudopotential.

70. L. J. Sham, Proc. Phys. Soc. 78, 895 (1961).
71. M. Lax, Symmetry Principles in Solid State and Molecular Physics, (Wiley, New York, 1974).
72. O. J. Glembocki and F. H. Pollak, Phys. Rev. Lett. 48, 415 (1982).
73. S. Pantelides, private communication; J. Bernholc, N. O. Lipari and S. Pantelides, Phys. Rev. B 21, 5545 (1980).
74. M. L. Cohen and T. K. Bergstresser, Phys. Rev. 141, 789 (1966).
75. In order to obtain good results, the calculation must include at least fifth nearest neighbors.
76. P. B. Allen, private communication; W. Weber, Phys. Rev. B 15, 4789 (1977).
77. In Ref. 68, the importance of the large  $q$  region is noted for phonon calculations.
78. The calculations of Ref. 72 used 77 K values for the indirect transitions and 300 K values for the other important optical transitions. In this thesis, we have used only values at 300 K. The energy differences calculated in this fashion were within 10 % of those obtained from M. Welkowsky and R. Braunstein, Phys. Rev. B 5, 497 (1972). The 77 K numbers were not used because they did not include a value for the  $E'_0$  transition.
79. S. Bednarek and U. Rossler, Verhandl. DPG, 16, R 153 (1981); Phys. Rev. Lett. 48, 1296 (1982).
80. O. J. Glembocki and F. H. Pollak, Phys. Rev. B 25, 7865 (1982).
81. M. G. Craford, R. Shaw, A. H. Herzog and W. O. Groves, J. Appl. Phys. 43, 4075 (1972).
82. A. Onton and L. M. Foster, J. Appl. Phys. 43, 5084 (1972).

83. N. M. Sirota, I. V. Bodner, A. I. Lukomskii, G. F. Smirnova and L. M. Finkel'shtein, Sov. Phys. Semicond. 10, 671 (1976).
84. R. Tsu, Proc. Nato Advanced Study Inst. on "Excitations In Disordered systems", (Plenum Press, New York, 1981).
85. B. Batz, Ph.D. Thesis, Univ. Libre de Bruxelles, 1967, unpublished.
86. O. J. Glembocki and F. H. Pollak, in press, Proc. 16th Int. Conf. on Physics of Semicond., Montpellier, France, 1982.
87. K. Kunc and R. M. Martin, Phys. Rev. Lett. 24, 2311 (1981).

LIST OF TABLES

TABLE	PAGE
I.	Theoretical expressions for the oscillator strength in $\langle 001 \rangle$ indirect gap materials.....150
II.	Theoretical expressions for the oscillator strength in $\langle 111 \rangle$ indirect gap materials..... 151
III.	Experimental values of the spin orbit splittings, elastic compliance constants and various deformation potentials in Si and GaP..154
IV.	Summary of the allowed $\Gamma-L$ and $\Gamma-\Delta(X)$ transitions for stresses along $[001]$ and $[111]$ .....155
V.	Theoretical expressions for the LA phonon assisted transitions in GaP for stress along $[001]$ and $[111]$ and light polarized parallel and perpendicular to the stress.....156
VI.	Theoretical expressions for the TA and TO phonon assisted transitions in GaP for stress along $[001]$ and $[111]$ and light polarized parallel and perpendicular to the stress axis..157
VII.	Theoretical expressions for the LO phonon assisted transitions in GaP for stress along

	[001] and [111] and light polarized parallel and perpendicular to the stress axis.....	158
VIII.	Theoretical expressions for the LA phonon assisted transitions in Ge for stress along [001] and [111] and light polarized parallel and perpendicular to the stress axis.....	159
IX.	Experimental and theoretical values of the intensities of the LA phonon assisted transition in GaP as a function of stress and light polarization.....	161
X.	Experimental values of various optical transitions in Si, Ge and GaP.....	162
XI.	Phonon energies at various points in the Brillouin zone for Si, Ge and GaP.....	164
XII.	Optical matrix elements and various materials parameters in Si, Ge and GaP.....	165
XIII.	Experimental and theoretical values of the intensities for the TA phonon assisted transition in GaP as a function of stress and light polarization.....	167
XIV.	Values of the phonon occupation number and the slopes of $\sqrt{2\hbar\omega}$ for the TO phonon of Si. The	

	slopes are obtained from the data of Ref. 2....	168
XV.	Experimental values of the e-ph and h-ph matrix elements for the $\langle 001 \rangle$ TO phonon assisted transition of Si.....	169
XVI.	Experimental values of the absorption coefficient for the LA and TA $\langle 001 \rangle$ phonons of GaP.....	171
XVII.	Experimental values of the e-ph and h-ph matrix elements for the LA and TA $\langle 001 \rangle$ phonon assisted transitions of GaP.....	172
XVIII.	Theoretical and experimental values of the e-ph and h-ph matrix elements for the $\Gamma - \Delta$ transitions (TO, LO, TA, LA) of Si.....	173
XIX.	Theoretical and experimental values of the coefficient $A_{\text{ex}f_1}$ , for the $\Gamma - \Delta$ transitions of Si.....	174
XX.	Potential parameters for the Si form factor.....	175
XXI.	Potential parameters for the Ge form factor.....	176
XXII.	Calculated values of the e-ph and h-ph matrix elements for the $\Gamma - L$ transitions (LA, TO) of Ge.....	177

- XXIII. Theoretical and experimental values of the coefficient,  $A_{ex}$ , for the  $\Gamma - L$  transitions of Ge.....178
- XXIV. Theoretical and experimental values for the relative intensities of the LA phonon assisted transitions in Ge as a function of stress and light polarization.....179
- XXV. Theoretical and experimental values of the e-ph and h-ph matrix elements for the  $\Gamma - L$  transitions (LA and TO) in Si.....180
- XXVI. Theoretical and experimental values of the total of the  $\Gamma - \Delta$  and  $\Gamma - L$  contributions to the absorption coefficient of Si.....182
- XXVII. Theoretical values of the e-ph and h-ph matrix elements in Si, for scattering midway into the zone along  $\Delta$ . Also listed are the individual contributions of each phonon to the absorption coefficient.....183
- XXVIII. Calculated values of the e-ph and h-ph matrix elements for  $\Gamma - \Delta$  scattering in Ge, both midway into the Brillouin zone and to  $\vec{k} = (2\pi/a)(0,0,0.85)$ .....184
- XXIX. Calculated values of the e-ph and h-ph matrix

elements in Ge for scattering midway into the  
Brillouin zone along  $\Lambda$  .....185

XXX. Summary of all of the e-ph and h-ph matrix  
elements for  $\Gamma - \Delta(X)$  scattering in Si, Ge and  
GaP.....186

XXXI. Summary of all of the e-ph and h-ph matrix  
elements for  $\Gamma - L$  scattering in Si and Ge....187

TABLE I. Theoretical expressions for the "oscillator strengths" of the LA-, LO-, TA-, and TO- (creation) phonon-assisted transitions in (001) indirect materials. The subscript  $\ell$  refers to the phonon branch being considered.

Phonon branch ( $\ell$ )	Oscillator strength ( $f_\ell$ ) <sup>a</sup>
TA, TO (Si, GaP, AlSb, AlAs)	$\frac{6}{5} [U_\ell^2 + (U_\ell + V_\ell)^2]$
LA (GaP, AlSb) LO (Si, AlAs)	$\frac{4}{3} [W_\ell^2 + 2(W_\ell + V_\ell)^2]$
LO (GaP, AlSb) LA (Si, AlAs)	$\frac{6}{5} (U_\ell + V_\ell)^2$
	$U_\ell = \frac{\langle \Gamma_{8,v}^2   p_x   \Gamma_{15,c}^2 \rangle \langle \Gamma_{15,c}^2   \mathcal{H}^2   X_{1,c} \rangle^2}{E(X_{1,c}) - E(\Gamma_{15,c}) - (\hbar\omega)_\ell}$
	$W_\ell = \frac{\langle \Gamma_{8,v}^2   p_x   \Gamma_{1,c} \rangle \langle \Gamma_{1,c}   \mathcal{H}   X_{1,c} \rangle^2}{E(X_{1,c}) - E(\Gamma_{1,c}) - (\hbar\omega)_\ell}$
	$V_\ell = \frac{\langle \Gamma_{8,v}^2   \mathcal{H}^2   X_{5,v}^2 \rangle \langle X_{5,v}^2   p_x   X_{1,c} \rangle^2}{E(\Gamma_{8,v}) - E(X_{5,v}) + (\hbar\omega)_\ell}$

<sup>a</sup>These expressions apply to the zinc-blende materials. For Si,  $\Gamma_{8,v}^2$  becomes  $\Gamma_{25,v}^2$ ,  $\Gamma_{15,c}$  is replaced by  $\Gamma_{2,c}$ ,  $X_{5,v}^2$  becomes  $\Delta_{5,v}^2$ , and  $X_{1,c}$  is replaced by  $\Delta_{1,c}$ . For the TO phonon,  $\mathcal{H}^2$  becomes  $\mathcal{H}$ .

Table II. Theoretical expressions for the oscillator strength of the  $\Gamma-L$ , LA and TO phonon assisted transitions. Expressions are also listed for the transitions from the spin orbit split valence band. For the LA phonon, the conduction band scattering via the  $\Gamma_{15,c}$  state is included.

Phonon	Initial State	$\Gamma_{8,v}^+$	$\Gamma_{7,v}^+$ (a)
LA		$\frac{4}{3} \left[ 2 \left( W_{LA} + \frac{5V_{LA}}{3} - U_{LA} \right)^2 + \left( U_{LA} - \frac{2V_{LA}}{3} \right)^2 \right]$	$\frac{1}{3} (W_{LA} + U_{LA})^2 + (W_{LA} + \frac{8V_{LA}}{9} - \frac{1}{3}U_{LA})^2 + \frac{2}{9} \left( \frac{2V_{LA}}{3} - U_{LA} \right)^2$
TO		$\frac{1}{3} \left[ U_{TO}^2 + \frac{16}{3} \left( U_{TO} - \frac{5X_{TO}}{3} \right)^2 + \frac{5}{3} \left( U_{TO} + \frac{4}{3} \cdot 2 V_{TO} \right)^2 \right]$	$\frac{1}{6} U_{TO}^2 + \frac{16}{3} \left( U_{TO} - \frac{5X_{TO}}{3} \right)^2 + \frac{5}{3} \left( U_{TO} + \frac{4}{3} \cdot 2 V_{TO} \right)^2$

Table II. continued

$$W_{LA} = \frac{\langle L_{1,c} | H_{LA} | \Gamma_{2,c} \rangle \langle \Gamma_{2,c} | P_x^- | \Gamma_{8,v}^+ \rangle}{E(L_{1,c}) - E(\Gamma_{8,v}^+) - \hbar\omega_{LA}}$$

$$U_{LA} = \frac{\langle L_{1,c} | H_{LA} | \Gamma_{2,c} \rangle \langle \Gamma_{2,c} | P_z^- | \Gamma_{8,v}^+ \rangle}{E(L_{1,c}) - E(\Gamma_{8,v}^+) - \hbar\omega_{LA}}$$

$$V_{LA} = \frac{\langle \Gamma_{8,v}^+, \bar{x} | H_{LA} | \bar{x} | L_{3',v} \rangle \langle L_{3',v} | P_x^- | L_{1,c} \rangle}{E(\Gamma_{8,v}^+) - E(L_{3',v}) + \hbar\omega_{LA}}$$

$$U_{TO} = \frac{\langle L_{1,c} | H_{TO} | \Gamma_{15,c} \rangle \langle \Gamma_{15,c} | P_z^- | \Gamma_{8,v}^+ \rangle}{E(L_{1,c}) - E(\Gamma_{8,v}^+) - \hbar\omega_{LA}}$$

$$V_{TO} = \frac{\langle \Gamma_{8,v}^+, \bar{x} | H_{TO} | \bar{x} | L_{3',v} \rangle \langle L_{3',v} | P_x^- | L_{1,c} \rangle}{E(\Gamma_{8,v}^+) - E(L_{3',v}) + \hbar\omega_{TO}}$$

Table II continued.

$$X_{TO} = \frac{\langle \Gamma_{8,v}^{+,z} | H_{TO}^{\bar{x}} | L_{3',v}^{\bar{x}} \rangle \langle L_{3',v}^{\bar{x}} | P_{\bar{x}} | L_{1,c} \rangle}{E(\Gamma_{8,v}^{+}) - E(L_{3',v}) + \hbar\omega_{TO}}$$

a. For the spin orbit split band,  $\Gamma_{7,v}^{+}$  replaces  $\Gamma_{8,v}^{+}$ . When the spin orbit splitting is neglected,  $\Gamma_{25',v}$  will be used instead of the above notation for the valence band.

Table III. Experimental values of the spin orbit splitting, elastic compliance constants and various deformation potentials in Si and GaP. Ge is not included, because its values are not needed.

	$\Delta_o$ (eV)	$S_{11}$ ( $10^{-12}$ dyn $^{-1}$ -cm $^2$ )	$S_{12}$ ( $10^{-12}$ dyn $^{-1}$ -cm $^2$ )	$S_{44}$ ( $10^{-12}$ dyn-cm $^2$ )	$\xi_2$ (eV)	
Si <sup>a</sup>	0.044	0.863	-0.213	1.249	8.7 ± 0.4	
Gap <sup>b</sup>	0.090	0.973	-0.299	1.490	6.3 ± 0.9	
	$\xi_1^{+a_1}$ (eV)	$a_2$ (eV)	$b_1$ (eV)	$b_2$ (eV)	$d_1$ (eV)	$d_2$ (eV)
Si <sup>a</sup>	1.5±0.3	0.0	-1.9±0.15	-0.1±0.15	-4.7±0.25	-0.005±0.25
Gap <sup>b</sup>	2.7±0.5	-0.4±0.3	-1.9±0.3	0.2±0.2	-5.2±0.2	0.3±0.2

a. Ref. 9.  
b. Ref. 12.

Table IV. Summary of the various allowed  $\Gamma-L$  and  $\Gamma-\Delta(X)$  transitions for stresses along (001) and (111). The label inside the parenthesis refers to the  $\Gamma-L$  transitions, while the one outside is used for the  $\Gamma-\Delta(X)$  processes.

Transition	$\Gamma-\Delta(X)$	$\Gamma-L$
$\Gamma-\Delta(\Gamma-L)$	$\vec{x} \parallel [001]$	$\vec{x} \parallel [111]$
$A_1 (B_1)$	$v_1 \rightarrow (100), (010), (001)$	$v_1 \rightarrow (111), (111), (111)$
$A_2 (B_2)$	$v_2 \rightarrow (100), (010), (001)$	$v_2 \rightarrow (111), (111), (111)$
$B_1 (A_1)$	$v_1 \rightarrow (001)$	$v_1 \rightarrow (111)$
$B_2 (A_2)$	$v_2 \rightarrow (001)$	$v_2 \rightarrow (111)$
$B_3 (A_3)$	$v_1 \rightarrow (100), (010)$	$v_1 \rightarrow (111), (111), (111)$
$B_4 (A_4)$	$v_2 \rightarrow (100), (010)$	$v_2 \rightarrow (111), (111), (111)$

Table V. Theoretical expressions for the relative intensities of the LA-phonon-assisted indirect transition in GaP (LO-phonon-assisted transition in Si) as a function of stress, for  $\bar{X}||[001]$  and  $\bar{X}||[111]$  and light polarized parallel and perpendicular to the stress axis. The quantities  $n_0$ ,  $m_0$ ,  $n_1$ ,  $m_1$ ,  $\delta E'_{001}$ , and  $\delta E'_{111}$  are defined in Chpt. III. The matrix elements of  $\mathcal{H}_{LA}$  are referred to the (001) valley.

	$\bar{E}  \bar{X}$	$\bar{E}  \bar{X}$
$\bar{X}  [001]$		
$B_1 [v_1 \rightarrow (001)]$	$\frac{2}{3} \eta_2^0 W_{LA}^2$	$\frac{1}{6} \eta_1^0 (W_{LA} + V_{LA})^2$
$B_2 [v_2 \rightarrow (001)]$	0	$\frac{1}{2} (W_{LA} + V_{LA})^2$
$B_3 [v_1 \rightarrow (100), (010)]$	$\frac{4}{3} \eta_2^0 (W_{LA} + V_{LA})^2$	$\frac{1}{6} \eta_1^0 [(W_{LA} + V_{LA})^2 + W_{LA}^2]$
$B_4 [v_2 \rightarrow (100), (010)]$	0	$\frac{1}{2} [(W_{LA} + V_{LA})^2 + W_{LA}^2]$
$\bar{X}  [111]$		
$A_1 [v_1 \rightarrow (001), (010), (100)]$	$2\eta_2^0 (W_{LA}^2 + \frac{4}{3} W_{LA} V_{LA} + \frac{1}{3} V_{LA}^2)$ $-\frac{1}{9} (\mu - \frac{1}{3} \gamma) V_{LA}^2$ $\frac{1}{3} V_{LA}^2$	$\frac{1}{3} \eta_1^0 (W_{LA}^2 + \frac{4}{3} W_{LA} V_{LA} + V_{LA}^2)$ $+\frac{1}{9} (\mu + \frac{1}{3} \gamma) V_{LA}^2$ $\frac{1}{3} (3W_{LA}^2 + 4W_{LA} V_{LA} + \frac{2}{3} V_{LA}^2)$
$A_2 [v_2 \rightarrow (001), (010), (100)]$		
$W_{LA} = \langle \Gamma_{8,p}^+   p_x   \Gamma_{1,c} \rangle \langle \Gamma_{1,c}   \mathcal{H}_{LA}   X_{1,c} \rangle / [E(X_{1,c}) - E(\Gamma_{1,c}) - (\hbar\omega)_{LA}]$		
$V_{LA} = \langle \Gamma_{8,p}^+   \mathcal{H}_{LA}   X_{3,p}^+ \rangle \langle X_{3,p}^+   p_x   X_{1,c} \rangle / [E(\Gamma_{8,p}) - E(X_{3,p}) + (\hbar\omega)_{LA}]$		
$\eta_1^0 = [n_0(n_0 - m_0)]^{-1} [(n_0 - m_0) - \delta E'_{001}]^2$		
$\eta_2^0 = [n_0(n_0 - m_0)]^{-1} [\frac{1}{2}(n_0 - m_0) + \delta E'_{001}]^2$		
$\eta_1 = [n_1(n_1 - m_1)]^{-1} [(n_1 - m_1) - \delta E'_{111}]^2$		
$\eta_2 = [n_1(n_1 - m_1)]^{-1} [\frac{1}{2}(n_1 - m_1) + \delta E'_{111}]^2$		
$\mu = \frac{1}{3} (\eta_2 - \eta_1)$		
$\gamma = \delta E'_{111} / n_1$		

Table VI. Theoretical expressions for the relative intensities of the TO- and TA-phonon-assisted indirect transition in GaP as a function of stress for  $\bar{X}||[001]$  and  $\bar{X}||[111]$  and light polarized parallel and perpendicular to the stress axis. The quantities  $n_0$ ,  $n_1$ ,  $m_1$ ,  $\delta E'_{001}$ , and  $\delta E'_{111}$  are defined in Chapter I. In the expressions below, the subscript  $T$  refers to either TO or TA phonon. The matrix elements of  $\mathcal{R}_T^0$  are referred to the (001) valley. Note that the  $\eta_j$  and  $\eta'_j$  of this table correspond, respectively, to  $\eta_j$  and  $\eta'_j$  in Ref. 7. For the TO phonon  $\mathcal{R}_T^0$  becomes  $\mathcal{R}_T^*$ .

	$\bar{E}  \bar{X}$	$\bar{E}  \bar{X}$
$\bar{X}  [001]$		
$B_1 [v_1 \rightarrow (001)]$	$\frac{1}{3} \eta_1^0 U_T^2$	$\frac{2}{3} \eta_1^0 (U_T + V_T)^2$
$B_2 [v_2 \rightarrow (001)]$	$U_T^2$	0
$B_3 [v_1 \rightarrow (100), (010)]$	$\frac{1}{3} \eta_1^0 (U_T + V_T)^2$	$(\frac{1}{6} \eta_1^0 + \frac{2}{3} \eta_2^0) U_T^2 + \frac{1}{6} \eta_1^0 (U_T + V_T)^2$
$B_4 [v_2 \rightarrow (100), (010)]$	$(U_T + V_T)^2$	$\frac{1}{2} [U_T^2 + (U_T + V_T)^2]$
$\bar{X}  [111]$		
$A_1 [v_1 \rightarrow (001), (010), (100)]$	$2\eta_1^0 (U_T^2 + U_T V_T) + \frac{2}{3} V_T^2$	$\eta_1^0 (U_T^2 + U_T V_T) + \frac{2}{3} V_T^2$
$A_2 [v_2 \rightarrow (001), (010), (100)]$	$\frac{2}{3} (U_T^2 + V_T^2 + U_T V_T)$	$\frac{1}{3} (5U_T^2 + 2V_T^2 + U_T V_T)$
$U_T = (\Gamma_{15,c}^*   p_x   \Gamma_{15,c}^* \langle \mathcal{R}_T^0   X_{1,c} \rangle / [E(X_{1,c}) - E(\Gamma_{15,c}) - (\hbar\omega)_T]$		
$V_T = (\Gamma_{15,c}^*   p_x   \mathcal{R}_T^0 \langle X_{3,c}^*   p_x   X_{1,c} \rangle / [E(\Gamma_{15,c}) - E(X_{3,c}) + (\hbar\omega)_T]$		
$\eta_1^0 = [n_0(n_0 - m_0)]^{-1} [(n_0 - m_0) - \delta E'_{001}]^2$		
$\eta_2^0 = [n_0(n_0 - m_0)]^{-1} [\frac{1}{3}(n_0 - m_0) + \delta E'_{001}]^2$		
$\eta_3^0 = [n_1(n_1 - m_1)]^{-1} [(\delta E'_{111})^2 + \frac{1}{3}(n_1 - m_1)^2 + \frac{2}{3}\delta E'_{111}(n_1 - m_1)]$		
$\eta_4^0 = [n_1(n_1 - m_1)]^{-1} [(\delta E'_{111})^2 + \frac{2}{3}(n_1 - m_1)^2 - \frac{2}{3}\delta E'_{111}(n_1 - m_1)]$		

Table VII. Theoretical expressions for the relative intensities of the LO-phonon-assisted indirect transition in GaP (LA-phonon-assisted transition in Si) as a function of stress for  $\bar{X}||[001]$  and  $\bar{X}||[111]$  and light polarized parallel and perpendicular to the stress axis. The quantities  $n_0$ ,  $m_0$ ,  $n_1$ ,  $\delta E'_{001}$ , and  $\delta E'_{111}$  are defined in Chpt. III. The matrix elements of  $\mathcal{H}_{LO}$  are referred to the (001) valley.

	$\bar{E}  \bar{X}$	$\bar{E}\perp\bar{X}$
$\bar{X}  [001]$		
$B_1 [v_1 \rightarrow (001)]$	0	$\frac{1}{6} \eta_1^2 (U_{LO} + V_{LO})^2$
$B_2 [v_2 \rightarrow (001)]$	0	$\frac{1}{2} (U_{LO} + V_{LO})^2$
$B_3 [v_1 \rightarrow (100), (010)]$	$\frac{1}{3} \eta_1^2 (U_{LO} + V_{LO})^2$	$\frac{2}{3} \eta_1^2 (U_{LO} + V_{LO})^2$
$B_4 [v_2 \rightarrow (100), (010)]$	$(U_{LO} + V_{LO})^2$	0
$\bar{X}  [111]$		
$A_1 [v_1 \rightarrow (001), (010), (100)]$	$\frac{1}{9} (\frac{1}{2} \eta_1 + 8\eta_2 + \frac{1}{2} \eta_3) (U_{LO} + V_{LO})^2$	$\frac{1}{9} (\frac{1}{2} \eta_1 + 2\eta_2 + \eta_3) (U_{LO} + V_{LO})^2$
$A_2 [v_2 \rightarrow (001), (010), (100)]$	$\frac{1}{3} (U_{LO} + V_{LO})^2$	$\frac{2}{3} (U_{LO} + V_{LO})^2$
$U_{LO} = \langle \Gamma_{15,c}^+   p_x   \Gamma_{15,c}^+ \rangle \langle \Gamma_{15,c}^+   \mathcal{H}_{LO}^+   X_{1,c} \rangle \langle X_{1,c}   E(X_{1,c}) - E(\Gamma_{15,c}) - (\hbar\omega)_{LO} \rangle$		
$V_{LO} = \langle \Gamma_{15,c}^+   p_x   \mathcal{H}_{LO}^+   X_{3,p}^+ \rangle \langle X_{3,p}^+   p_x   X_{1,c} \rangle \langle X_{1,c}   E(\Gamma_{15,c}) - E(X_{3,p}) + (\hbar\omega)_{LO} \rangle$		
$\eta_1^0 = [n_0(n_0 - m_0)]^{-1} [(n_0 - m_0) - \delta E'_{001}]^2$		
$\eta_2^0 = [n_0(n_0 - m_0)]^{-1} [\frac{1}{2}(n_0 - m_0) + \delta E'_{001}]^2$		
$\eta_1^1 = [n_1(n_1 - m_1)]^{-1} [(n_1 - m_1) - \delta E'_{111}]^2$		
$\eta_2^1 = [n_1(n_1 - m_1)]^{-1} [\frac{1}{2}(n_1 - m_1) + \delta E'_{111}]^2$		
$\eta_3^1 = [n_1(n_1 - m_1)]^{-1} [(n_1 - m_1) + \delta E'_{111}]^2$		

Table VIII. Polarization dependent relative intensities of the LA phonon assisted  $\Gamma_2$ -L transition for  $\vec{X} \parallel [111]$  and  $\vec{X} \parallel [001]$  and  $\vec{E} \perp \vec{X}$  and  $\vec{E} \parallel \vec{X}$ . Scattering from  $\Gamma_{15,c}$  is included. The quantities  $W_{LA}$ ,  $U_{LA}$  and  $V_{LA}$  are defined in Table II.

$\vec{X} \parallel [111]$	$\vec{E} \parallel \vec{X}$	$\vec{E} \perp \vec{X}$
$A_1$	$\frac{2}{3}(W_{LA} + U_{LA})^2$	$\frac{1}{6}(W_{LA} - \frac{1}{2}U_{LA} + V_{LA})^2$
$A_2$	0	$\frac{1}{2}(W_{LA} - \frac{1}{2}U_{LA} + V_{LA})^2$
$A_3$	$2(W_{LA} - \frac{1}{3}U_{LA} + V_{LA})^2$ $+ \frac{4}{81}(V_{LA} - \frac{3}{2}U_{LA})^2$	$\frac{1}{6}(W_{LA} - \frac{1}{2}U_{LA} + V_{LA})^2$ $+ \frac{1}{3}(W_{LA} + \frac{1}{2}U_{LA} + \frac{1}{3}V_{LA})^2$ $+ \frac{4}{27}(V_{LA} - \frac{3}{2}U_{LA})^2$
$A_4$	$\frac{4}{27}(V_{LA} - \frac{3}{2}U_{LA})^2$	$\frac{1}{2}(W_{LA} - \frac{1}{2}U_{LA} + V_{LA})^2$ $+ (W_{LA} + \frac{1}{2}U_{LA} + \frac{1}{3}V_{LA})^2$ $+ \frac{4}{27}(V_{LA} - \frac{3}{2}U_{LA})^2$

Table VIII. continued

$\vec{x} \parallel [001]$	$\vec{E} \parallel \vec{x}$	$\vec{E} \perp \vec{x}$
$B_1$	$\frac{8}{3} (w_{LA} + \frac{2}{3}v_{LA})^2$ $+ \frac{4}{27} (v_{LA} - \frac{3}{2}u_{LA})^2$	$\frac{2}{3} (w_{LA} + \frac{2}{3}v_{LA})^2$ $+ \frac{10}{27} (v_{LA} - \frac{3}{2}u_{LA})^2$
$B_2$	$\frac{4}{9} (v_{LA} - \frac{3}{2}u_{LA})^2$	$2 (w_{LA} + \frac{2}{3}v_{LA})^2$ $+ \frac{2}{9} (v_{LA} - \frac{3}{2}u_{LA})^2$

Table IX. Experimental and theoretical values of the intensities for the LA phonon assisted transition in GaP as a function of stress for  $\vec{X} \parallel [001]$  and  $\vec{X} \parallel [111]$  and  $\vec{E} \parallel \vec{X}$  and  $\vec{E} \perp \vec{X}$ . The relative and actual (in parentheses in units of  $\text{cm}^{-1}$ ) experimental values were obtained by multiplying  $d\alpha/dE$  by the broadening parameter  $\Gamma$ . The theoretical values were calculated from the expressions in Table V using  $W_{\text{LA}}/V_{\text{LA}} = -4.5$ .

$\vec{X} \parallel [001]$ ( $X = 5.68 \times 10^9 \text{ dyn-cm}^{-2}$ )	$\vec{E} \parallel \vec{X}$		$\vec{E} \perp \vec{X}$	
	Exp.	Theory	Exp.	Theory
B <sub>1</sub>	52% (0.338)	45%	6% (0.018)	4%
B <sub>2</sub>	0%	0%	19% (0.054)	23%
B <sub>3</sub>	48% (0.308)	55%	16% (0.042)	11%
B <sub>4</sub>	0%	0%	59% (0.165)	62%
$\vec{X} \parallel [111]$ ( $X = 7.35 \times 10^9 \text{ dyn-cm}^{-2}$ )	$\vec{E} \parallel \vec{X}$		$\vec{E} \perp \vec{X}$	
	Exp.	Theory	Exp.	Theory
A <sub>1</sub>	100% (0.261)	99%	12% (0.027)	14%
A <sub>2</sub>	0%	1%	88% (0.195)	86%

Table X. Experimental values of various optical transitions (in eV) in Si, Ge, and GaP. Also listed is exciton Rydberg (eV).

	Si <sup>a</sup>	Ge <sup>b</sup>	GaP
R	0.0143 <sup>c</sup>	0.0039 <sup>d</sup>	0.020 <sup>e</sup>
E <sub>ind</sub> (primary)	1.10 <sup>f</sup>	0.735 <sup>g</sup>	2.320 <sup>e,h</sup>
E <sub>0</sub> ( $\Gamma_{25',v} \rightarrow \Gamma_{2',c}$ )	4.0 <sup>a</sup>	0.880 <sup>i</sup>	2.870 <sup>j</sup>
E' <sub>0</sub> ( $\Gamma_{25',v} \rightarrow \Gamma_{15,c}$ )	3.32 <sup>a</sup>	3.23 <sup>a,k</sup>	4.47 <sup>j</sup>
E <sub>1</sub> (L <sub>3,v</sub> ' $\rightarrow$ L <sub>1,c</sub> )	3.37 <sup>a</sup>	2.375 <sup>i</sup>	- <sup>l</sup>
E <sub>2</sub> ( $\Delta_{5,v} \rightarrow \Delta_{1,c}$ )	4.31 <sup>a</sup>	- <sup>l</sup>	5.21 <sup>m</sup>
E' <sub>ind</sub> (secondary gap)	1.65 <sup>n</sup>	1.0 <sup>o</sup>	- <sup>l</sup>

- a. Ref. 50. These are 300 K values, except for E'<sub>ind</sub>, which is a low temperature number.
- b. All values are at 77 K.
- c. Ref. 13.
- d. Ref. 37.
- e. Ref. 11.
- f. Ref. 2.
- g. Ref. 1.
- h. Ref. 9. This is a 77 K value.

Table X continued.

- 
- i. Ref. 51.
  - j. Ref. 52.
  - k. The value of Ref. 50 is a 300 K number. In order to estimate the 77 K value, we added 0.10 eV to the 300 K number. The accuracy of this quantity is not critical to the calculation in Ge.
  - l. Values which are not listed were not needed in our work.
  - m. Ref. 53. This is a 2 K value.
  - n. Ref. 54.
  - o. Ref. 43.
- 
-

Table XI. Phonon energies at various points in the Brillouin zone for Si, Ge and GaP. The values are listed in units of  $10^{-3}$ eV (meV).

(X)	LA	TA	TO	LO
Si ( $\Delta$ )	44.0 <sup>a</sup>	18.0 <sup>a</sup>	57.0 <sup>a</sup>	55.0 <sup>a</sup>
Ge ( $\Delta$ )	25.0 <sup>b</sup>	10.0 <sup>b</sup>	33.0 <sup>b</sup>	29.0 <sup>b</sup>
GaP (X)	31.0 <sup>c</sup>	13.0 <sup>c</sup>	47.0 <sup>c</sup>	44.0 <sup>c</sup>
$\vec{k} = \frac{2\pi}{a}(0,0,0.5)$	LA	TA	TO	LO
Si	31.0 <sup>a</sup>	16.0 <sup>a</sup>	61.0 <sup>a</sup>	60.0 <sup>a</sup>
Ge	17.0 <sup>b</sup>	9.00 <sup>b</sup>	34.0 <sup>b</sup>	33.0 <sup>b</sup>
$\vec{k} = \frac{\pi}{a}(1,1,1)$ (L)	LA	TA	TO	LO
Si	48.0 <sup>d</sup>	15.0 <sup>d</sup>	59.0 <sup>d</sup>	52.0 <sup>d</sup>
Ge	26.0 <sup>b</sup>	7.00 <sup>b</sup>	33.0 <sup>b</sup>	29.0 <sup>b</sup>
$\vec{k} = \frac{\pi}{2a}(1,1,1)$	LA	TA	TO	LO
Ge	16.0 <sup>b</sup>	6.80 <sup>b</sup>	37.0 <sup>b</sup>	25.0 <sup>b</sup>

a. The LO, TO and TA values are from Ref. 13, while the LA number is from Ref. 55.

b. Ref. 56.

c. Ref. 5.

d. Ref. 57.

Table XII. Various materials parameters (in atomic units) of Si, Ge and GaP. Also listed are the optical matrix elements of select transitions at the Brillouin zone center and near the X and L points.

	Si	Ge	GaP
	3.38 <sup>a</sup>	4.0 <sup>b</sup>	3.33 <sup>a</sup>
$a/a_0$	10.2 <sup>c</sup>	10.7 <sup>c</sup>	10.3 <sup>d</sup>
$M_v^*/m_0$	0.52 <sup>c</sup>	0.34 <sup>c</sup>	- <sup>e</sup>
$m_c/m_0$ ( $\Delta$ )	0.92 <sup>f</sup>	0.799 <sup>f</sup>	1.7 <sup>f</sup>
$m_c/m_0$ ( $\Delta$ )	0.19 <sup>f</sup>	0.20 <sup>f</sup>	0.19 <sup>f</sup>
$m_c/m_0$ (L)	1.418 <sup>f</sup>	1.588 <sup>f</sup>	- <sup>e</sup>
$m_c/m_0$ (L)	0.130 <sup>f</sup>	0.0815 <sup>f</sup>	- <sup>e</sup>
$\langle \Gamma_{25',v}   p_x   \Gamma_{2',c} \rangle$	0.600 <sup>f</sup>	0.680 <sup>f</sup>	0.610 <sup>f,g</sup>
$\langle \Gamma_{25',v}   p_x   \Gamma_{2',c} \rangle$	0.525 <sup>f</sup>	0.535 <sup>f</sup>	0.500 <sup>f,g</sup>
$\langle \Delta_{5,v}   p_x   \Delta_{1,c} \rangle$	0.570 <sup>f</sup>	0.525 <sup>f</sup>	0.430 <sup>f,g</sup>
$\langle L_{3',v}   p_x   L_{1,c} \rangle$	0.600 <sup>f</sup>	0.655 <sup>f</sup>	- <sup>e</sup>

a. References 37 and 38.

Table XII continued

---

b. Ref. 58.

c. References 37 and 58

d. Ref. 59.

e. Values not listed were not used in this thesis,

f. Ref. 45,

g. The notation is that of Si and Ge. For zincblende materials,  
 $X_{1,c}$  replaces  $\Delta_{1,c}$ ,  $\Gamma_{2',c}$  becomes  $\Gamma_{1,c}$  and  $\Gamma_{8,v}$  ( $\Gamma_{7,v}$ )  
replaces  $\Gamma_{25',v}$ .

---

---

Table XIII. Experimental and theoretical values of the intensities for the TA phonon assisted transitions in GaP as a function of stress for  $\vec{X} \parallel [00]$  and  $\vec{X} \parallel [111]$  and  $\vec{E} \parallel \vec{X}$  and  $\vec{E} \perp \vec{X}$ . The relative and actual (in parentheses in units of  $\text{cm}^{-1}$ ) experimental values were obtained by multiplying  $d\alpha/dE$  by the broadening parameter. The theoretical values were calculated from the expressions in Table VI using  $U_{TA}/V_{TA} = -1.6$ . The dashes represent transitions which were not observed.

$\vec{X} \parallel [00]$ ( $X = 2.84 \times 10^{-9} \text{ dyn-cm}^{-2}$ )	$\vec{E} \parallel \vec{X}$		$\vec{E} \perp \vec{X}$	
	Exp.	Theory	Exp.	Theory
$B_1$	(0.073)	19%	-	3%
$B_2$	-	71%	-	0%
$B_3$	-	2%	-	39%
$B_4$	(0.046)	8%	-	58%

$\vec{X} \parallel [111]$ ( $X = 2.63 \times 10^{-9} \text{ dyn-cm}^{-2}$ )	$\vec{E} \parallel \vec{X}$		$\vec{E} \perp \vec{X}$	
	Exp.	Theory	Exp.	Theory
$A_1$	69% (0.045)	68%	25% (0.030)	26%
$A_2$	31% (0.021)	32%	75% (0.089)	74%

Table XIV. Values of the phonon occupation number,  $n_Q$  and the slopes of the experimental data of Ref. 2 for the TO phonon of Si. The slope,  $\sqrt{A_{e-h}^{fT0}}$ , is given in units of  $10^{-4} (a_0 \text{Ry})^{-1/2}$ . The superscripts a, e refer to phonon absorption and emission respectively.

Temperature	4.2 K	170. K	363 K
$n_Q$	0.0	0.021	0.190
$\sqrt{A_{e-h}^{faT0}}$	0.0	23.9	67.1
$\sqrt{A_{e-h}^{feT0}}$	161.0	162.3	-

Table XV. Experimental values of  $S_{e-ph_{TO}}$  and  $S_{h-ph_{TO}}$  (units of  $10^{-3} \text{ Ry}$ ) for the

$\langle 001 \rangle$  TO phonon of Si in the free electron-hole pair and excitonic regions. Both phonon absorption and emission processes are considered.

Temperature	Phonon Absorption		Phonon Emission	
	$S_{e-ph}$	$S_{h-ph}$	$S_{e-ph}$	$S_{h-ph}$
1.6 K	-	-	15.7 <sup>a</sup>	-20.6 <sup>a</sup>
	-	-	18.7 <sup>b</sup>	-24.5 <sup>b</sup>
4.2 K	-	-	17.4 <sup>c</sup>	-22.9 <sup>c</sup>
	-	-	17.9 <sup>d</sup>	-23.6 <sup>d</sup>
170 K	17.3 <sup>d</sup>	-23.2 <sup>d</sup>	17.9 <sup>d</sup>	-23.6 <sup>d</sup>
363 K	16.1 <sup>d</sup>	-21.6 <sup>d</sup>	-	-
<u>Average values</u>				
$S_{e-ph_{TO}} = 17.3 \pm 2.3 \text{ mRy}$		$S_{h-ph_{TO}} = -22.9 \pm 3.4 \text{ mRy}$		

Table XV. continued

- 
- a. From the experimental data of Ref. 3 in the excitonic region.
  - b. From the experimental data of Ref. 48 in the excitonic region.
  - c. From the experimental data of Ref. 2 in the excitonic region.
  - d. From the experimental data of Ref. 2 in the free electron-hole pair energy range.
- 
-

Table XVI. Experimental values of the quantities  $D_{LA}$  and  $D_{TA}$  (units of  $\text{cm}^{-1} \text{eV}^{-1/2}$ ) at various temperatures. Both phonon absorption and emission processes are considered. The numbers in this table are from Ref. 5.

Temperature	Absorption		Emission	
	LA	TA	LA	TA
1.6 K	0.0	0.0	64.0	17.0
77 K	0.36	2.60	67.0	20.0
120 K	1.60	6.60	68.0	25.0
218 K	5.00	11.0	74.0	<sup>a</sup>

a. Due to broadening effects, Dean et. al. (Ref. 5) could not obtain an accurate value for this number and consequently did not report it in this reference.

Table XVII. Values of  $e$ -ph, and  $h$ -ph, (in atomic units) for the (001) LA and TA phonons of GaP in the excitonic energy region.

Temperature (K)	LA phonon			TA phonon		
	Absorption $S_{e-ph_{LA}}$ ( $10^{-3}$ Ry)	Emission $S_{h-ph_{LA}}$ ( $10^{-3}$ Ry)	$S_{h-ph_{LA}}$ ( $10^{-3}$ Ry)	Absorption $S_{e-ph_{TA}}$ ( $10^{-3}$ Ry)	Emission $S_{h-ph_{TA}}$ ( $10^{-3}$ Ry)	$S_{h-ph_{TA}}$ ( $10^{-3}$ Ry)
1.6						
77	-6.2	-11.5	-8.3	18.7	17.1	19.8
120	-7.2	-12.4	-8.3	19.4	17.5	18.7
218	-5.2	-8.3	-7.9	16.0	14.4	19.4
Average values*						
LA phonon						
$S_{e-ph_{LA}} = -7.6 \pm 1.1 \times 10^{-3}$ Ry						
$S_{h-ph_{LA}} = -13.0 \pm 2.0 \times 10^{-3}$ Ry						
TA phonon						
$S_{e-ph_{TA}} = 19.2 \pm 2.8 \times 10^{-3}$ Ry						
$S_{h-ph_{TA}} = 17.4 \pm 2.5 \times 10^{-3}$ Ry						

\*The averages do not include the 218 K data.

Table XVIII. Theoretical and experimental values of  $S_{e-ph}$  and  $S_{h-ph}$  (units of  $10^{-3}$  Ry) for the  $\Gamma-\Delta$  transitions (TO,LO,TA,LA) of Si. Results are listed for the three different interpolations of Fig. 14.

Interpolation	TO		LO		TA		LA	
	$S_{e-ph}$	$S_{h-ph}$	$S_{e-ph}$	$S_{h-ph}$	$S_{e-ph}$	$S_{h-ph}$	$S_{e-ph}$	$S_{h-ph}$
Histogram	19.0	-24.0	-13.0	-36.0	-2.0	7.0	23.0	25.0
Curve a	19.0	-23.0	-12.0	-36.0	-3.3	0.3	25.0	28.0
Curve b (oscillating tail)	19.0	-23.0	-13.0	-36.0	-4.4	0.3	25.0	28.0
Experiment (present results)	$17.3 \pm 2.6$	$-22.9 \pm 3.4$	-	-	-	-	-	-

Table XIX. Experimental and theoretical values (in units of  $10^{-9} \text{Ry}^{1/2} a_0^{-1}$ ) of the coefficient  $A_{\text{ex}1}$  for the TO, LO, TA, and LA ( $\Gamma - \Delta$ ) phonons of Si. Theoretical results are listed for the three interpolations of Fig. 14, as discussed in the text. The LA phonon transition is so weak that it is not observed experimentally.

Interpolation	TO	LO	TA	LA
Histogram	31.0	5.6	1.1	0.31
Curve a	30.0	5.1	0.43	0.27
Curve b	30.0	4.8	0.76	0.27
<u>Experiment</u>				
Ref. 2	26.9	-	0.72	-
Ref. 3	21.8	3.23	0.64	-
Ref. 48	30.9	3.40	0.80	-

Table XX. Potential parameters for the interpolation of the S1 form factor given by Eq. 5.12. The form factor is taken to be zero beyond  $q = 5$ . The units of  $q$  in this table are  $2\pi/a$ .

Range	a	b	c	d
$q^2 < 3$	0.0	0.153	0.087	-0.830
$3 \leq q^2 \leq 11$	0.103	-0.910	2.748	-2.783
$q^2 > 11$	0.0	0.021	-0.221	0.586

Table XXI. Potential parameters for the interpolation of the Ge form factor given by Eq. 5.14. The wave vector,  $q$ , is in units of  $2\pi/a$ .

Range	Parameter	$u_0$	$r_1$	$k_0^2$	$k_1^2$	$k_2^2$
$q^2 < 3$		-2.438	0.5775	2.8	-0.044	0.0
$3 \leq q^2 \leq 11.2$		-2.438	0.5775	2.8	0.0	0.0
$q^2 > 11.2$		-2.438	0.5775	2.8	0.0	-5.0

Table XXII. Theoretical values of  $S_{e-ph}$  and  $S_{h-ph}$  (units of  $10^{-3}$  Ry) for the  $\Gamma-L$  phonon assisted transitions in Ge. For  $S_{e-ph}$ ,  $\Gamma_{25,v}$  and  $\Gamma_{\bar{X},\bar{Y}}$  transform as  $\Lambda_{1,v}$  and  $\Lambda_{3,v}$  respectively.  $\bar{X}$ ,  $\bar{Y}$  and  $\bar{Z}$  are defined in the text.

<u><math>S_{e-ph}</math></u>				
Phonon Intermediate state	LA	TO	LO	TA
$\Gamma_{2',c}$	-9.0	0.0	0	0
$\Gamma_{15,c}$	21.0	-4.0	0	0
<u><math>S_{h-ph}</math></u>				
Phonon Final state	LA	TO	LO	TA
$\Gamma_{\bar{X}}_{25',v}$ or $\Gamma_{\bar{Y}}_{25',v}$	21.0	-26.0	0	0
$\Gamma_{\bar{Z}}_{25',v}$	0.0	10.0	0	0

Table XXIII. Theoretical and experimental values of the coefficient  $A_{\text{ex}1}^{\text{f}}$  for the LA and TO ( $\Gamma$ -L) phonon assisted transitions in Ge. The numbers are listed in atomic units and a commonly used mixed unit.

Phonon $A_{\text{f}2}$	<u>LA</u>		<u>TO</u>	
	<u>Theory</u>	<u>Expt.</u>	<u>Theory</u>	<u>Expt.</u>
$(10^{-9}\text{Ry}\frac{1}{2}\text{a}^{-1})$	11.2	11.6 <sup>a</sup> 12.2 <sup>b</sup>	1.3	- <sup>a</sup> 1.8 <sup>b</sup>
$(\text{cm}^{-1}\text{eV}\frac{1}{2})$	7.8	8.1 <sup>a</sup> 8.5 <sup>b</sup>	0.9	- <sup>a</sup> 0.7 <sup>b</sup>

a. Reference 1.

b. From the analysis of the wavelength modulated absorption spectrum of Ref. 8.

Table XXIV. Theoretical and experimental (Ref. 8) values for the intensities of the LA phonon assisted transition in Ge, for stress,  $\vec{X}$ , along  $[111]$  and  $[001]$  for the electric field vector,  $\vec{E}$ , of the incident light polarized parallel and perpendicular to  $\vec{X}$ . Scattering from the  $\Gamma_{15,c}$  state is included.

$X \parallel [111]$	$\vec{E} \parallel \vec{X}$		$\vec{E} \perp \vec{X}$	
	Expt.	Theory	Expt.	Theory
A <sub>1</sub>	16%	9%	6%	8%
A <sub>2</sub>	0%	0%	24%	24%
A <sub>3</sub>	84%	89%	17%	18%
A <sub>4</sub>	0%	2%	53%	50%

$X \parallel [001]$	$\vec{E} \parallel \vec{X}$		$\vec{E} \perp \vec{X}$	
	Expt.	Theory	Expt.	Theory
B <sub>1</sub>	100%	95%	25%	27%
B <sub>2</sub>	0%	5%	75%	73%

Table XXV. Theoretical values (units of  $10^{-3}$ Ry) of  $S_{e-ph}$  and  $S_{h-ph}$  for the  $\Gamma-L$  phonon scattering (LA,TO,LO,TA) in Si. The notation for the states is the same as in Table XXII for the case of Ge. The transformation rules for the valence band states are also the same as in Ge.

<u><math>S_{e-ph}</math></u>					
Phonon Intermediate state	LA	TO	LO	TA	
$\Gamma_{2',c}$	-15.0 <sup>a</sup> -16.0 <sup>b</sup>	0.0 <sup>a,b</sup>	0 <sup>a,b</sup>	0 <sup>a,b</sup>	0 <sup>a,b</sup>
$\Gamma_{15,c}$	18 <sup>a</sup> 16 <sup>b</sup>	-6.2 <sup>a</sup> -5.8 <sup>b</sup>	0 <sup>a,b</sup>	0 <sup>a,b</sup>	0 <sup>a,b</sup>
<u><math>S_{h-ph}</math></u>					
Phonon Final state	LA	TO	LO	TA	
$\bar{X}_{25',v}$ or $\bar{Y}_{25',v}$	31.0 <sup>a</sup> 31.0 <sup>b</sup>	-33.0 <sup>a</sup> -32.0 <sup>b</sup>	0 <sup>a,b</sup>	0 <sup>a,b</sup>	0 <sup>a,b</sup>
$\bar{Z}_{25',v}$	0.0 <sup>a,b</sup>	11.0 <sup>a</sup> 9.7 <sup>b</sup>	0 <sup>a,b</sup>	0 <sup>a,b</sup>	0 <sup>a,b</sup>

Table XXV continued.

- 
- a. Obtained by using curve a (Fig. 14) for the interpolation of the form factor.
  - b. Obtained by using curve b of Fig. 14 for the interpolation of the form factor.
- 
-

Table XXVI. Theoretical and experimental values (units of  $\text{cm}^{-1/2} - \text{ev}^{-1/2}$ ) for the quantity  $A_{e-h}^f$  total in Si, of the total  $\Gamma-L$  and  $\Gamma-A$  contributions. The experimental values are obtained from Fig. 19 and Ref. 2 (MMQR).

	$\Gamma-L$	$\Gamma-A$
Theory (curve a of Fig. 14)	110.0 <sup>a</sup>	76.0 <sup>a</sup>
<u>Experiment</u>		
Fig. 19	189.0	100.0
Ref. 2 (MMQR)	<sub>-b</sub>	64.0

a. Only curve a was used, because the total absorption coefficient is not very sensitive to the differences between the two interpolations of Fig. 14, curve a and b.

b. In this work, the absorption near the secondary indirect gap was not studied.

Table XXVII. Theoretical values of  $S_{e-ph}$  and  $S_{h-ph}$  (units of  $10^{-3}$ Ry) in Si, for  $\Gamma-\Delta$  scattering midway into the Brillouin zone  $\vec{k} = \pi/a(0,0,1)$ . Also listed are theoretical values of the quantity  $A_{e-h}^{f_1}$  in units of  $(eV-cm)^{-1/2}$  (for ease of comparison with Table XXVI).

Interpolation	TO		LO		TA		LA	
	$S_{e-ph}$	$S_{h-ph}$	$S_{e-ph}$	$S_{h-ph}$	$S_{e-ph}$	$S_{h-ph}$	$S_{e-ph}$	$S_{h-ph}$
Curve a	17.0	-27.0	-9.7	-38.0	-11.0	-0.88	16.0	18.0
Curve b	16.0	-25.0	-9.4	-38.0	-12.0	-0.89	15.0	18.0
$A_{e-h}^{f_1}$	TO		LO		TA		LA	
Curve a	76.0		41.0		28.0		3.7	
Curve b	71.0		41.0		31.0		1.8	

Table XXVIII. Calculated values (units of  $10^{-3}$  Ry) of  $S_{e-ph}$  and  $S_{h-ph}$  for  $\Gamma - \Delta$  scattering in Ge for the TO, LO, TA, and LA phonons. Numbers are listed for processes scattering to  $\vec{k} = 2\pi/a(0,0,0.85)$  and  $\vec{k} = 2\pi/a(0,0,0.5)$ .

Final point along	TO		LO		TA		LA	
	$S_{e-ph}$	$S_{h-ph}$	$S_{e-ph}$	$S_{h-ph}$	$S_{e-ph}$	$S_{h-ph}$	$S_{e-ph}$	$S_{h-ph}$
$2\pi/a(0,0,0.85)$	14.0	-21.0	-8.4	-26.0	3.4	0.65	21.0	22.0
$2\pi/a(0,0,0.5)$	14.0	-24.0	-8.8	-42.0	-1.3	-0.32	16.0	20.0

Table XXIX. Calculated values (units of  $10^{-3}$  Ry) of  $S_{e-ph}$  and  $S_{h-ph}$  for  $\Gamma - \Lambda$  scattering midway into the Brillouin zone,  $\vec{k} = \pi/2a(1,1,1)$ , in Ge. The LA, LO, TA and TO phonons are allowed.

<u><math>S_{e-ph}</math></u>					
Phonon Intermediate state	LA	TO	LO	TA	
$\Gamma_{2',c}$	-4.7	0.0	-5.0	0.0	
$\Gamma_{15,c}$	11.0	-4.8	17.0	-3.1	
<u><math>S_{h-ph}</math></u>					
Phonon Final state	LA	TO	LO	TA	
$\bar{X}_{25',v}$ or $\bar{Y}_{25',v}$	13.0	-26.0	21.0	-0.61	
$\bar{Z}_{25',v}$	0.0	14.0	0.0	-5.1	

Table XXX. Summary of the values (units of  $10^{-3}$  Ry) of  $S_{e-ph}$  and  $S_{h-ph}$  for  $\Gamma-\Delta$  (X) scattering in Si, Ge and GaP ( $\Gamma-X$ ). The numbers in parentheses refer to the point along to which the scattering occurs. The LO phonon matrix elements of Si and Ge should be compared to the LA ones of GaP (see Figs. 1-3).

	TO		LO		TA		LA	
	$S_{e-ph}$	$S_{h-ph}$	$S_{e-ph}$	$S_{h-ph}$	$S_{e-ph}$	$S_{h-ph}$	$S_{e-ph}$	$S_{h-ph}$
$\Gamma-\Delta$ (X) $2\pi/a(0,0,0.85)$								
Si (curve a)	19.0	-23.0	-12.0	-36.0	-3.3	0.30	25.0	28.0
Ge	14.0	-21.0	-8.4	-26.0	3.4	0.65	21.0	22.0
GaP (to X point) (experiment)	-	-	-	-	19.2	17.4	-7.6	-13.0
$\Gamma-\Delta$ $2\pi/a(0,0,0.5)$	TO		LO		TA		LA	
	$S_{e-ph}$	$S_{h-ph}$	$S_{e-ph}$	$S_{h-ph}$	$S_{e-ph}$	$S_{h-ph}$	$S_{e-ph}$	$S_{h-ph}$
Si (curve a)	17.0	-27.0	-9.7	-38.0	-11.0	-0.88	16.0	18.0
Ge	14.0	-24.0	-8.8	-42.0	-1.3	-0.32	16.0	20.0

Table XXXI. Summary of all of the values (units of  $10^{-3}$  Ry) of  $S_{e-ph}$  and  $S_{h-ph}$  for the  $\Gamma$ -L scattering in Si and Ge. The LO and TA phonon matrix elements are not listed because they are zero (symmetry forbidden).

Intermediate state \ Phonon		$S_{e-ph}$			
		LA		TO	
		Si <sup>a</sup>	Ge	Si <sup>a</sup>	Ge
$\Gamma_{2',c}$		-15.0	-9.0	0.0	0.0
$\Gamma_{15,c}$		18.0	21.0	-6.2	-4.0
Final state \ Phonon		$S_{h-ph}$			
		LA		TO	
		Si <sup>a</sup>	Ge	Si <sup>a</sup>	Ge
$\Gamma_{\bar{X},\bar{Y}}$ $\Gamma_{25',v}$		31.0	21.0	-33.0	-26.0
$\Gamma_{\bar{Z}}$ $\Gamma_{25',v}$		0.0	0.0	11.0	10.0

a. For Si, we list only the value obtained by using curve a as the interpolation of the form factor of Fig. 14.

FIGURE CAPTIONS

FIGURE	PAGE
1. Schematic representation of the band structure of Si, showing the allowed $\Gamma - \Delta$ transitions.....	190
2. Schematic representation of the band structure of Ge, showing the allowed $\Gamma - L$ transitions.....	191
3. Schematic representation of the band structure of GaP, showing the allowed $\Gamma - X$ transitions.....	192
4. Schematic representation of the effects of stress along [001] and [111] on the $\Gamma - L$ transitions.....	193
5. Schematic representation of the effects of stress along [111] and [001] on the $\Gamma - \Delta(X)$ transitions.....	194
6. Schematic diagram of the optics and electronics used in wavelength modulated absorption.....	195
7. Diagram of the stress rig used in the experiment...	196
8. Wavelength modulated absorption spectra, with and without stress for the indirect excitons of GaP at 77 K.....	197

9.	Theoretical fit to the $A_2^\perp$ (LA) peak at a stress of $7.35 \times 10^9 \text{ dyn-cm}^{-2}$ .....	198
10.	Theoretical fit to the $A_1^{\parallel}$ (LA) peak at a stress of $7.35 \times 10^9 \text{ dyn-cm}^{-2}$ .....	199
11.	Theoretical fit to the $A_1^{\parallel}$ (TA) peak at a stress of $2.63 \times 10^9 \text{ dyn-cm}^{-2}$ .....	200
12.	Theoretical fit to the $A_2^\perp$ (TA) peak at a stress of $2.63 \times 10^9 \text{ dyn-cm}^{-2}$ .....	201
13.	Decomposition of the absorption coefficient in Si at 4.2 K (Ref. 2).....	202
14.	Form factor interpolation in Si.....	203
15.	The wavelength modulated absorption spectrum of Ge at 77 K showing the LA and TO phonon lines.....	204
16.	Interpolation of the form factor in Ge.....	205
17.	Fit of $F(W)$ to the TO phonon peak of Fig. 15.....	206
18.	Fit of $F(W)$ to the LA phonon peak of Fig. 15.....	207
19.	The absorption curve for Si in the range of 1.4 eV to 3.0 eV.....	208
20.	The dispersion curves for Si (Ref. 57).....	209

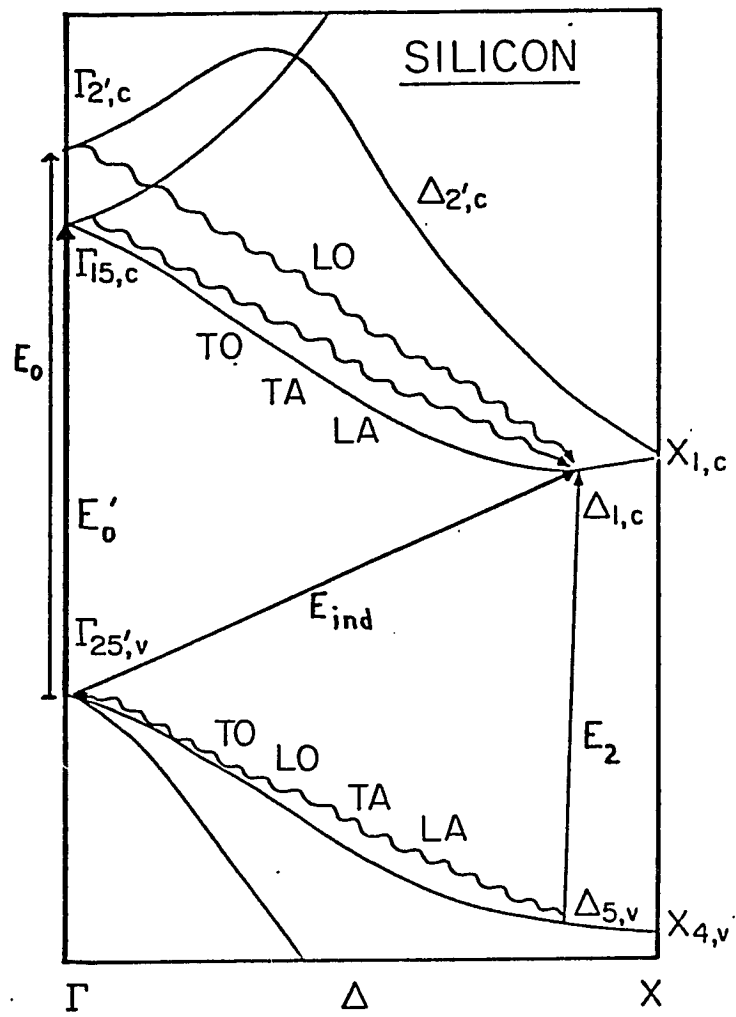


Fig. 1

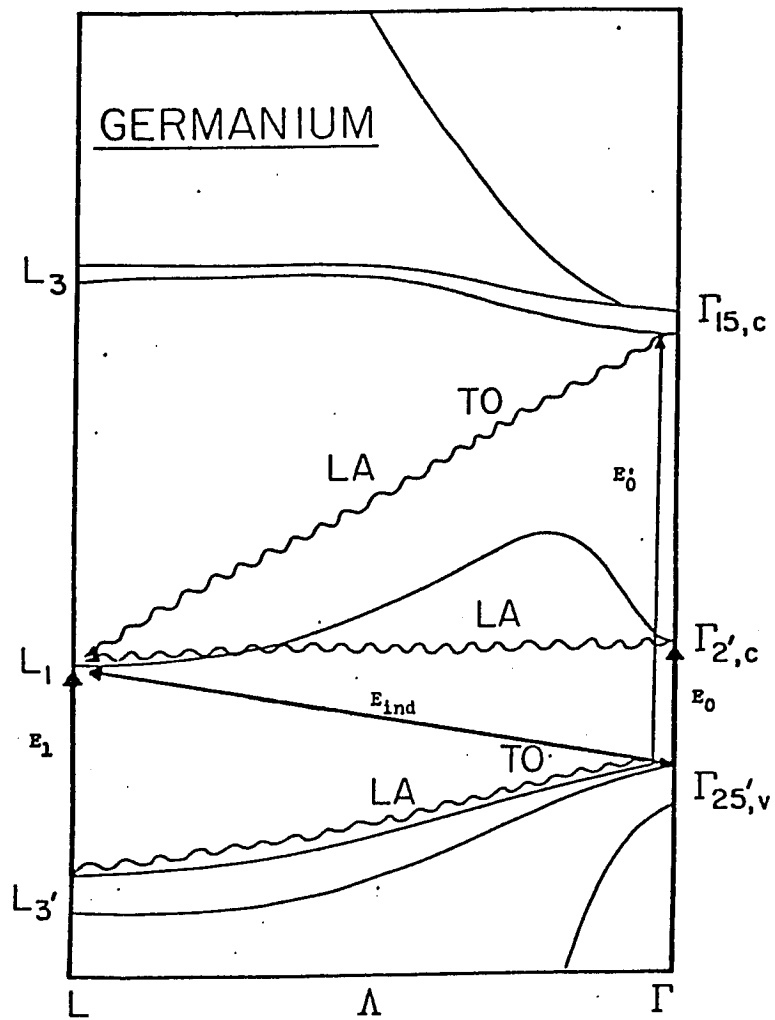


Fig. 2

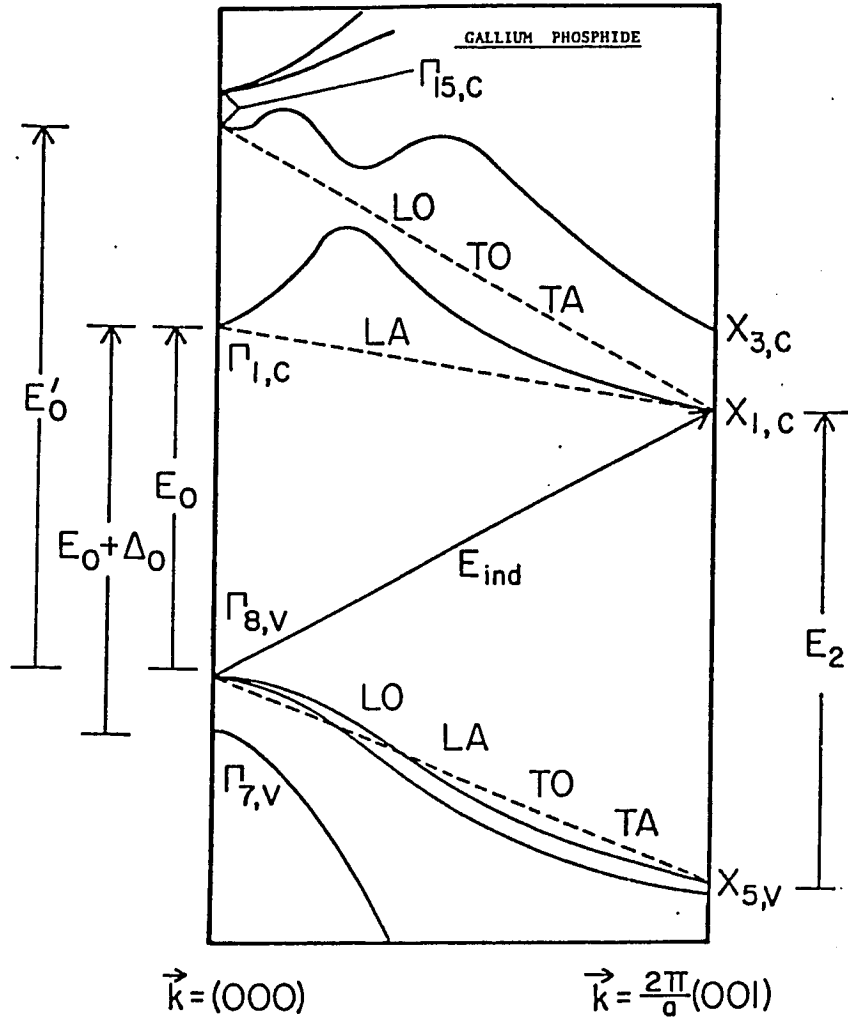
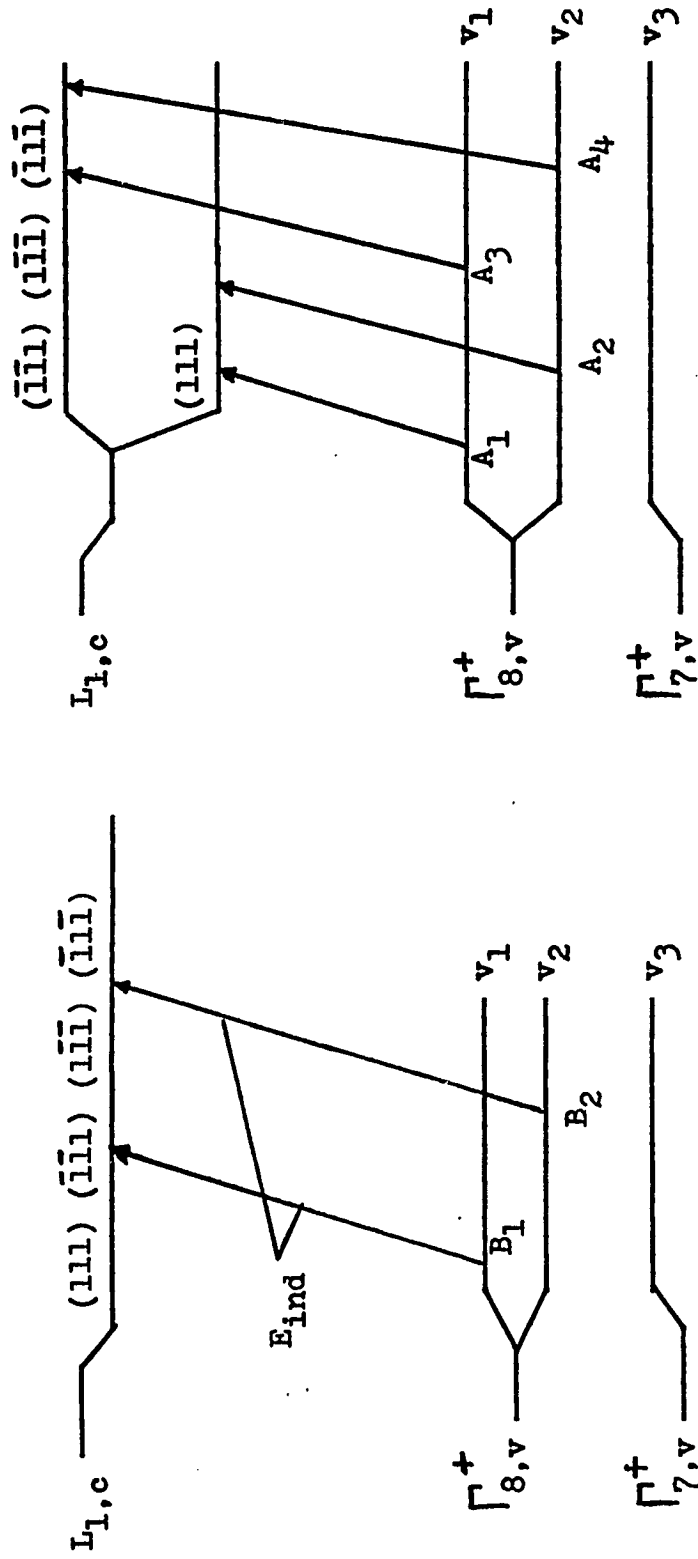


Fig. 3

$\Gamma$  - L Transitions



$\vec{x} \parallel [001]$

$\vec{x} \parallel [111]$

Fig. 4

$\Gamma$ -X( $\Delta$ ) Transitions

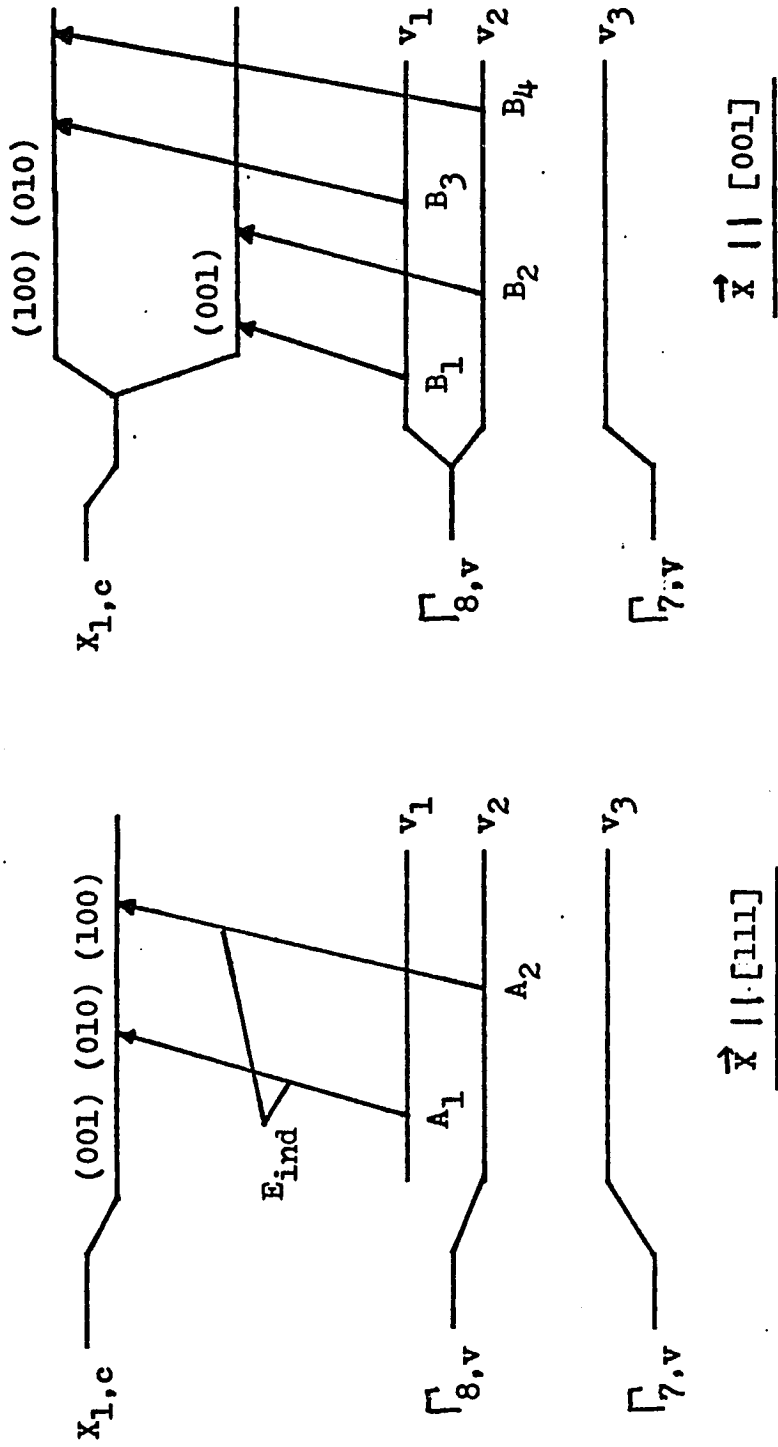


Fig. 5

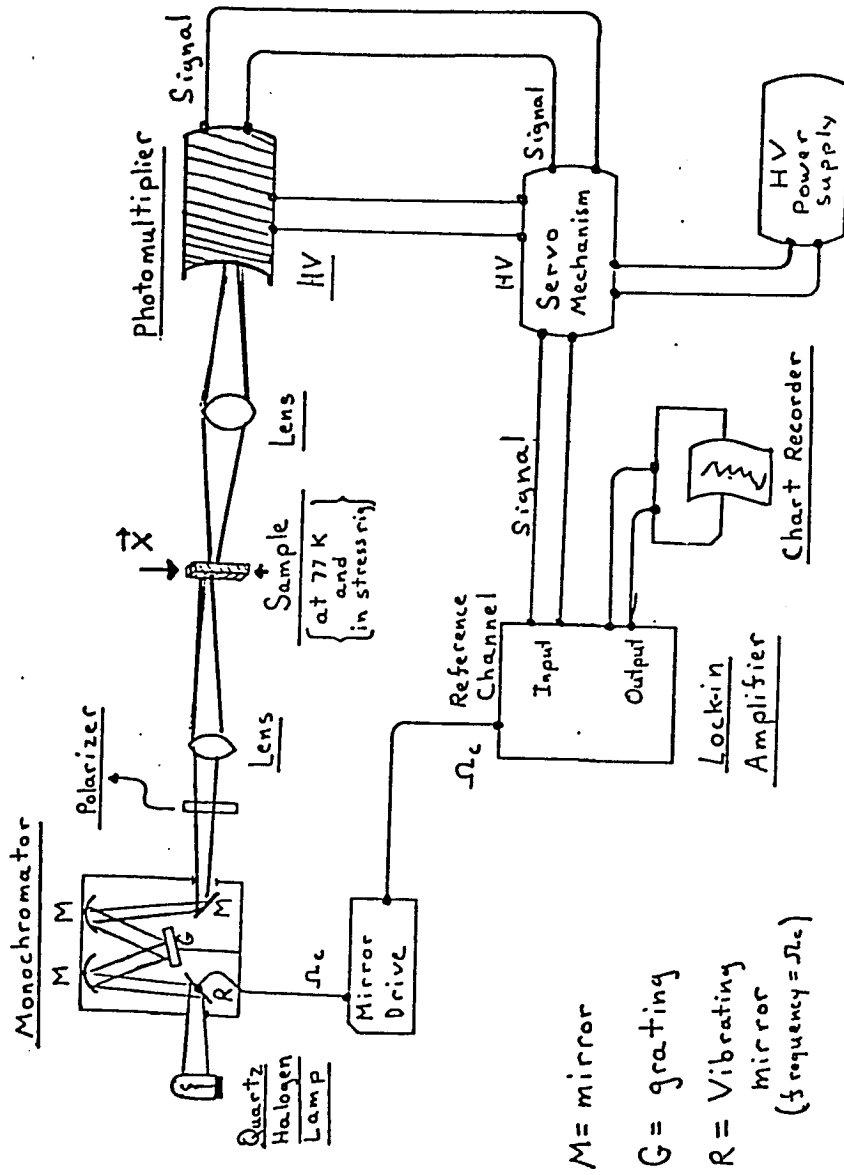


Fig. 6

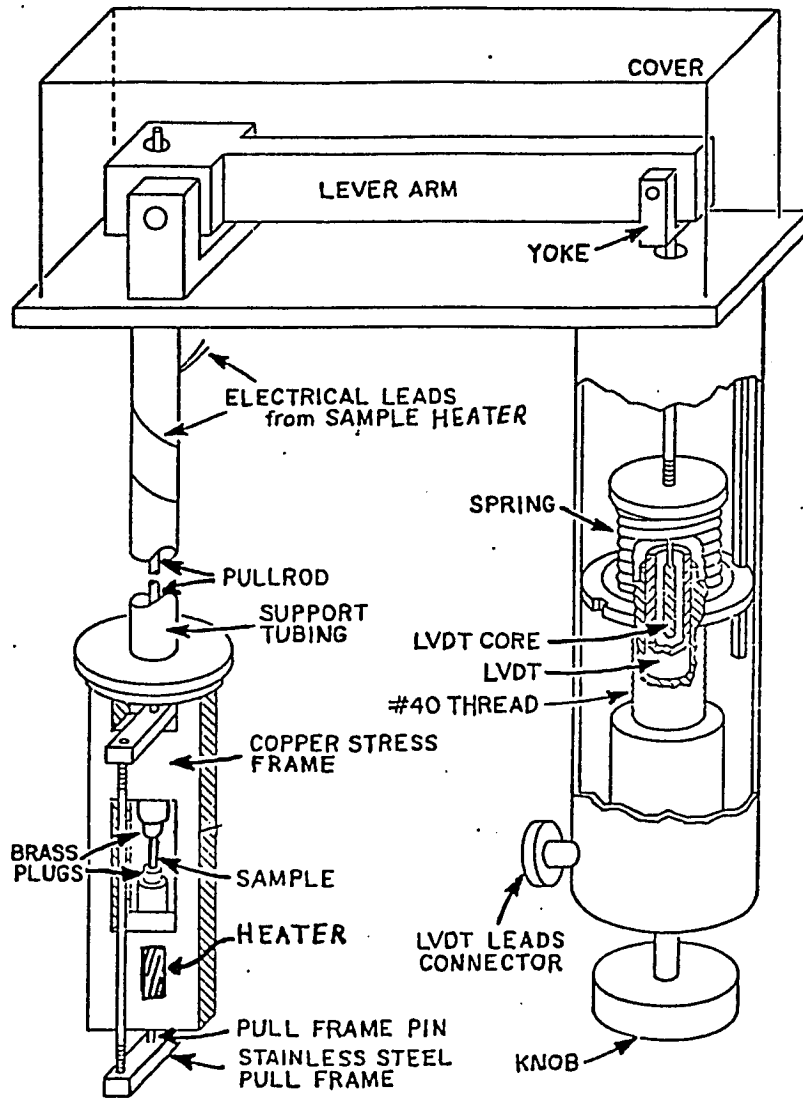


Fig. 7

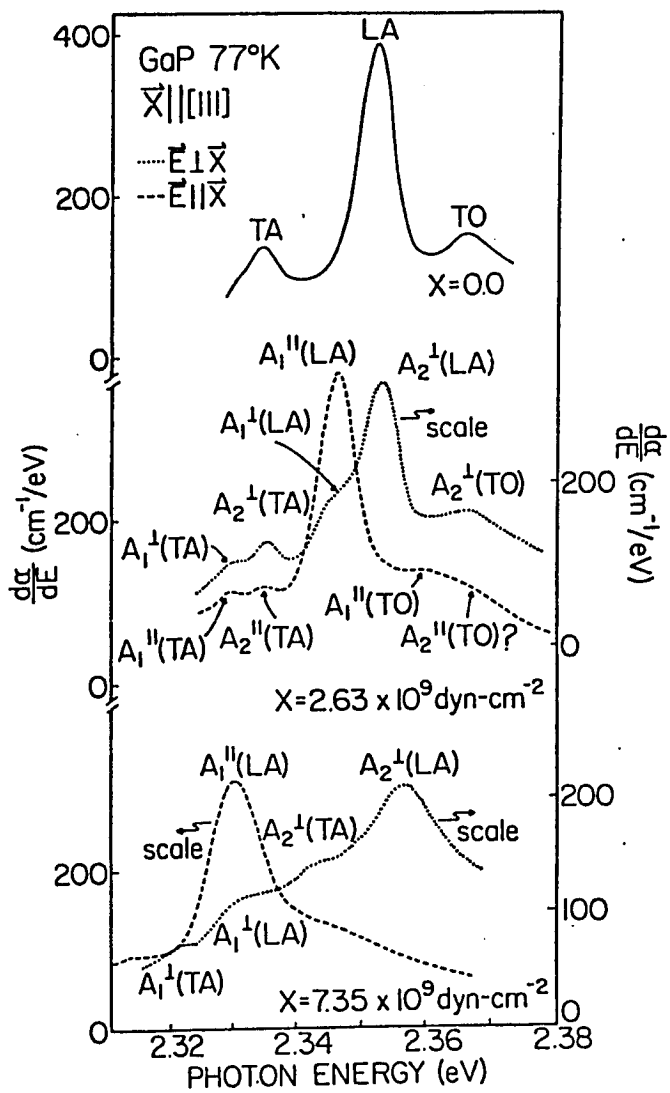


Fig. 8

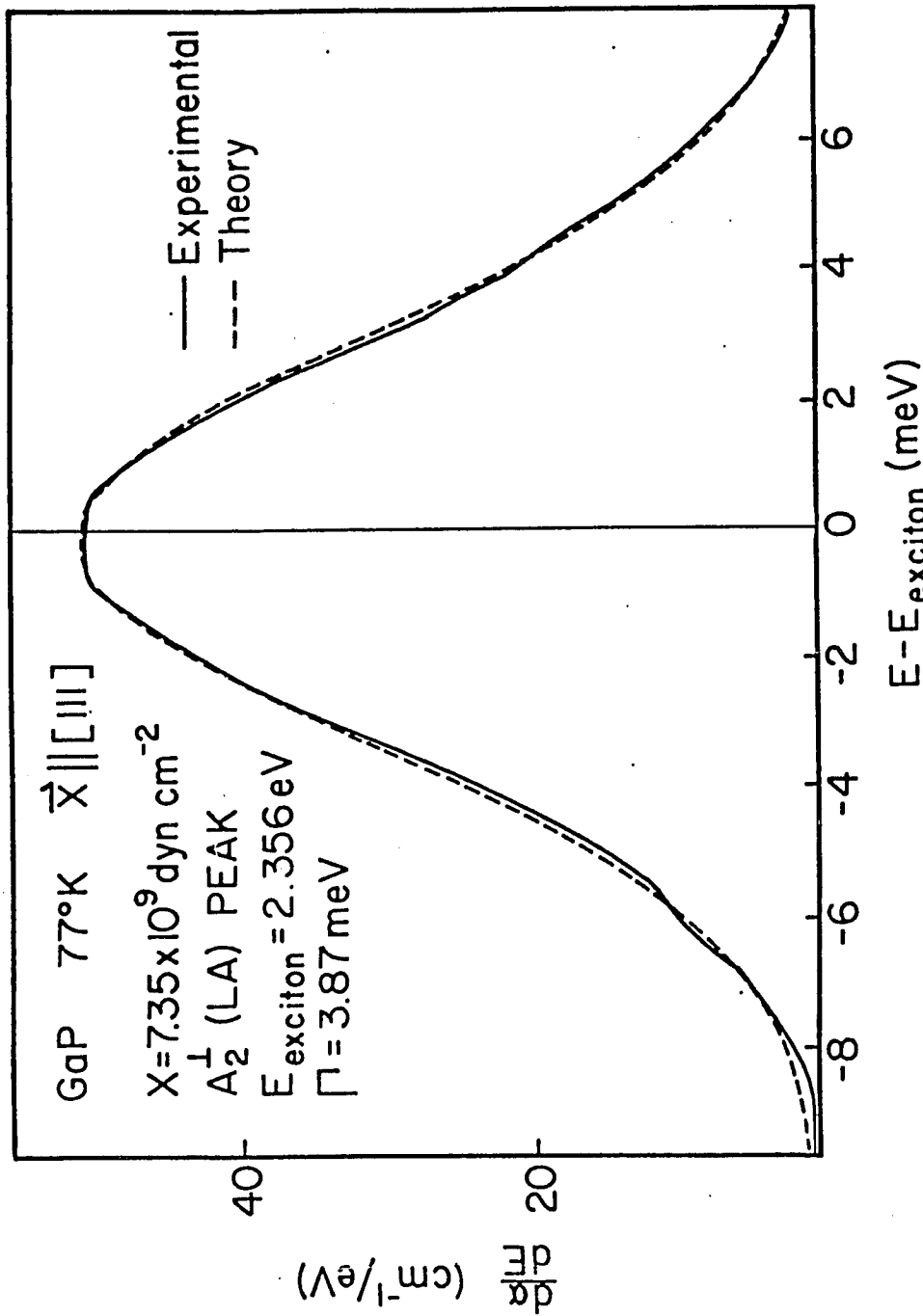


Fig. 9

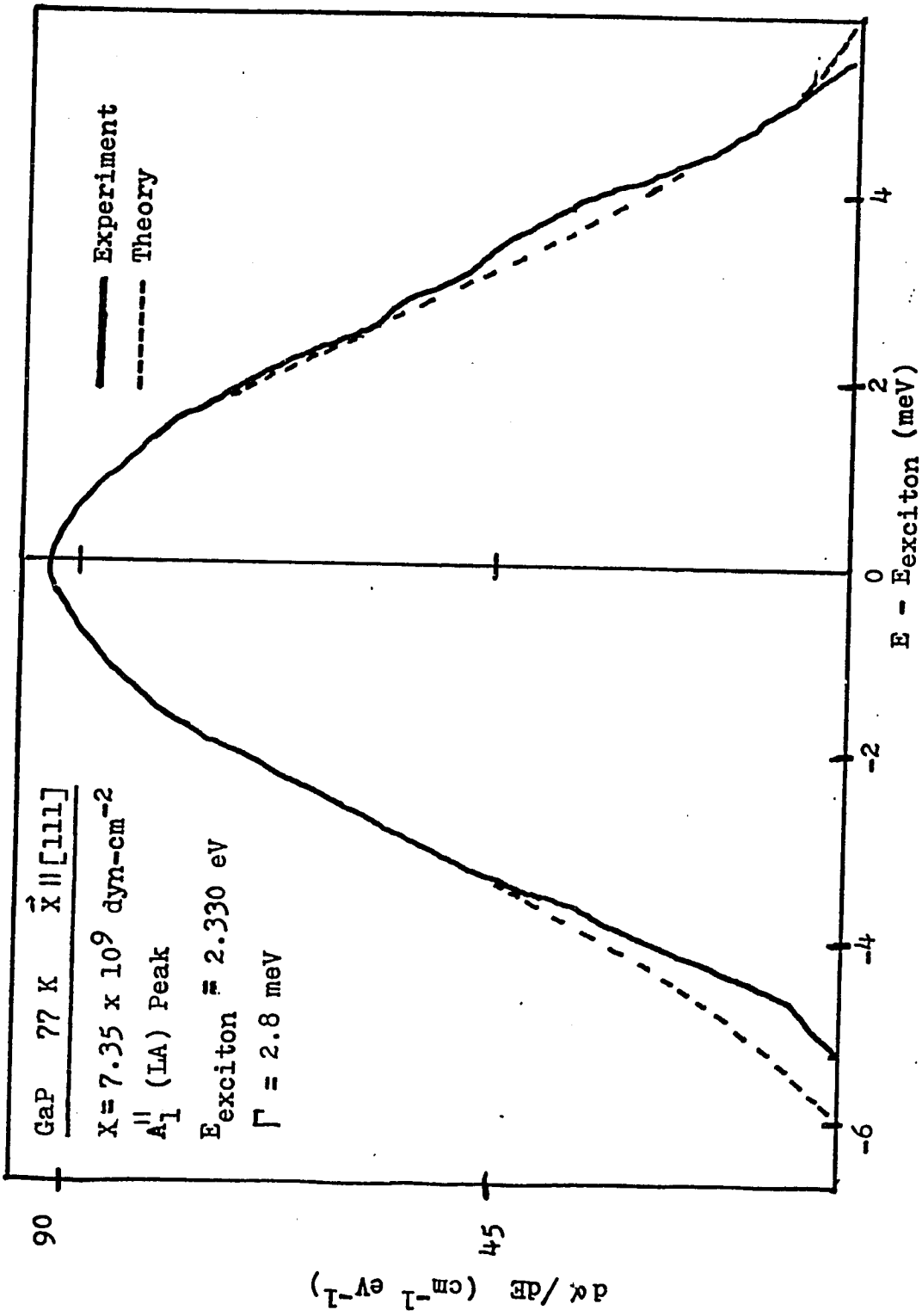


FIG. 10

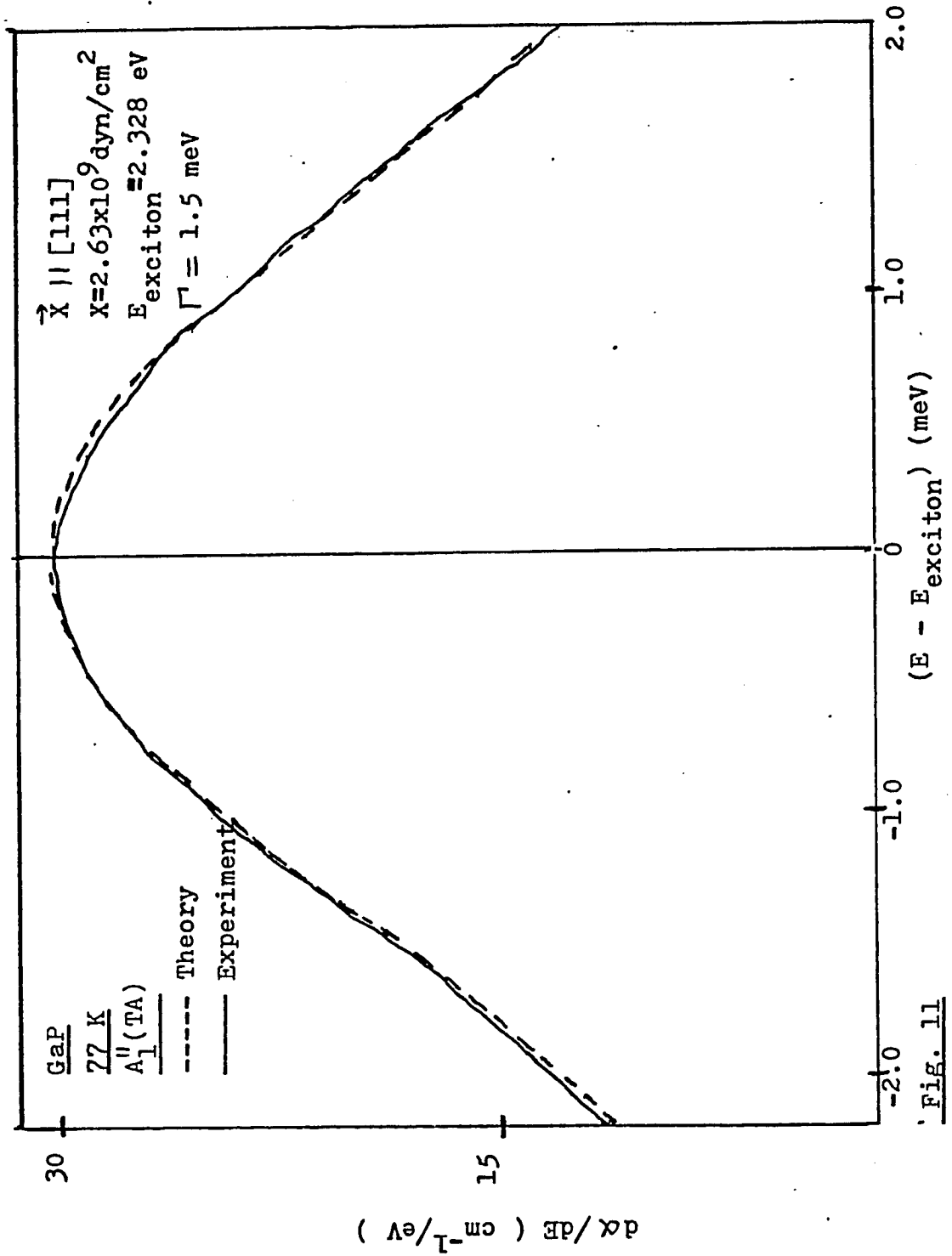


Fig. 11

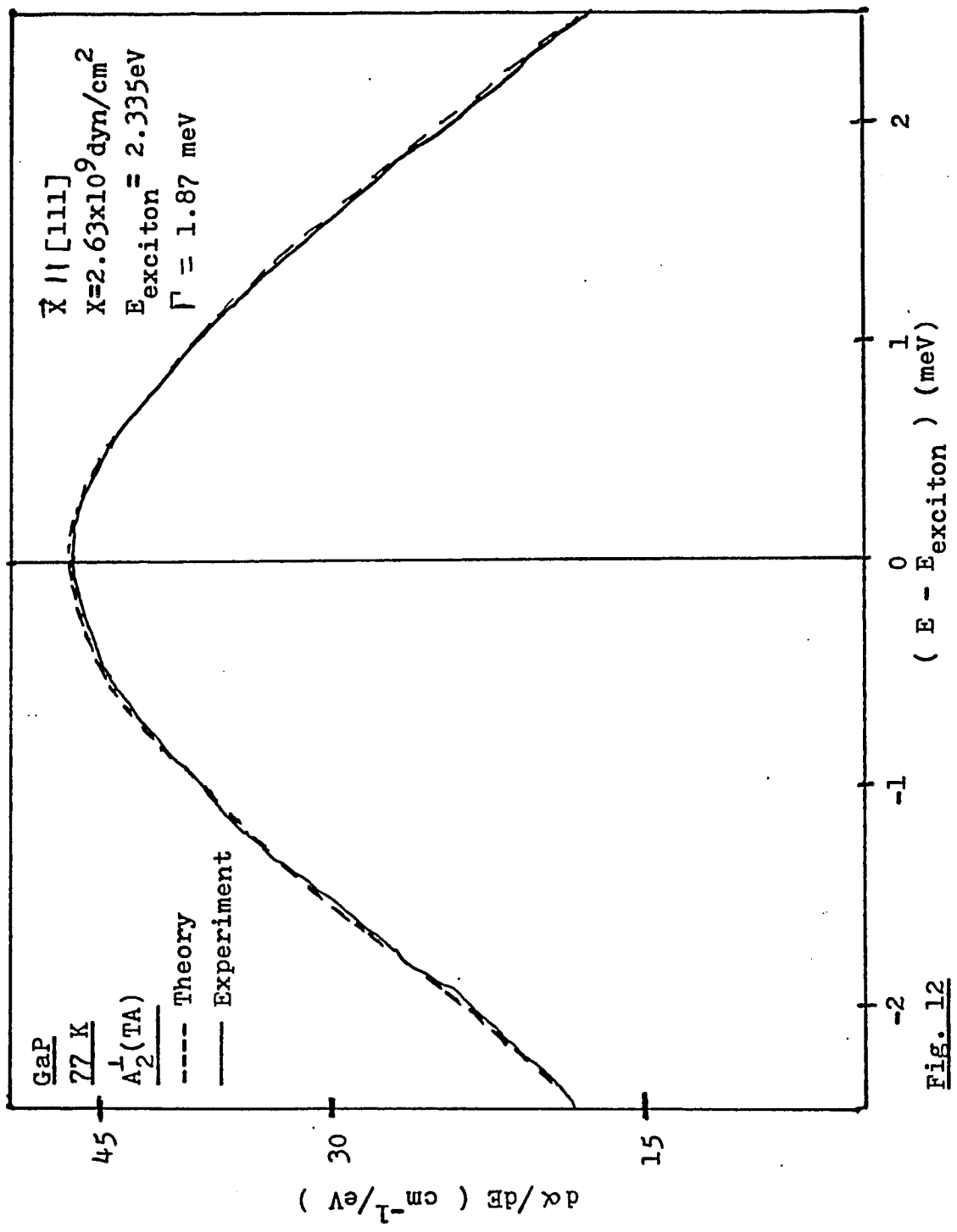


Fig. 12

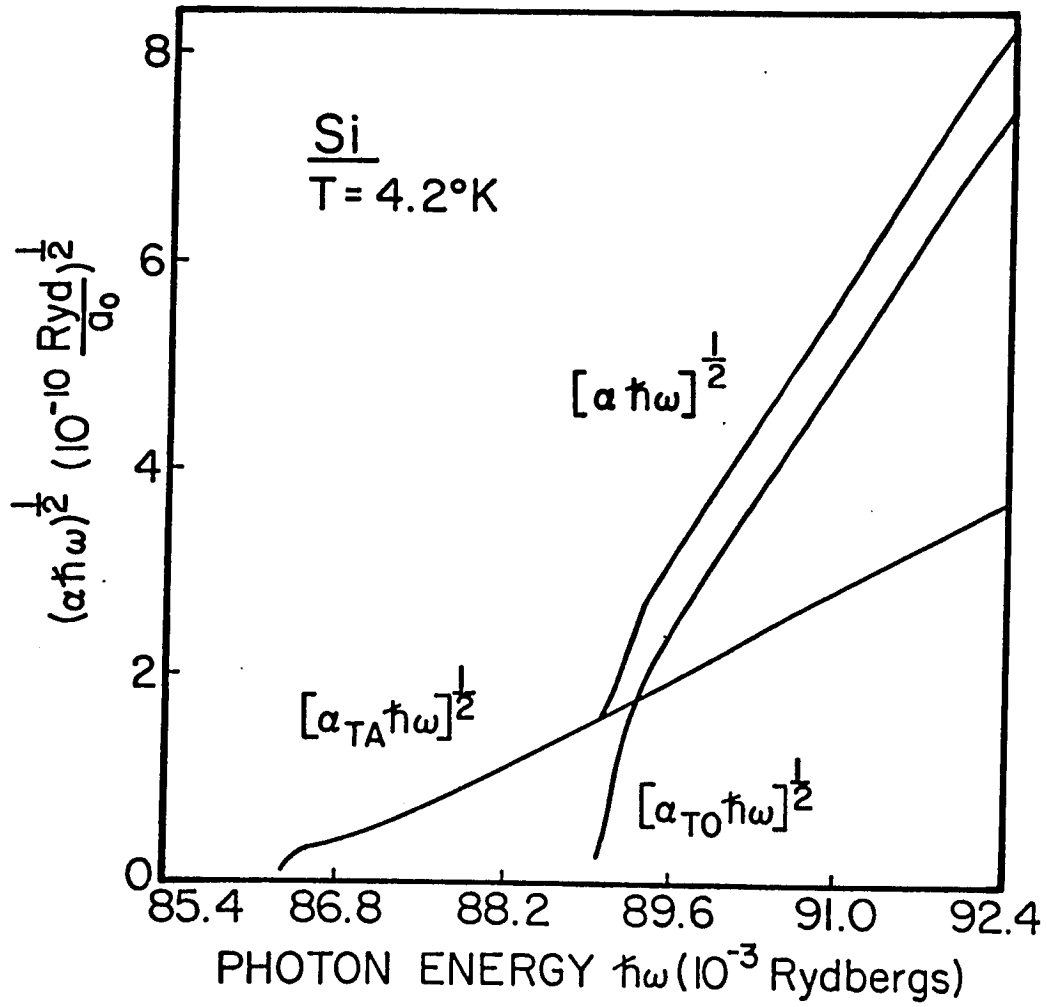


Fig. 13

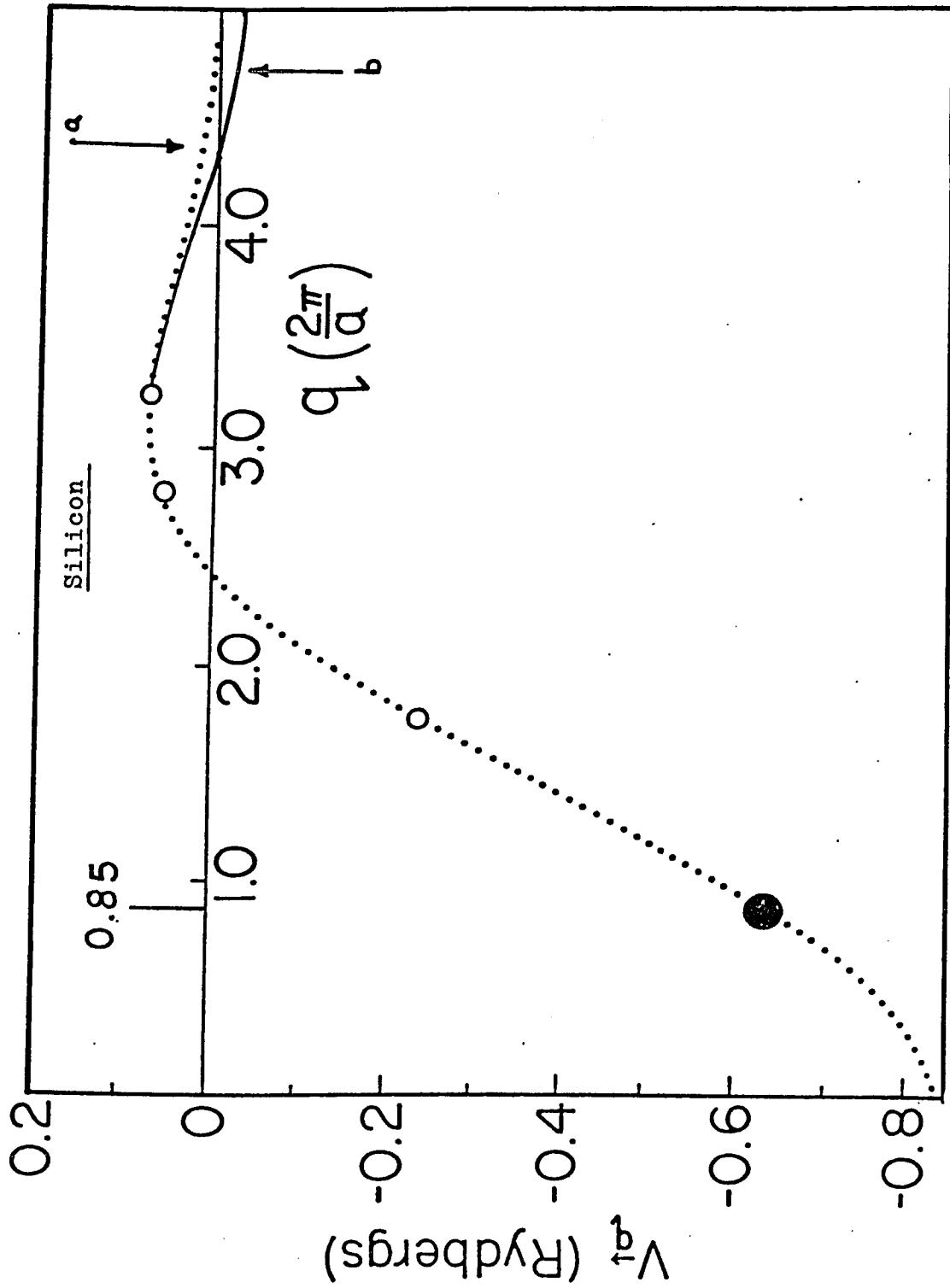
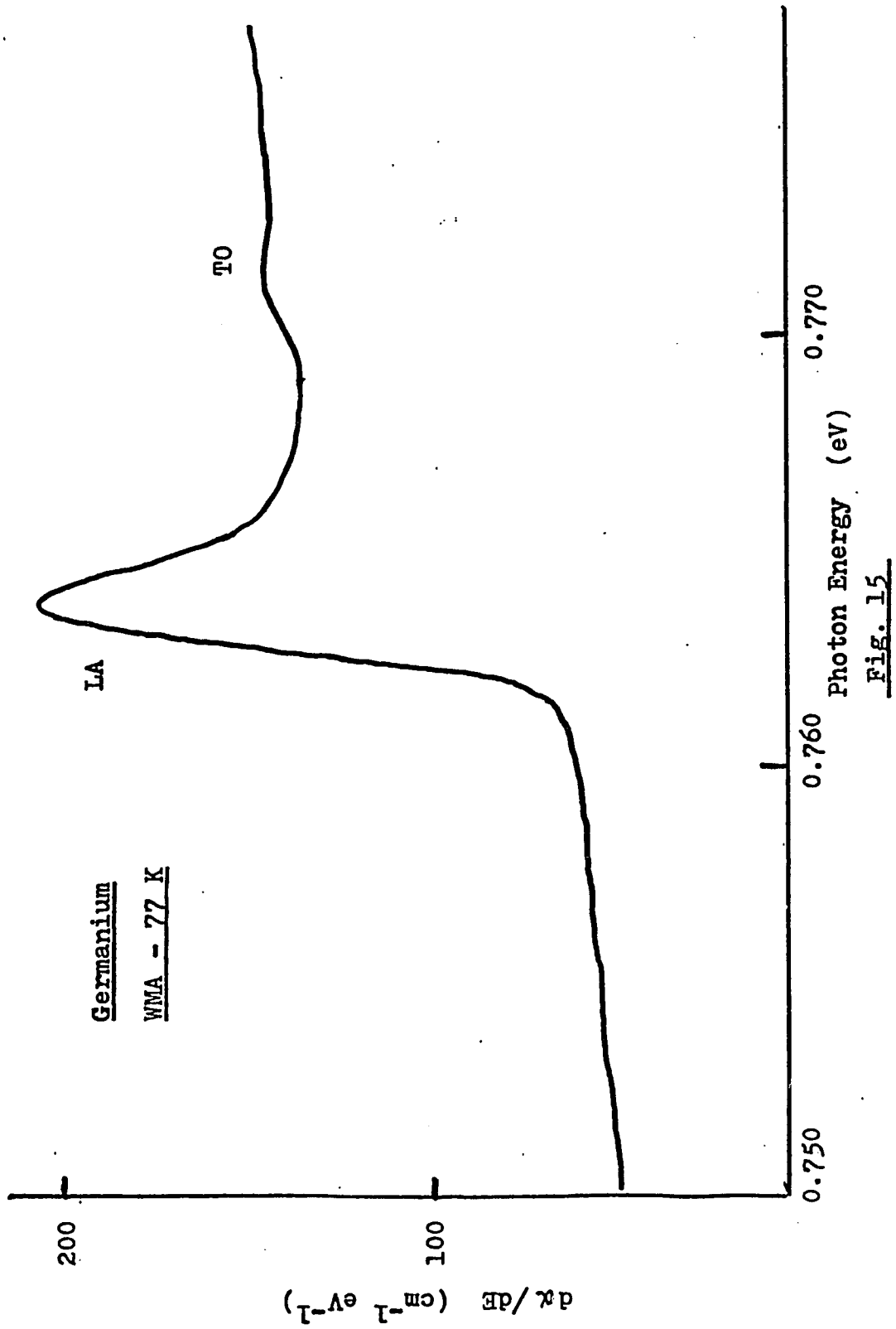


Fig. 14



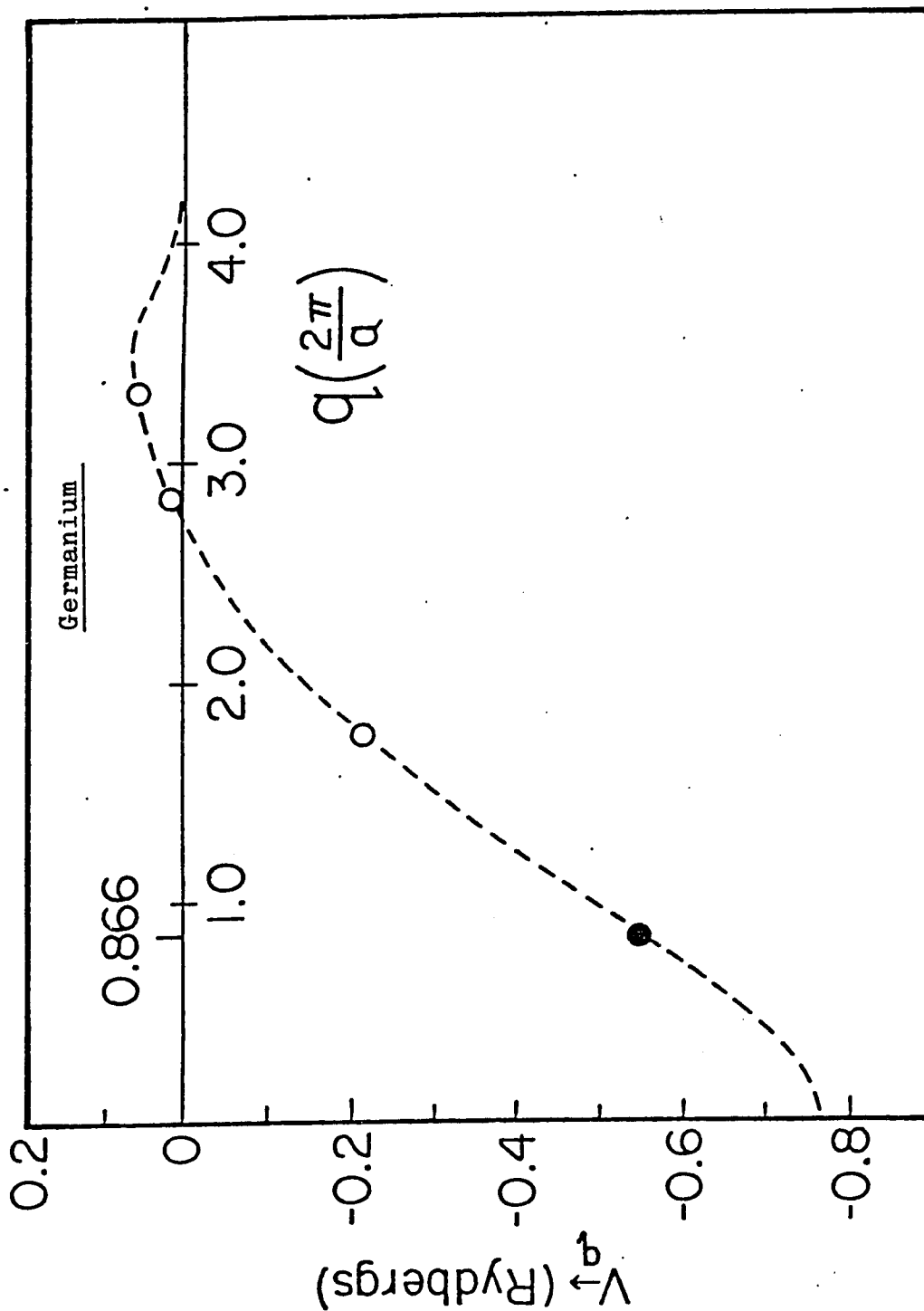


Fig. 16

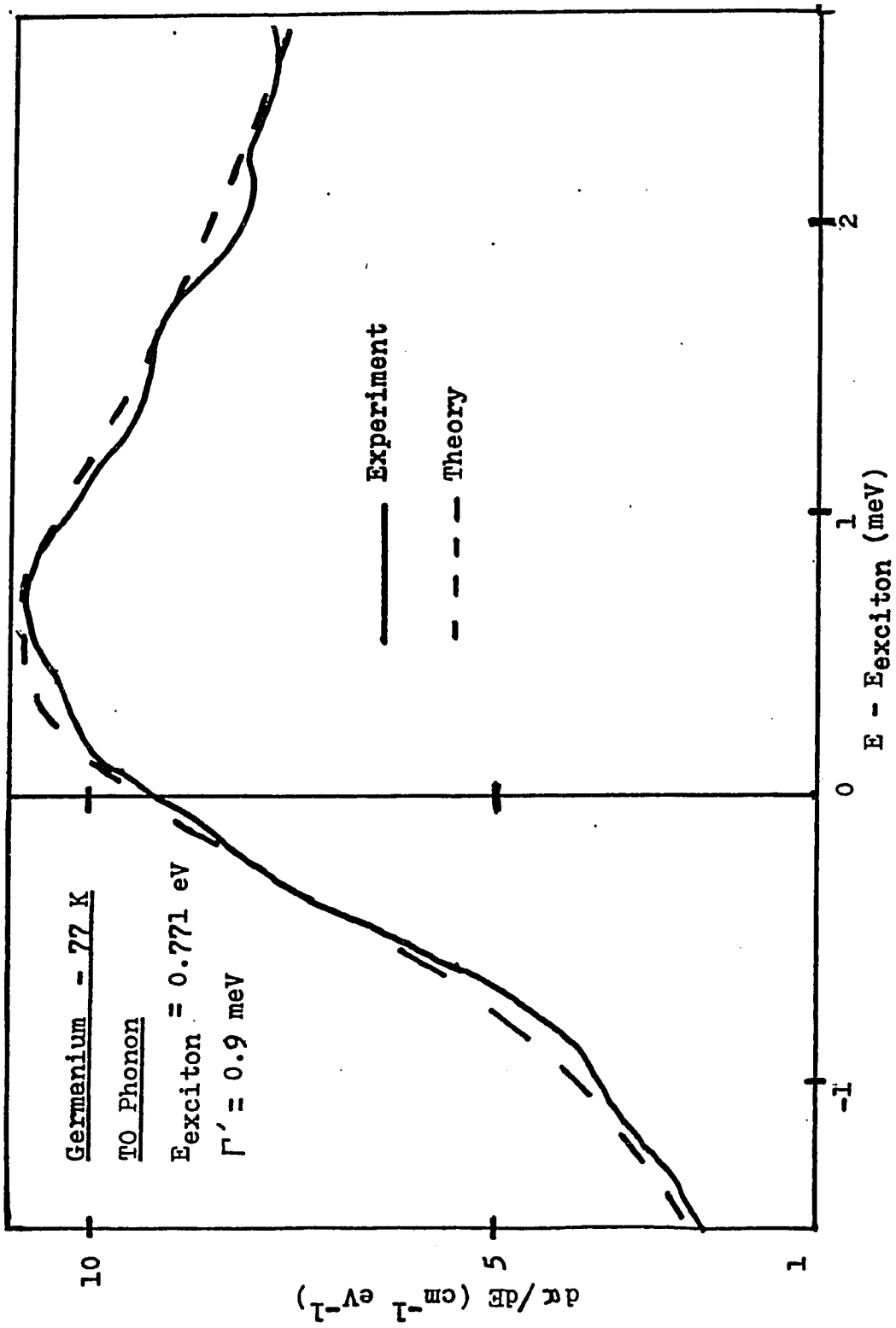


Fig. 17

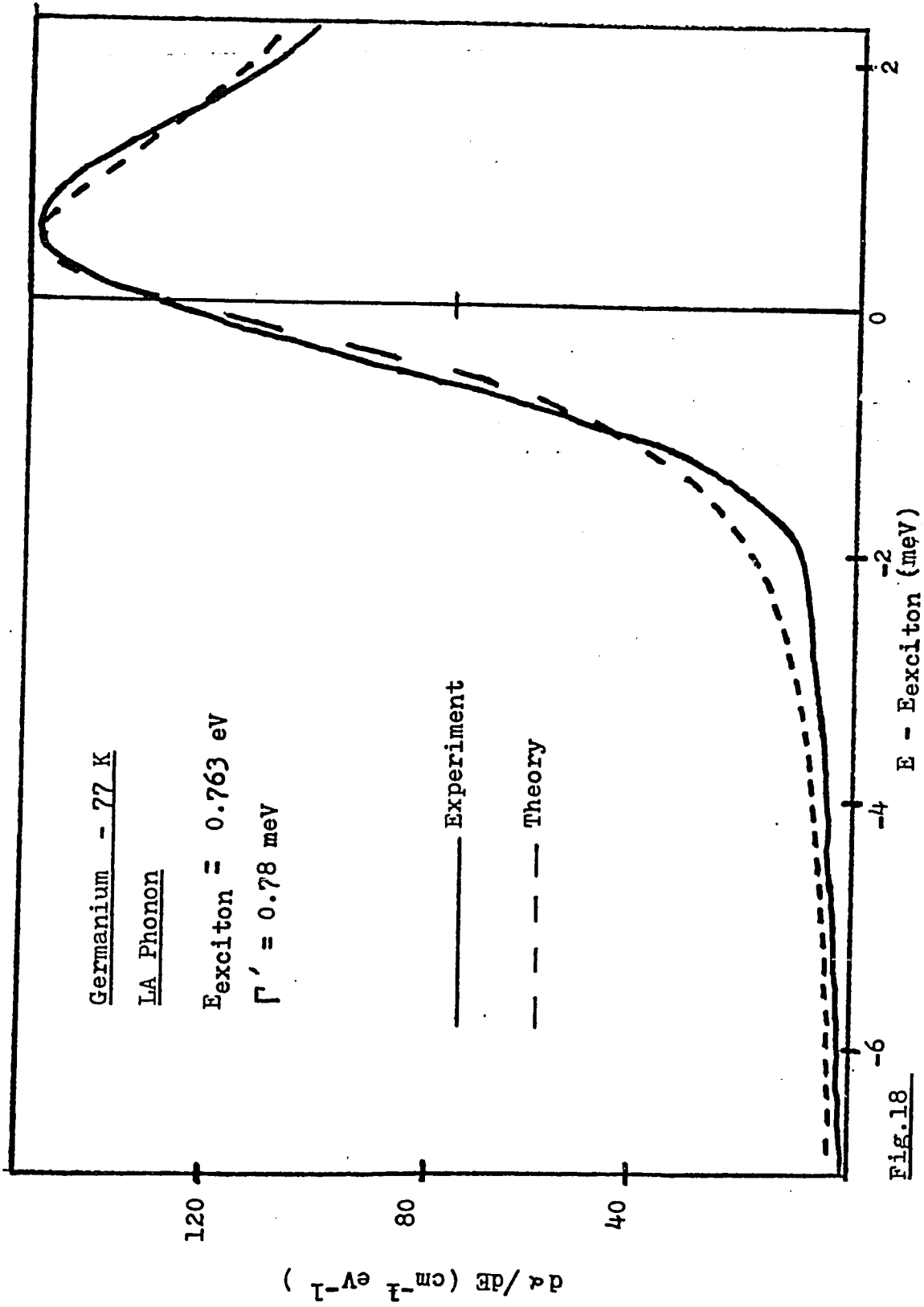


FIG. 18

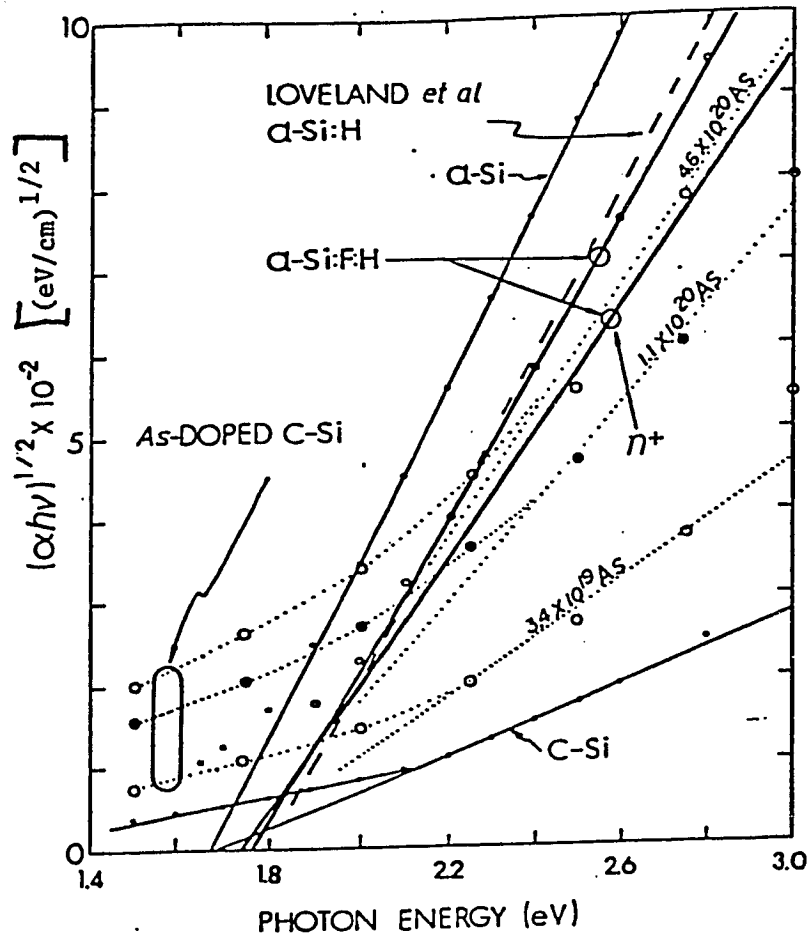


Fig. 19

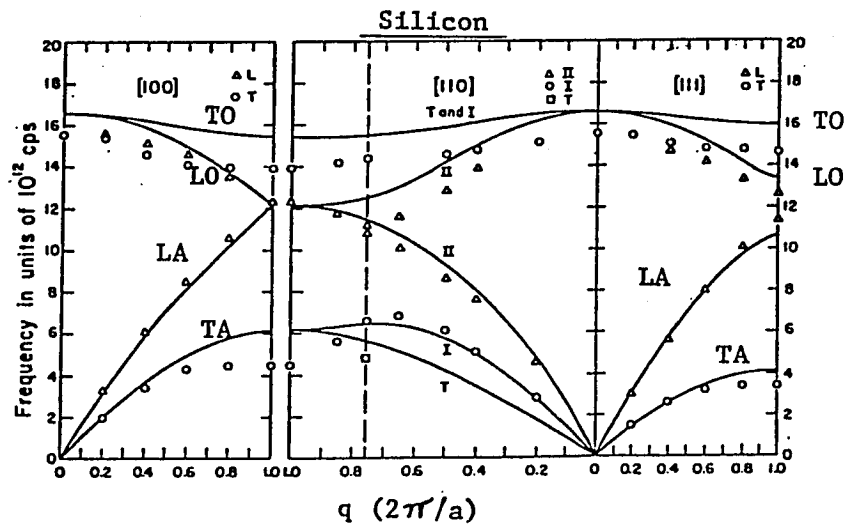


Fig. 20

LIST OF PUBLICATIONS

1. O. J. Glembocki and A. M. Halpern, Angular Distributions in Proton-Hydrogen Charge Transfer Collisions, Phys. Rev. A 16, 530 (1977).
2. O. J. Glembocki and F. H. Pollak, Piezospectroscopic Determination of the Ratio of the Electron-Phonon to Hole-Phonon Scattering Matrix Elements For the LA and TA Phonons of GaP, Phys. Rev. B 25, 1179 (1982).
3. O. J. Glembocki and F. H. Pollak, Relative Intensities of Indirect Transitions: Electron-Phonon and Hole-Phonon Scattering Matrix Elements in Si (TO) and GaP (LA,TA), Phys. Rev. B 25, 1193 (1982).
4. O. J. Glembocki and F. H. Pollak, Calculation of the  $\Gamma$ - $\Delta$  Electron-Phonon and Hole-Phonon Scattering Matrix Elements in Silicon, Phys. Rev. Lett. 48, 415 (1982).
5. O. J. Glembocki and F. H. Pollak, Calculation of the  $\Gamma$ -L Electron-Phonon and Hole-Phonon Scattering Matrix Elements in Germanium, 7863 (1982).
6. O. J. Glembocki and F. H. Pollak, Intervalley Electron-Phonon and Hole-Phonon Scattering Matrix Elements in Germanium, in press, Proc. 16th Int. Conf. on Physics of Semicond., 1982, Montpellier, France.